CELLULAR DYNAMICS IN THE NICHE OF INFREQUENTLY DIVIDING HAIR FOLLICLE STEM CELLS IN THE MOUSE MUS MUSCULUS

by Ying Zhang

CELLULAR DYNAMICS IN THE NICHE OF INFREQUENTLY DIVIDING HAIR FOLLICLE STEM CELLS IN THE MOUSE *MUS MUSCULUS*

A Dissertation

Presented to the Faculty of the Graduate School

of Cornell University

In Partial Fulfillment of the Requirements for the Degree of

Doctor of Philosophy

by

Ying Zhang

August 2010

CELLULAR DYNAMICS IN THE NICHE OF INFREQUENTLY DIVIDING HAIR FOLLICLE STEM CELLS IN THE MOUSE *MUS MUSCULUS*

Ying Zhang

Cornell University 2010

Tissue stem cells (TSCs) are cells that can self-renew for extended periods of time and differentiate into all cell lineages within the regenerating tissue. Self-renewal and differentiation are the two defining properties of TSCs, and failure of either will lead to the disruption of tissue homeostasis. In invertebrates, it has been shown that TSCs adopt asymmetric cell divisions to accomplish self-renewal and differentiation simultaneously. However, whether this mechanism universally applies to mammalian TSCs remains unclear. In our lab, we use the mouse hair follicle as a model system to study the regulatory mechanism for TSC functions.

Mouse hair grows in a cyclic pattern consisting of quiescence, growth, and regression phases. The hair follicle stem cells (HFSCs) are documented to reside in storage stem cell niche - the bulge. Our cell division tracking results using *Tet-off H2B-GFP* transgenic mice confirm the infrequently dividing property of bulge cells and suggest that differentiation of progenitor cells occurs at different times and tissue locations than self-renewal of stem cells. Further single bulge cell lineage tracing using the inducible *Cre* system reveals that a single bulge cell will either leave the bulge to contribute to the new hair growth, or stay in the bulge to replenish the stem cell pool. Long term single bulge cell tracing data indicate a symmetric daughter-cell fate determination model for HFSCs. Moreover, we provide data suggesting that the self-renewing divisions of HFSCs within the bulge are symmetric with respect to an important niche component the basement membrane; whereas the divisions of

differentiating progenitors are both symmetric and asymmetric. Finally, we identify *Gata6* as a crucial transcription factor for HFSC differentiation whose loss impairs the proliferation, differentiation and survival of progenitors in the skin epithelium. Collectively, our findings propose a population mechanism for clustering TSCs whose maintenance involves symmetric cell division and fate determination, as well as specific genetic regulators.

BIOGRAPHICAL SKETCH

Ying Vincent Zhang was the only son born to Zuolan Yang and Shufang Zhang in Maanshan City, China in July of 1982. Ying spent his entire childhood in this serene small town while his parents were especially indulgent for his special interest in capturing and keeping uncommon pets including owls, snakes, mentises, crabs, etc. He set his goal of becoming a biologist from such a hobby at the age of 7. Thanks to his parents' genetics, Ying encountered little competition in his early school days. From 1994, he attended the Maanshan No.2 Junior/Senior High School where he not only extended his interest in science but also met his future wife Chen Li although they didn't start dating until after high school. Ying attended University of Science and Technology of China (USTC) as a biological science major in the College of Life Science. As an undergraduate, he conducted independent research under Dr. Xuebiao Yao investigating the kinetochore protein interaction network in mammalian cells, and under Dr. Wenming Chen exploring new materials in concentrating proteins by radioactive synthesis.

After graduating from USTC with an honors thesis, one publication, one patent, and a Bachelor of Sciences, Ying traveled half of the globe to Ithaca, another small town, entering the Biochemistry, Molecular, and Cell Biology (BMCB) graduate program at Cornell University in August 2005. Interest in understanding the function and exploring the potential application of mammalian stem cells led him to the lab of Dr. Tudorita Tumbar where he studied hair follicle stem cells in the mouse skin. After graduation, Ying plans to extend the studies presented here and continue his research on stem cells in hematopoietic system.

Dedicated to my parents,

to my wife Chen Li for everything,

and to Emilia.

ACKNOWLEDGMENTS

I would first like to express my deepest appreciation to my mentor, Dr. Tudorita Tumbar, who has taught me a great deal about science and faith. She is a thorough, self-critical, and earnest scientist who believes nothing is impossible, and I hope I have acquired these traits for my future career in academia. She has also created a lab where enthusiasm and camaraderie are the norm. It has been my home for 5 years and I will sorely miss it once I have moved on.

I am greatly indebted to my special committee members, Drs. Michael Goldberg, Kelly Liu, and John Schimenti for advice and conversation. Their support is indispensible for my graduate life, both in research and in understanding life. I would also like to extend a special thank you to Dr. Kenneth Kemphues, who isn't my official committee member but has done nothing less.

I would like to acknowledge my dear labmates for many intellectual and personal conversations and support. To David McDermitt, Karen Osorio, Songeun Lee, Jayhun Lee, Cornelia Scheitz, Sanjeev Waghmare, Janice Cheong, Nichita Ciapurin, Colleen Thurman, Karin Lilja, Shu Lu, Charlene Hoi, Tae Lee, and others I am greatly indebted for everything. And to Drs. Brian White and David Shalloway, I thank their professional analysis and fruitful collaboration. I am also grateful to several other faculty members – Drs. Mariana Wolfner, Lis John, Bik Tye, Ailong Ke, Robert Weiss, Sylvia Lee, and Bill Brown for advice and reagents.

I want to thank several special friends for enriching my life in so many ways during my years at Cornell. To Changrui Lu, Wenyu Liu, Xue Xia, Yi Liu, Haitao Wang, Hui Zhang, and Damien Garbett I owe a big thank you for being wonderful and encouraging.

And last, but most importantly, my wife, Chen Li, has been a source of constant support and encouragement through my studies. I thank her for being with me in this 5 years and giving birth to our first daughter Emilia.

Finally, I would like to acknowledge the financial support from VERGE at Cornell University, and from the Presidential Fellowship of Life Science.

TABLE OF CONTENTS

LIST OF FIGURES

LIST OF TABLES

LIST OF ABBREVIATIONS

aPKC	atypical protein kinase C
BAT-GAL	beta-catenin-activated transgene driving expression of nuclear beta-galactosidase reporter
BM	basement membrane
BMP	bone morphogenetic protein
BrdU	5-bromo-2-deoxyuridine
Bu	bulge
CD34	cluster of differentiation molecule 34
cDNA	complementary DNA
Cre	Cre recombinase
DAPI	4',6-diamidino-2-phenylindole
Doxy	doxycycline
DP	dermal papillae
ER	estrogen receptor
FACS	fluorescence activated cell sorting
GAPDH	glyceraldehyde 3-phosphate dehydrogenase
Gata3	GATA binding protein 3
Gata6	GATA binding protein 6
GFP	green fluorescent protein
H&E	hematoxylin & eosin
H2B	histone 2B
HF	hair follicle
HG	hair germ
IRS	inner root sheath
JAK	janus kinase

JZ	junctional zone
K1	keratin 1
K14	keratin 14
K15	keratin 15
K5	keratin 5
Lgr5	leucine-rich repeat-containing G-protein coupled receptor 5
LRC	label retaining cell
Lrig1	leucine-rich repeats and immunoglobulin-like domains protein 1
mRNA	messenger RNA
Mx	matrix
ORS	outer root sheath
PAR	abnormal embryonic partitioning of cytoplasm
PD	postnatal day
PG	post-grafting day
PIE-1	pharynx and intestine in excess-1
QRT-PCR	quantitative real time polymerase chain reaction
SC	stem cell
SEM	standard error of mean
STAT	signal transducer and activator of transcription
TCF/LEF	T cell factor / lymphoid enhancer-binding factor
Tet	tetracycline
TSC	tissue stem cell

CHAPTER 1

THE FUNDAMENTALS OF STEM CELLS

Stem cells are defined by three criteria. First, they self-renew by cell divisions to maintain the stem cell pool. Second, stem cells undergo lineage commitment giving rise to differentiated progenitors, transient amplifying precursors, and eventually terminal differentiated cell lineages. Third, stem cells contribute to the development of an organism for extended periods of time. The two broad types of stem cells are embryonic stem cells from the inner cell mass of blastocysts and adult stem cells found in a variety of regenerating tissues. Over several decades, a tremendous amount of information has become available concerning the properties and functions of stem cells, especially on the self-renewal and differentiation mechanisms in adult stem cells. Recently, the successful combination of classic molecular biology methods with mouse genetics, as well as new experimental approaches including Fluorescence Activated Cell Sorting, has enabled researchers to identify, isolate, and analyze specific stem cell populations *in vivo*. This thesis describes molecular and cellular analyses on the proliferation dynamics, daughter cell fate determination, and genetic regulation of stem cells in the mouse *Mus Musculus* hair follicle system. A review of background knowledge and recent progress specifically relevant to the work in individual chapters is presented in the Introductions to those chapters. In this chapter, I will review briefly the stem cell concepts in a broader sense to provide a general context from which the work in this thesis can be accessed.

Definition for Stem Cells

Stem cells are functionally defined as cells that can self-renew to generate more stem cells, and can differentiate into various lineages of a certain tissue (Smith, 2001; Weissman et al., 2001). In other words, stem cells have the capacities to make daughter cells identical to their mother to "self-renew" the stem cell pool, as well as to generate progeny that will "differentiate" to maintain tissue homeostasis. These two criteria alone would be sufficient to define the function of embryonic stem cells because they transiently exist in the inner cell mass at the blastocyst stage, and can contribute to all tissues of the adult organism. A third definition, however, is needed to distinguish the adult stem cells from other short-lived precursors (such as in the case of hematopoietic stem cells versus primitive blood precursors). The criterion is that stem cells should contribute to the regenerating tissue for extended periods of time - usually the entire life span of an organism (van der Kooy and Weiss, 2000). Besides this tripartite definition, stem cells also possess several functional hallmarks including unlimited self-renewal capacity, clonality from single cells, and extended potency toward multiple lineages.

The first of these hall marks is that stem cells have unlimited proliferative potential. In cell culture, most somatic cells will deplete their proliferative capacity within 80 population doublings before reaching senescence or mitotic arrest (Shay and Wright, 2000; Sherr and DePinho, 2000). In contrast, both embryonic stem cells and some adult stem cells (such as neural stem cells) display unlimited (>160 doublings) proliferative ability *in vitro* (Morrison et al., 1997a; Smith, 2001). Besides this cell culture evidence, results from serial transplantation assays using single stem cells have supported this unlimited self-renewal capacity as a general property for stem cells in the adult hematopoietic system and hair follicles (Claudinot et al., 2005; Iscove and

Nawa, 1997). As such, adult stem cells are able to sustain tissue regeneration for the entire lifetime of the animal.

Second, single stem cells can create more stem cells both in cell lines and in the native tissue. Although the composition of cellular populations proves heterogeneous in most embryonic and adult stem cell lines, hand-picked single stem cells from a Petri dish should at least contain, if not exclusively, cells that are able to reconstitute the specific stem cell line (Weissman et al., 2001). However, our limited understanding of the cell culture condition and transplantation technology delays the final verdict on whether these *in vitro* characteristics would reflect the *in vivo* behavior of stem cells. The most persuasive evidence is derived from the hematopoietic system where single stem cells can reconstitute the entire blood in lethally irradiated recipients upon serial transplantations (Purton and Scadden, 2007).

The third general characteristic is the extended potency of stem cells toward multiple lineages. Within an organism, the embryonic stem cell stands at the top of the lineage hierarchy as pluripotent, i.e., capable of making all types of somatic cells in the adult animal (Weissman et al., 2001). Within a regenerating tissue, the adult stem cell for that specific tissue is multipotent to make all cell types below its rank: from progenitors, to committed precursors, and all the way down to terminally differentiated cell lineages (Weissman et al., 2001). Sometimes, progenitors and precursors are referred to as "oligopotent" or even "multipotent" partially because of a lack of clear boundaries to distinguish them from the adult stem cells. In this thesis, a structure of hierarchical cell definitions is adopted where multipotent adult stem cells give rise to progenitors, which will later become transient amplifying cells that generate terminally differentiated lineages.

In summary, a stem cell is a self-renewing clonogenic cell with both long-term proliferative potential and the pluripotency to differentiate into all cellular lineages of the regenerating tissue.

Stem Cell Niches

Both embryonic and adult stem cells reside in specialized microenvironments known as stem cell niches where the stem cell pool is maintained with regard to cellular properties, proliferative capability, and differentiation potential. During embryonic development, embryonic stem cells are derived directly from the inner cell mass of pre-implantation embryos after the formation of a cystic blastocyst (Papaioannou, 2001). While the inner cell mass are short-lived in the blastocyst once placed in the culturing conditions they live essentially forever, as far as we can tell. This was the first clear indication that the microenvironmentof the stem cell niche is essential for its behavior and for its long-term maintenance. Adult stem cells are maintained for extended periods of time in regenerating tissues, a property which allows closer investigation of the stem cell niche function. Studies from invertebrate systems such as *Drosophila* germ lines, and from mammalian tissues including bone marrow, skin, brain, and intestine have revealed various stem cell - niche interactions at the molecular level that govern cell adhesion, intracellular signaling, and cell cycle regulation. Candidate niches (cells or cellular compartments) have been identified in those tissues. Based on the organization of stem cells in the niche (Ohlstein et al., 2004), I will discuss the stem cell – niche interactions in three categories: simple niches, complex niches, and storage niches (Fig. 1.1).

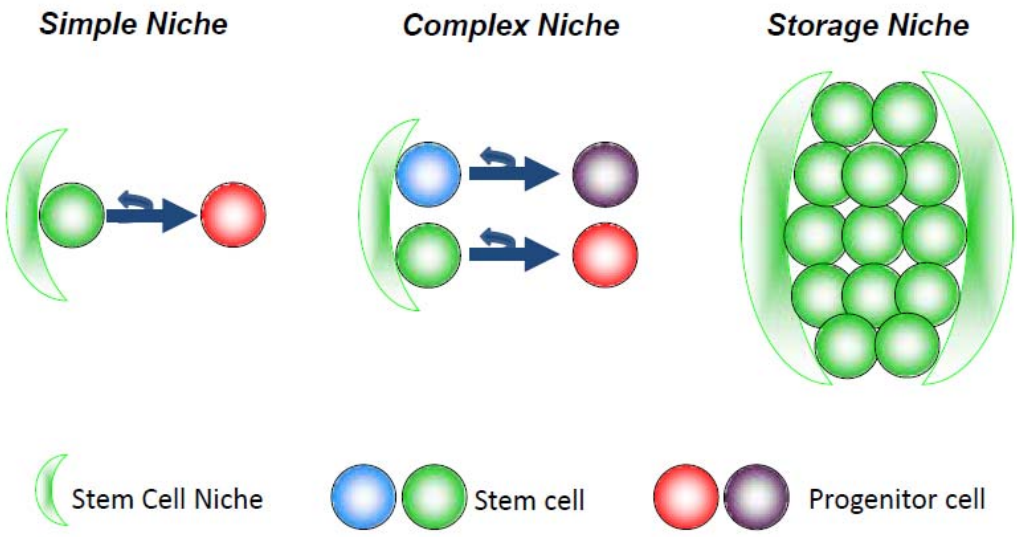

Figure 1.1. Stem cell niche types.

In a "Simple Niche", scarce stem cells attach to the niche cell via tight cellular junctions to receive crucial maintenance signals. Stem cells divide asymmetrically to generate a differentiating progenitor and a renewed stem cell daughter simultaneously. In a "Complex Niche", more than one stem cell types co-exist and produce their specific downstream progenitors respectively. Asymmetric divisions are generally adopted in the complex niche, and there are usually more than 1 supporting niche cells. In a "Storage Niche", dozens of stem cells reside in a specialized environment where they maintain low proliferation activity. Little is known about how stem cells regulate differentiation and self-renewal in the storage niche.

The best studied stem cell niche model is the "simple niche" initially found in the *Drosophila* germ line stem cell systems (Lin, 2002). A stem cell is attached to a permanent stromal niche cell via adherens junctions (Song et al., 2002) and/or through interactions with extracellular matrices (Frye et al., 2003). Such tight association of stem cells with the niche ensures the delivery of critical intercellular signals to the stem cells. For example, bone morphogenetic protein (BMP) signaling directly regulates the growth, and suppresses the differentiation, of *Drosophila* germ line stem cells in both ovaries and testes via the stem niche cap cell and the hub cell, respectively (Decotto and Spradling, 2005). Other signaling pathways have also been identified at the stem niche to control stem cell functions in these systems, such as insulin levels (Spradling et al., 2008). However, one needs to be careful when categorizing these signaling pathways as stem cell specific, as they might in fact be ubiquitous types of physiological signaling that will affect every cell type within the tissue environment. The same standard also applies to studies in the genetic regulation of stem cell functions. Only when the loss of a certain signaling affects a subset of cells in the regenerating tissue (stem cells, progenitors, or terminally differentiated lineages), can we propose that the signaling may play a specific role in stem cell function.

In addition to the maintenance of stem cells, the simple niche model also governs the differentiation of stem cell daughters as they lose contact with the niche. A common mechanism is the adoption of oriented stem cell divisions: When the differentiation signal is absent, niche cells signal, directly or through an underlying basement membrane, to the stem cells to block differentiation. The division of stem cells at this stage will align parallel to the niche and will generate two daughter cells that are both self-renewed stem cells. When a lineage commitment signal arrives, stem cell division orientation instead turns 90 degrees to be perpendicular to the niche.

The daughter cells generated at the distal pole will no longer have contact with the niche, and will thus start differentiating and migrating. At both stages, the nature of cell division can be both symmetric and asymmetric depending on the local factors and the fate of the daughter cells (Spradling et al., 2001). Another important aspect of simple niches is their ability to maintain the niche environment without the presence of stem cells, and attract transplanted stem cells to the niche in the *Drosophila* ovary, and mouse spleen, testis, and bone marrow (Morrison and Spradling, 2008).

Due to the scarcity of stem cells in the simple niche, lost stem cells must be immediately replenished without affecting the homeostasis of the regenerating tissue. Replacement of lost stem cells in the *Drosophila* ovary by rare symmetric divisions of adjacent stem cells or rare de-differentiation of nearby progenitors maintains the stem cell pool at the niche cap cell (Xie and Spradling, 2000). In mouse testes, stem cell niches are constantly filled by the seminiferous tubules after germ cell introduction. Such a mechanism maximizes the number of occupied stem cell niches for optimal production of differentiated sperm (Ryu et al., 2003). More interestingly, the hematopoietic stem cells have adopted a dynamic remodeling system of stem cell niches. Depending on the location and number of niche osteoblasts, hematopoietic stem cells display a dynamic distribution in the bone (Calvi et al., 2003). As such, accidental loss of a single hematopoietic stem cell at one niche will be well compensated by the continuous re– setting all stem cell – niche interactions to ensure uninterrupted production of the differentiated lineages.

The second general category of stem cell niche is the “complex niche”. In these niches, two or more types of stem cells co-exist and all directly attach to the niche cells. Their activity is coordinately regulated to generate multiple product cells (orange and yellow) by niche regulatory signals. For example, the mammalian neural stem cells found at the sub-ventricular zone closely associate with other stem cells /

precursors at the niche including neuroblasts, astrocytes, ependymal cells, and endothelial cells (Alvarez-Buylla and Lim, 2004). The reason behind this complex stem cell – niche structure is probably the inherit complexity of the future neural tissue made from all these stem cells. It is apparently most efficient to place all necessary stem cells together to achieve balanced production of differentiated lineages by mechanisms not yet fully understood.

Sometimes, the definition of a complex niche can be arbitrary, such that some of the simple niches discussed earlier can be also counted as complex: The *Drosophila* testis niche contains cyst stem cells which produce somatic cells to encase the developing germ cells. Similarly, supporting somatic stem cells contribute to the follicle microenvironment that accommodates the differentiating germ cells (Decotto and Spradling, 2005). Moreover, both niches utilize the BMP and JAK/STAT (Janus kinase and signal transducer and activator of transcription) signaling pathway to control the self-renewal and differentiation of stem cells (Decotto and Spradling, 2005). Regardless of how we categorize these niches, the coordinated activity of stem cells with somatic progenitors at the niche is the key to achieve stem cell function for the tissue.

Other complex niches without anatomical specificity also exist in mammalian tissues. Evidence has been found that hematopoietic stem cells could temporarily reside at vascular tissues outside the bone marrow (Il-Hoan and Kyung-Rim, 2010). In the mouse inter-follicular epidermis, the basement membrane houses sparse epidermal stem cells intermingled with differentiated lineages, although morphologically specific niche structures are not observed (Clayton et al., 2007). These findings provide insights for new stem cell – niche interaction models, and also lead to more questions that require further investigations: Is the arrival of stem cells at different tissues able to induce de-novo niche formation? How do stem cells maintain

their properties without dedicated niche support? Is the tight junction between stem cells and niche cells necessary in all regenerating tissues? And most importantly, can we in fact apply the vast knowledge obtained from *Drosophila* stem cell studies directly to mammalian systems?

The last and most relevant niche type for this thesis is the "storage niche". It is best represented by the mouse hair follicle system. During normal adult hair regenerations, epithelial stem cells and melanocyte progenitors contribute to hair follicle homeostasis (Blanpain and Fuchs, 2006). The bulge compartment below the sebaceous gland is the stem cell niche in the hair follicle. More than 100 cells reside in the bulge, which is surrounded by a basement membrane layer. Compared to differentiated cell lineages, bulge cells divide infrequently to preserve their genome from accumulating replicative errors (Cotsarelis et al., 1990). But upon new hair growth or under wounding conditions, some bulge cells are activated to exit the quiescence and contribute to the differentiated lineages of the tissue (Taylor et al., 2000). However, most reviews refer to the dermal papillae as niche cells – although the dermal papillae might not be involved in maintenance, it is likely involved in stem cell behavior – activation and differentiation. Little is known about the niche cell identity in the bulge compartment if they ever exist. It is also unclear whether bulge stem cells comprise distinct sub-types of committed progenitors for the various lineages of the hair and these cells migrate directly out of the niche, or the bulge stem cells only send their differentiating daughters to become transient multi-potent progenitors. Furthermore, the adhesive contacts and molecular signals found in simple and complex stem cell systems are yet to be characterized in the storage niche model (Morrison and Spradling, 2008). Finally, the storage niche is considered to be a generally quiescent stem cell reservoir for the regenerating tissues (Li and Clevers, 2010). Whether these stem cells contribute to the tissue growth under normal

physiological conditions or only serve as a reserve pool for emergency situations is one of the remaining key questions in the research field of stem cell – niche interactions.

Asymmetric and Symmetric Stem Cell Divisions

Self-renewal and differentiation are the defining characteristics of stem cells. To accomplish these two divergent biological functions, stem cells have adopted various division and fate assignment strategies. The simplest strategy is asymmetric cell division, where one stem cell divides to generate one stem cell daughter cell and a differentiating progenitor simultaneously (Betschinger and Knoblich, 2004; Clevers, 2005). However, if stem cells only divide asymmetrically, a specific stem cell pool will face quick depletion due to unpredicted losses of stem cells by senescence, apoptosis, and migration, as well as the inability to produce additional stem cells. Thus, most stem cells have also evolved to divide symmetrically, either during the establishment of its pool during the embryonic stage (Lechler and Fuchs, 2005; Morrison et al., 1995) or under stress conditions such as wounding (Doetsch et al., 2002; Wright et al., 2001). From one symmetric division, the two daughters from a single stem cell possess the same fate: Either both remain as stem cells to expand the stem cell pool; or both step on the differentiation path, resulting in a net loss to the stem cell population. In principle, a stem cell population can sustain itself through only asymmetric cell divisions, or a mixture of symmetric and asymmetric divisions. Next I will briefly review the functions and implications of asymmetric division, symmetric division, and a combination of both in stem cells.

Numerous studies have shown that stem cells, especially in invertebrate systems, widely adopt asymmetric cell divisions to regulate stem cell activities (Clevers, 2005;

Doe and Bowerman, 2001). There are two general mechanisms governing the asymmetric stem cell divisions: An intrinsic pathway, where intracellular fate determinants are segregated asymmetrically into two daughter cells during mitosis leading to distinct cellular property and fate; and an extrinsic pathway, where molecularly identical daughter cells are generated from mitosis, but they are exposed or placed into distinct cellular environments afterwards to achieve asymmetric fate determination. Mitotic spindle orientation is a common regulator shared by both intrinsic and extrinsic asymmetric stem cell division mechanisms.

One of the first and most intensively studied intrinsically controlled stem cell asymmetric division models is the *C. elegans* zygote (Doe and Bowerman, 2001). The zygote divides asymmetrically to generate a larger blastomere whose descendants will become the future ectoderm, and a smaller blastomere that makes mesoderm, endoderm and the germ line in subsequent asymmetric divisions (Guo and Kemphues, 1996). Although the zygote is not a typical adult stem cell, the asymmetric segregation of fate determinants has proven to be evolutionarily conserved in *Drosophila* neuroblasts (Wodarz, 2005) and mammalian stem cell systems. The initial asymmetry is achieved by the segregation of the PAR-3, PAR-6 and atypical protein kinase C (aPKC) complex to one pole of the dividing cell – the stem cell daughter side. Then the PAR proteins control the asymmetric localization of cell fate determinants including Mira, Lgl and Numb in mammalian cells to the opposite pole of the dividing cell – the differentiating progenitor side. Mitotic spindles are also directed by the molecular asymmetry in the cell through microtubule- centrosome interactions with fate determinants localized to the opposing poles.

For the extrinsic asymmetric stem cell division mechanism, the *Drosophila* germ line stem cell serves as the best example. Upon one cell division, the stem cell daughter remains attached to the niche (the hub cell in the testis or the cap cell in the

ovary); while the other daughter loses contact with the niche signaling and migrates away to differentiate (Yamashita et al., 2005). Known niche signaling pathways includes BMP and JAK/STAT to repress differentiation of stem cells attached to the niche (Decotto and Spradling, 2005). The orientation of the mitotic spindle is directed by centrosome components in the stem cells, similar to that in the intrinsic asymmetric division mechanism (Yamashita et al., 2003).

In mammalian systems, the conserved intrinsic asymmetric stem cell divisions have been characterized in central neural stem cells, muscle stem cells, and inter-follicular epidermal progenitors. The neural stem cells have been proposed to asymmetrically segregate the Numb protein to the progenitors destined for differentiation (Shen et al., 2002; Zhang et al., 2004; Zhong et al., 1996), while antagonizing Notch signaling maintains the stem cell daughter in the undifferentiated state (Cayouette and Raff, 2002; Wakamatsu et al., 1999). Similarly, the Numb signaling regulates the muscle stem cell asymmetric divisions by repressing stemness in the differentiating progenitors (Conboy and Rando, 2002). In the inter-follicular epidermis, epidermal progenitors rely on the PAR-aPKC protein complex to align the spindle perpendicularly to the basement membrane (Lechler and Fuchs, 2005). All these resemblance implies that the intrinsic stem cell asymmetric division mechanism is highly conserved through evolution. However, a mammalian system utilizing the the extrinsic asymmetric cell division mechanism as found in the *Drosophila* germ line stem cell systems has yet to be discovered.

Symmetric stem cell divisions have been found during development and adulthood in invertebrate and vertebrate tissues, as well as under stress conditions. In the *C. elegans* germ line, the original two germ line stem cells divide symmetrically during larval development to produce a stem cell/progenitor pool of ~ 2000 cells in the adult gonad (Kimble and White, 1981). Each stem cell division produces two

morphological and molecularly identical daughters, and the loss or repositioning of a fraction of the total stem cells does not affect the maintenance of the stem cell pool. More interestingly, duplication of the distal tip cell (DTC) niche results in the expansion of stem cell populations (Kipreos et al., 2000; Kostic et al., 2003; Lam et al., 2006). Unlike *Drosophila* germ line stem cells, *C. elegans* germ line stem cells utilize Notch signaling to regulate self-renewal and differentiation during both larva and adult stages (Kimble and Crittenden, 2007). These experimental findings indicate that *C. elegans* germ line stem cells have adopted a different scheme for self-renewal and differentiation control: Stem cells no longer act as individuals, but rather work together as a population to accomplish their jobs producing many stem cells with symmetric divisions, and assign part of them to become progenitors depending on their distance from the signaling niche.

In mammals, symmetric stem cell divisions have been characterized in the sub-ventricular zone neural stem cells, inter-follicular epidermal progenitors, and hematopoietic stem cells. By directly observing cultured slices of developing mouse cerebral cortex (Huttner and Kosodo, 2005) and epidermis (Lechler and Fuchs, 2005), researchers have documented the expansion of the stem cell pool by symmetric cell divisions before significant differentiation occurs. In both cases, the two daughters from one cell division align parallel to the stem cell niche either at the ventricular zone in the brain or at the epidermis basement membrane during early gestation stage. Although the comprehensive molecular properties of the two daughters have yet to be determined, their identical morphology, tissue location, and staining patterns for specific stem cell markers strongly imply that they have the same cellular identity and developmental fate. In the hematopoietic system, the total number of stem cells doubles every day during mid-gestation (Morrison et al., 1995), suggesting symmetric expansion events during embryonic development.

An interesting observation concerning some mammalian stem cells is their ability to utilize both symmetric and asymmetric stem cell divisions to fulfill the purposes of initial expansion, self-renewal during adulthood, and differentiation to sustain tissue regeneration. In the aforementioned sub-ventricular zone neural stem cell system, upon the stratification of differentiated neural cells in the forebrain, neural stem cells start dividing asymmetrically, to generate one stem cell that remains in the ventricular zone and a differentiating progenitor that migrates away from the stem cell niche to the neural stratification site (Noctor et al., 2004). Clonal analyses by retroviral labeling of individual stem cells in this tissue also support the idea that undifferentiated neural stem cells divide asymmetrically under steady-state conditions (Morshead et al., 1998; Reid et al., 1997). Similarly, during mid-gestation when stratification occurs at the embryonic epidermis, the previously expanding basal layer epidermal cells also initiate asymmetric cell division with the mitosis axis perpendicularly aligned to the niche (Lechler and Fuchs, 2005). Analyses of spindle orientation through embryonic development to early adulthood clearly illustrate that epidermal basal layer cells are down-toning symmetric divisions (paralleled orientation to the niche) and increasing the frequency of asymmetric divisions (perpendicularly to the niche) to accommodate the need of the developing organism (Lechler and Fuchs, 2005). Asymmetric cell divisions also maintain the homeostasis of other regenerative epithelial tissues, including the esophagus and the corneal epithelium (Seery and Watt, 2000; Sun and Lavker, 2004).

The switch from symmetric to asymmetric division in some mammalian stem cells can be reversed by stress conditions such as transplantation and injury. Upon transplantation, hematopoietic stem cells expand themselves symmetrically to reconstitute the entire blood system in the recipient mice (Wilson et al., 2008). In the rat forebrain, the sub-ventricular zone neural stem cells increase their frequency of

symmetric divisions following stroke-induced cell death (Zhang et al., 2004). Similar findings have been established in cultured hematopoietic stem cell and neural stem cell lines (Bodine et al., 1996; Morrison et al., 1997b).

Except for the sub-ventricular zone neural stem cells and epidermal stem cells in the epidermis basal layer, little is known about the division mechanism of other adult stem cells in mammals. One of the obstacles in this research is the scarcity of stem cell divisions in niches found in many systems, such as in the hematopoietic and the hair follicle systems. As a result, capturing a single division under the microscope and following the fate of the two daughter cells are very technically challenging. New cell division detection and daughter cell tracing strategies are required to facilitate the direct observation of stem cell division behavior *in vivo*. Another unsolved question is whether either the extrinsic asymmetric cell division mechanism found in *Drosophila* germ lines, or the population strategy for stem cell maintenance in *C. elegans* germ line, or both would apply to all mammalian stem cell systems. Current findings suggest that an exclusive asymmetric division model may not apply to mammalian stem cells, which tend to possess significant flexibility in division modes so that they can respond to various developmental and physiological conditions. It would not be surprising to discover more complex mechanisms to maintain the stem cell function in tissues that differ in niche structure, growth pattern, and surrounding biochemical microenvironment. Furthermore, as researchers are continuously claiming the discovery of new stem cells, the three criteria to define stem cells need to be reinforced in existing stem cell models. The vague boundaries between stem cells and progenitors, as well as between both and neighboring supporting cells, have imposed additional difficulties in focusing our research on true stem cells. Thus, *in vivo* data directly demonstrating the stem cell identity has recently become a priority in the stem cell research community.

Next I will briefly review the basics of the hair follicle in mouse skin which I use as a model system in an attempt to answer these remaining questions, and explore new regulatory mechanisms for stem cells.

Hair Follicle Stem Cells in the Mouse Skin

Hair follicles are epidermal appendages of the skin, and their morphogenesis involves a series of epithelial-mesenchymal interactions. In early embryogenesis, one single layer of ectodermal cells covers the whole embryo and attaches to an underlying basement membrane of extracellular matrix. These cells become the basal cells of mature skin that proliferate and differentiate vigorously. The result is a stratified epidermis consisting of multiple layers of terminally differentiated cells that accomplish the barrier function of the skin (Blanpain and Fuchs, 2006).

At the same time, some of the undifferentiated basal cells receive signals from the underlying dermis to form a cluster of elongated cells called the hair placode, which bears a hair follicle destiny. The epidermis in turn responds to the dermis by sending a signal to direct the dermal cells to condense and establish the dermal papilla, a future signaling compartment in a mature hair follicle. The dermal papilla induces the hair placode to invaginate and differentiate into the discrete lineages of the hair follicle (Blanpain and Fuchs, 2006; Schmidt-Ullrich and Paus, 2005). During this process, the cells at the base of the developing hair follicle maintain a highly proliferative state. As the hair follicle matures, these proliferating matrix cells differentiate into the inner root sheath (IRS), which serves as the envelope of the future hair shaft; the outer root sheath (ORS), which is contiguous with the epidermis and is surrounded externally by the basement membrane; and the new hair shaft.

Adult hair follicles undergo cyclical regeneration (Cotsarelis, 2006). At the end of morphogenesis, the matrix cells exhaust their proliferation capacity; and hair growth ceases and enters a regression stage (catagen), when the lower two-thirds of the hair follicle rapidly degenerate by apoptosis. The retracting epithelial strand lifts the dermal papilla upward to the base of the permanent portion of the hair follicle, called the bulge. After catagen, the hair follicle enters a quiescent stage (telogen). In the mouse, the first telogen lasts approximately one day; but in subsequent hair cycles, this phase becomes increasingly longer, with less synchronized hair cycle timing among follicles. After the first telogen, the hair follicles enter the growth stage (anagen), with the enlargement of the hair germ located between the bulge and the dermal papilla. Later, the hair germ is superseded by a new matrix structure which repeats the matrix contribution during hair morphogenesis to produce a new hair until the following catagen arrives (Muller-Rover et al., 2001). This periodic cycling of hair growth lasts for the entire life of the animal approximately 10 cycles in total, implying the existence of specific hair follicle stem cells.

Before the discovery of hair follicle stem cells, researchers had summarized several distinctive hallmarks for adult stem cells from studies stratified squamous and simple epithelia, as well as in the hematopoietic system: relatively undifferentiated status; long-term proliferative potential; slow cycling to conserve proliferative potential and to protect DNA from replicative errors; prompt responses to wounding and growth stimuli; proximal localization with respect to rapidly proliferating cells usually called “transient amplifying cells” in the stem cell - progenitor cell – transient amplifying cell - terminally differentiated cell hierarchy; and residence in a well-protected area called the stem cell niche (Cotsarelis et al., 1990). One of these distinguishing features, infrequent division, is utilized to identify the hair follicle stem cells by nucleotide label-retaining assays using 5-bromo-2-deoxy-uridine (BrdU).

After the initial BrdU labeling (pulse) in newborn mice, the level of BrdU in individual cells is examined over time (chase). The most proliferative cells dilute their label rapidly through mitosis, while only the infrequently dividing cells retain high BrdU levels as label-retaining stem cells, most of which reside in the bulge region of the hair follicle – the putative stem cell niche (Cotsarelis et al., 1990). Results from later studies have provided further evidence for the model that hair follicle stem cells divide infrequently. *In vitro* clonogenicity assays have shown that in rat-whisker follicles, 95% of the single cell-derived holoclones come from cells of the bulge, whereas less than 5% of the growing colonies derive from the matrix region (Kobayashi et al., 1993). Colonies from cultured single bulge cells are able to contribute to hair growth on recipient mice after serial transplantations over a long period of time, which proves the long term potential of stem cells from the bulge (Claudinot et al., 2005). Moreover, labeled bulge cells and their derivatives contribute to wound healing in the epidermis by migration from the bulge (Claudinot et al., 2005; Ito et al., 2005; Taylor et al., 2000). Although direct *in vivo* evidence is still missing to ultimately confirm the stem cell identity, these previous studies strongly suggest the bulge contains most, if not all, the hair follicle stem cells.

As mentioned earlier in this chapter, the scarcity of stem cell divisions has been one of the major obstacles for tracking the fate of stem cell progeny. The nucleotide label-retaining technology only allows semi-quantitative microscopic analysis of stem cell proliferation, and only for 3 divisions in a limited number of hair follicles (Waghmare et al., 2008). In an attempt to improve the scope and resolution of label-retaining essays, Dr. Tumbar and colleagues developed a Tet-off inducible H2B-GFP transgenic mouse line (Tumbar et al., 2004). In the absence of doxycycline, all the skin epithelium nuclei accumulate H2B-GFP to the same level (pulse). When doxycycline is fed to the mice (chase), the expression of H2B-GFP shuts off quickly,

and the level of H2B-GFP protein is diluted by cell divisions. After four weeks of doxycycline chase, only the bulge cells still retain a high level of H2B-GFP protein (Tumbar et al., 2004). Additional work using the bulge cell markers CD34 and α6 integrin in Fluorescence Activated Cell Sorting (FACS) confirmed that the H2B-GFP protein level is diluted by exactly 2 fold by each additional cell division (Trempus et al., 2003; Waghmare et al., 2008). This *in vivo* stem cell division counting system provides for the first time the opportunity to monitor precisely the proliferation dynamics of stem cells in their native tissue. It also offers an experimental approach to isolate and analyze stem cells in specific developmental states for genetic regulation studies. Moreover, with the only storage niche known thus far in mammalian tissues, the hair follicle stem cell system is of special interest for testing the evolutionary conservation of stem cell symmetric or asymmetric division mechanisms and exploring further the complex regulation of mammalian stem cells.

Dissertation Outline

This dissertation describes cellular dynamics in the niche of infrequently dividing hair follicle stem cells.

Chapter 2 documents the proliferation dynamics of hair follicle stem cells in the bulge using the inducible H2B-GFP system, as well as the gene expression identification of stem cell or progenitor cell populations in differentiation and self-renewal stages. This chapter also describes the *in vivo* tracking of H2B-GFP label-retaining hair follicle stem cells at the start of a new hair regenerating cycle. In addition, a retrospective single stem cell lineage tracing study is presented, which supports a population fate deterministic strategy for stem cell maintenance. Collectively, the work described in Chapter 2 proposes a temporal-spatial proliferation

regulation of hair follicle stem cells during which stem cell daughters are assigned with symmetric fate determinations.

Chapter 3 describes further applications of the division counting and single cell lineage tracing systems elucidated in Chapter 2. Direct analysis of the alignment of two daughters from one stem cell division suggests mostly symmetric divisions for stem cell self-renewal, while progenitor maintenance involves both symmetric and asymmetric divisions. Chapter 3 also presents evidence for the dynamic relocalization of cells in the bulge to accommodate hair morphology changes through the hair cycle. Furthermore, this chapter includes a mathematical model for bulge cell dynamics which leads to the conclusion of an unanticipated loss of 42% of bulge cells during one hair cycle. Finally, characterization of the proliferation dynamics for a newly identified stem cell population at the junctional zone of the hair follicle indicates more vigorous proliferation than the bulge stem cells.

Chapter 4 describes analyses of *Gata6* knock-out in the skin during the quiescence and growth stages of the hair cycle. It also presents the cellular defects in the knockout skin with regard to differentiation, proliferation, and apoptosis. Data from these experiments suggest that *Gata6* is required for the maintenance and proper differentiation of hair follicle progenitors, but not for the stem cells in the bulge.

Chapter 5 is an overall summary and discussion of the main results described in this thesis in relation to the current status of stem cell research. Chapter 5 also discusses research directions in the immediate future suggested by my work in Chapter 4.

CHAPTER 2

DISTINCT SELF-RENEWAL AND DIFFERENTIATION PHASES IN THE NICHE OF INFREQUENTLY DIVIDING HAIR FOLLICLE STEM CELLS

Summary

In homeostasis of adult vertebrate tissues, stem cells are thought to self-renew by infrequent and asymmetric divisions that generate another stem cell daughter and a progenitor daughter cell committed to differentiate. This model is based largely on *in vivo* invertebrate or *in vitro* mammal studies. Here we examine the dynamic behaviour of adult hair follicle stem cells in their normal setting by employing mice with repressible H2B-GFP expression to track cell divisions and Cre inducible mice to perform long-term single cell lineage tracing. We provide direct evidence for the infrequent stem cell division model in intact tissue. Moreover, we find that differentiation of progenitor cells occurs at different times and tissue locations than self-renewal of stem cells. Distinct fates of differentiation or self-renewal are assigned to individual cells in a temporal-spatial manner. We propose that large clusters of tissue stem cells behave as populations, whose maintenance involves unidirectional daughter-cell fate decisions.

This chapter has been published in *Cell Stem Cell* (Zhang, Y.V., Cheong, J., Ciapurin, N., McDermitt, D.J., and Tumbar, T. (2009). Cell Stem Cell 5, 267-278.), and is reprinted with permission. The following is detailed contribution of authors: Tumbar T and Zhang YV designed the experiments and analyzed the data presented in all figures. Zhang YV performed experiments in all figures. Cheong J performed experiments and contributed to Fig. 2.10B, E. Ciapurin N contributed RT-PCR data to Fig. 2.3D. McDermitt DJ performed the initial analyses for K14CreER : Rosa26R mouse line, and assisted in the experiments in Fig. 2.12B. Zhang YV and Tumbar T made the figures and wrote the paper.

Introduction

Stem cells (SCs) have the ability to self-renew and differentiate for extended periods of time. Their dynamic behaviour within tissues is key in regulating normal tissue homeostasis and injury repair (Morrison and Kimble, 2006). Based on *in vivo* work in invertebrates, and supported by *in vitro* transplantation (functional) assays in mammalian systems adult SCs are thought to have several characteristics: reside in a protective environment or niche important for their long-term maintenance; divide infrequently during life; generate at division two daughter cells that acquire asymmetric fates (one daughter remains in the niche and becomes another SC, and the other leaves the niche and becomes a short-lived rapidly dividing transit-amplifying or progenitor cell); be multipotent or capable to generate all cell types in their own lineage (Lansdorp, 2007). However, due to the complexity of vertebrate tissues, the lack of specific markers, and the overall scarcity of adult SCs, there are few studies demonstrating these features for mammalian tissues in normal settings, without transplantation injury (Morrison and Kimble, 2006). Recently, long-term lineage tracing in intact tissue (referred to here as "*in vivo*") in mouse epidermis, hair follicle (HF), and intestine (Barker et al., 2007; Clayton et al., 2007; Jaks et al., 2008), challenged the infrequently dividing/ "slow-cycling" SC model, previously best supported by *in vitro* data from blood and HF single-cell transplantation assays (Blanpain et al., 2004; Foudi et al., 2009; Wilson et al., 2008). Here we employ the mouse HF system to re-examine the dynamic behaviour of long-lived adult SCs in their normal setting.

HFs form beneath the skin surface during mouse embryonic life and emerge in early post-natal life as fully differentiated organelles with a cylindrical structure, made of an upper permanent region (bulge), containing epithelial SCs, and a temporary

region (bulb) containing differentiated cells (Fig. 2.1A). Concentric layers of cells surround the centrally located hair shaft, and the SCs are localized in the outer most layer, called the outer root sheath (ORS). At the bulb base there is a pocket of progenitor cells known as matrix (Mx), which divide rapidly and generate terminally differentiated cells forming the inner root sheath (IRS) and the hair shaft. The matrix encloses a mesenchymal pocket of cells called dermal papillae (DP), a signalling centre with fate instructive properties (Fig. 2.1A). Around 3 weeks into postnatal life HFs begin a cyclic process of degeneration and regeneration known as the hair cycle (Cotsarelis, 2006), which consists of recognizable and synchronous phases: catagen, telogen and anagen (Fig. 2.1B). Catagen is the destructive phase in which bulge cells cease proliferation, bulb cells undergo massive apoptosis, and DP cells are lifted upwards towards the bulge. Telogen is the resting quiescent phase, in which HFs consist of bulge and hair germ (HG). The HG is a small epithelial structure generated at least in part by cells at the bulge base (Cotsarelis, 2006; Jaks et al., 2008) Fig. 2.1B). Anagen is a phase of intense growth, when rapidly dividing progenitor Mx cells emerge underneath the bulge at the HG location and produce a new hair bulb (Greco et al., 2009; Legue and Nicolas, 2005). In later life these phases occur repeatedly, albeit less synchronously (Plikus et al., 2008), and are marked by long periods of rest. Bulge cells can be identified in the skin by their infrequent divisions and specific surface expression of CD34 and α6-integrin (Cotsarelis, 2006). Single bulge-cell transplantation assays showed contribution to HF regeneration in transplantation assays, which deemed the bulge as the SC compartment. In addition, data in intact skin revealed that at least some infrequently dividing bulge cells contributed progeny cells to the bulb in anagen in short-term assays. Finally, both K15 or LGR5 promoters marked collectively both bulge and HG cells in lineage tracing experiments, and confirmed the long-term contribution of bulge/germ cell

Figure 2.1. Distinct characteristics of bulge cells newly generated at different hair cycle stages.

(A) The hair follicle structure. (B) Hair cycle phases of growth (anagen), degeneration (catagen) and quiescence (telogen) (see text). (C) Doxycycline (doxy) chases in 1st (synchronous) hair cycle to document cell proliferation quantitatively. PD, postnatal day. (D) FACS dot plot of live (PI negative) skin cells stained for CD34 and a6-integrin surface expression (PD21-PD28 chase). Red dots, secondary antibody alone for CD34 staining. (E) FACS histograms of CD34+/a6+ bulge cells from individual mice at stages indicated. Note distinct proliferation profiles at different stages (pink arrows). (F) Cells were sorted and analyzed by RT-PCR for expression of bulge-preferred factors (Tumbar et al, 2004). (G) Skin images from 3-day BrdU labeled and doxy treated mice showed BrdU staining in hair germ (hg) at PD18-PD21 and in bulge (Bu) at PD22-PD25. Arrows indicate CD34+/BrdU+ proliferating cells. Note that lower CD34 levels at the bulge/germ transition zone at PD18- PD21. All experiments were repeated in $\geq$ 3 mice per stage. DP, dermal papillae. Scale bar in G, 10mm.

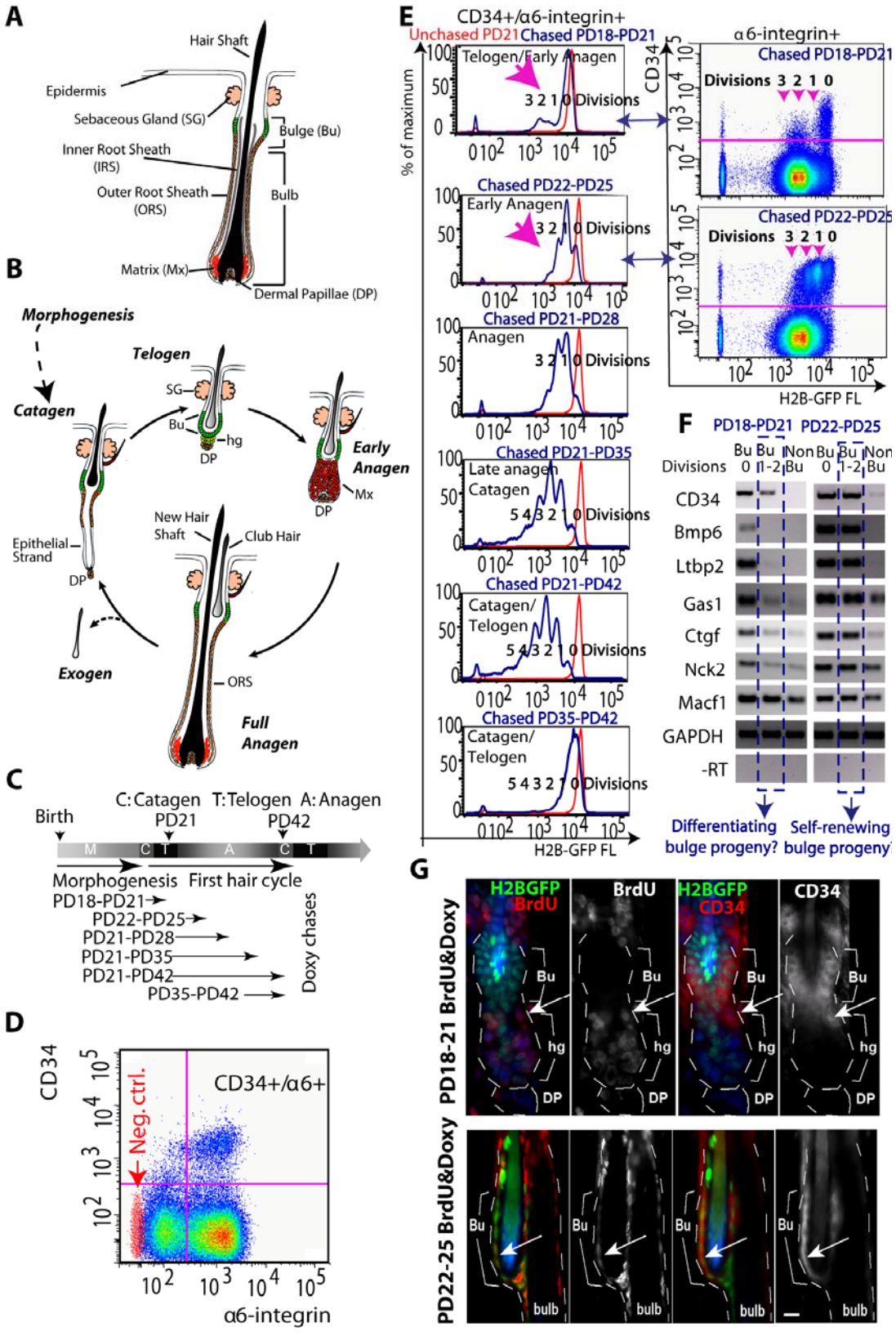
A
Hair Shaft
Epidermis
Sebaceous Gland (SG)
Bulge (Bu)
Inner Root Sheath (IRS)
Outer Root Sheath (ORS)
Bulb
Matrix (Mx)
Dermal Papillae (DP)
B
Morphogenesis
Telogen
Catagen
SG
Bu
hg
DP
Early Anagen
Mx
New Hair Shaft
Club Hair
Epithelial Strand
Exogen
ORS
Full Anagen
C
C: Catagen T: Telogen A: Anagen
Birth
PD21
PD42
Morphogenesis
First hair cycle
PD18-PD21
PD22-PD25
PD21-PD28
PD21-PD35
PD21-PD42
PD35-PD42
Doxy chases
D
CD34
Neg.ctrl.
CD34+/α6+
α6-integrin
E
CD34+/α6-integrin+
Unchased PD21
Chased PD18-PD21
Telogen/Early Anagen
Divisions
% of maximum
Chased PD22-PD25
Early Anagen
Chased PD21-PD28
Anagen
Chased PD21-PD35
Late anagen
Catagen
Chased PD21-PD42
Catagen/ Telogen
Chased PD35-PD42
H2B-GFP FL
α6-integrin+
CD34
F
PD18-PD21
PD22-PD25
Bu 0
Bu 1-2
Non Bu
CD34
Bmp6
Ltbp2
Gas1
Ctgf
Nck2
Macf1
GAPDH
-RT
Differentiating bulge progeny?
Self-renewing bulge progeny
G
H2BGFP BrdU
BrdU
H2BGFP CD34
CD34
PD18-21 BrdU&Doxy
PD22-25 BrdU&Doxy
Bu
hg
DP
bulb

progeny to all hair compartments (Cotsarelis, 2006). In this paper we marked for the first time the single bulge cells apart from the HG cells and test their long-term fate in intact tissue, in the absence of injury induced by cell isolation, transplantation, or dermabrasion. Specifically, we ask whether long-lived functional bulge HFSCs divide infrequently in unperturbed tissue homeostasis and whether their daughter cells undergo asymmetric fate decision throughout life.

Materials and Methods

Transgenic mice

All experiments were approved by Cornell IACUC and carried out using standard procedure, as described (Waghmare et al, 2008). We generated Tet-off H2B-GFP mice by crossing hemizygous pTRE–H2B–GFP (Tumbar et al., 2004) (CD1) and K5tTA (FVB1) mice and identified GFP-expressing animals with an ultraviolet-based portable lamp (BLS Ltd). Mice were fed with 1 g doxy/kg mouse chow (Bio-serv), and sacrificed at various time points. For lineage tracing, we crossed K14-CreER (Vasioukhin et al., 1999) and Rosa26R (Soriano, 1999) mice, and genotyped with PCR using CRE primers (5'-GCG GTC TGG CAG TAA AAA CTA TC-3', 5'-GTG AAA CAG CAT TGC TGT CAC TT-3'). Tamoxifen delivered intraperitoneally to induce labelling (100 ug/g body weight) was dissolved in corn oil.

FACS analysis

We used SPHERO Rainbow particles, 3.0–3.4 um (Spherotech), to calibrate the FACS machine. All experiments were performed on a FACS Aria (BD Biosciences) in

the Cornell University Flow Cytometry Facility and analyzed with FlowJo software. Skin cells were isolated from fresh tissue using trypsin digestion (0.25%) and stained with biotin-labelled CD34 antibody (eBioscience) and phycoerythrin-labelled a6-integrin (CD49f) antibody (BD Pharmingen). CD34 secondary antibody was Streptavidin-APC (BD Pharmingen). Live cells were those not stained by propidium iodide (PI; Sigma).

Tissue Staining and Microscopy

Staining procedure for immunofluorescence and Hematoxylin and Eosin (H&E) were as described previously (Tumbar et al., 2006). Nuclei were labeled by 4',6'-diamidino-2-phenylindole (DAPI). Primary antibodies: α6 integrin (1:100, BD Pharmingen), CD34 (1:150, BD Pharmingen) and BrdU (1:300, Abcam), active capase 3 (1:500, R&D Systems), Ki67 (1:100, Novocastra), Secondary antibodies were coupled to the following fluorophores: FITC, Texas-Red or Cy5 (Jackson Laboratories). For X-gal staining, frozen skin sections were fixed 1 hr in 4% paraformaldehyde at 4°C, PBS washed 3x30 min., stained 24hrs at 37°C with X-gal buffer (Osorio et al., 2008), and incubated 3 hrs in 1M Na2CO3 to maximize sensitivity (Tanahashi and Tabira, 2000). For immuno-fluorescence and X-gal staining, images were acquired using the IP-Lab software (MVI) on a light fluorescence microscope (Nikon) equipped with a CCD 12-bit digital camera (Retiga EXi, QImaging). For confocal microscopy, frozen tissue sections (100 um) were fixed for 1 h in 4% paraformaldehyde and stained overnight with TOPRO3 (1:2000 dilution; Invitrogen). Confocal Z-sections were collected using a Leica microscope with details described in (Osorio et al., 2008; Waghmare et al., 2008).

Microarray and (Q)RT–PCR

RNA isolation, cDNA generation and RT-PCR were described (Osorio et al., 2008; Waghmare et al., 2008); see Table 2.1 for primers. Quantitative (Q) RT-PCR performed on MyiQ thermocycler (Bio-Rad), as manufacturer instructed. Signals from triplicate wells per primer pair were normalized to GAPDH. For microarrays we collected ~35,000 sorted cells/sample, and 5 ng of high quality RNA (Bioanalyzer, Agilent) were amplified (Ovation Amplification; Nugene) in the Cornell Microarray Core Facility (Ithaca, NY). GeneChip IVT labelling was followed by Gene Chip MOE 430 2.0 hybridization and GeneArray 3000 scanning (Affymetrix). GCOS software generated present calls and signal values from raw signals, which were scaled to default target of 500. Heat map and correlation tree among subpopulations was generated by un-supervised hierarchical average linkage cluster analysis with Cluster 3.0 software (http://bonsai.ims.u-tokyo.ac.jp/), using log2 data normalized to the average value across all samples for each probe.

Results

Distinct characteristics of newly generated CD34+/α6-integrin+ cells at two hair cycle stages

We began by analyzing the proliferation and differentiation status of newly generated bulge cells during the first adult hair cycle, when HF remodelling phases are synchronous (Fig. 2.1B). We employed double transgenic mice, K5tTA x pTRE-H2B-GFP in which an epithelial Keratin 5 (K5) promoter drove repressible histone H2B-GFP expression (Diamond et al., 2000; Tumbar et al., 2004). Repression is achieved by feeding the mice doxycycline (doxy) for a period of time (chase), when

the H2B-GFP dilutes in cells by 2-fold at division. This allowed us to quantify precise proliferation history *in vivo*, from the amount of H2B-GFP fluorescence retained in cells after chase (Waghmare et al., 2008). After various chase periods (Fig. 1C) we sacrificed mice at different ages corresponding to distinct phases of hair cycle, as confirmed by microscopy (Fig. 2.2A). We isolated skin cell suspensions from these mice and stained them for surface expression of bulge markers CD34 and α 6-integrin. Fluorescence-activated cell sorting (FACS) revealed histograms with distinct peaks of 2-fold median H2B-GFP intensity corresponding to distinct divisions (Fig. 2.1D,E). These data quantified the bulge proliferation during the first hair cycle, and provided information on kinetics and fraction of divided bulge cells. The data showed in Fig. 2.1E indicated that CD34+/α6+ cells began to divide at the telogen-anagen transition (Postnatal day (PD)18-PD21 chase) and continued on in anagen (PD22-PD25&PD21-PD28 chases). The cells slowed-down divisions by late anagen (PD21-PD35 chase) and became quiescent in catagen (PD21-PD42&PD35-PD42 chases). Most CD34+/α6+ cells divided infrequently (1-3x) during the PD21-PD42 chase, in line with our previous data from a full hair cycle chase (PD21-PD49; (Cotsarelis, 2006; Waghmare et al., 2008).

Since single CD34+/α6+ sorted cells gave rise to rapidly dividing progenitor Mx cells upon transplantation (Blanpain et al., 2004), we examined FACS profiles for emergence of a more rapidly dividing cell population of cells. Histograms from PD18-PD21 doxy chases indicated 2-3 divisions, which occurred in <15% of CD34+/α6+ cells (Fig. 2.1E, top). In contrast, the histograms from PD22-PD25 chases showed on average only ~1 division in >80% CD34+/α6+ cells. In addition, the CD34 surface levels appeared largely reduced in PD18-PD21 divided cells (Fig. 2.1E right panels & Fig. 2.2C). To probe this observation further, we sorted skin cells subpopulations as CD34+/α6+ bulge (Bu) cells, with H2B-GFP signals indicating they

Figure 2.2. H2B-GFP chases at different hair cycle stages to elucidate proliferation dynamics of bulge cells.

(A) Skin collected from mice after 3 days (d) or 1-3 weeks (wk) of doxy feedings, were frozen embedded in OCT, sectioned and stained with DAPI (blue); H2B-GFP is green. Age of mice indicated at top (PD21-42). DP, dermal papillae; hg, hair germ. (B) CD34 and a6-integrin (CD49f) together mark specifically the HF bulge. Shown are skin sections in the second anagen (PD56) after 4 weeks of doxy chase, stained for CD34 (top) and a6 (bottom), shown in red. H2B-GFP is green, and blue is DNA DAPI staining. Note high H2B-GFP signal in the bulge (Bu) at all times (A&B). (C) Histograms of all live skin cells isolated from mice after 3-days doxy chase at stages indicated, stained for surface expression of CD34 and a6-integrin. Note lower CD34 signal for bulge progeny with 1-2 divisions relative to undivided cells at PD21. Scale bars, 50 μm. (D) FACS plot of PD18-PD21 3-day chase experiment for live a6+ skin cells sorted as follows: CD34+/a6+ divided cells; CD34+/a6+ undivided cells sorted as CD34-medium (comparable in level with divided cells) and CD34-high. QRT PCR for differentiation markers tested in Fig. 2 were expressed at equally low levels in the undivided fractions irrespective of CD34 level. N=2 mice.

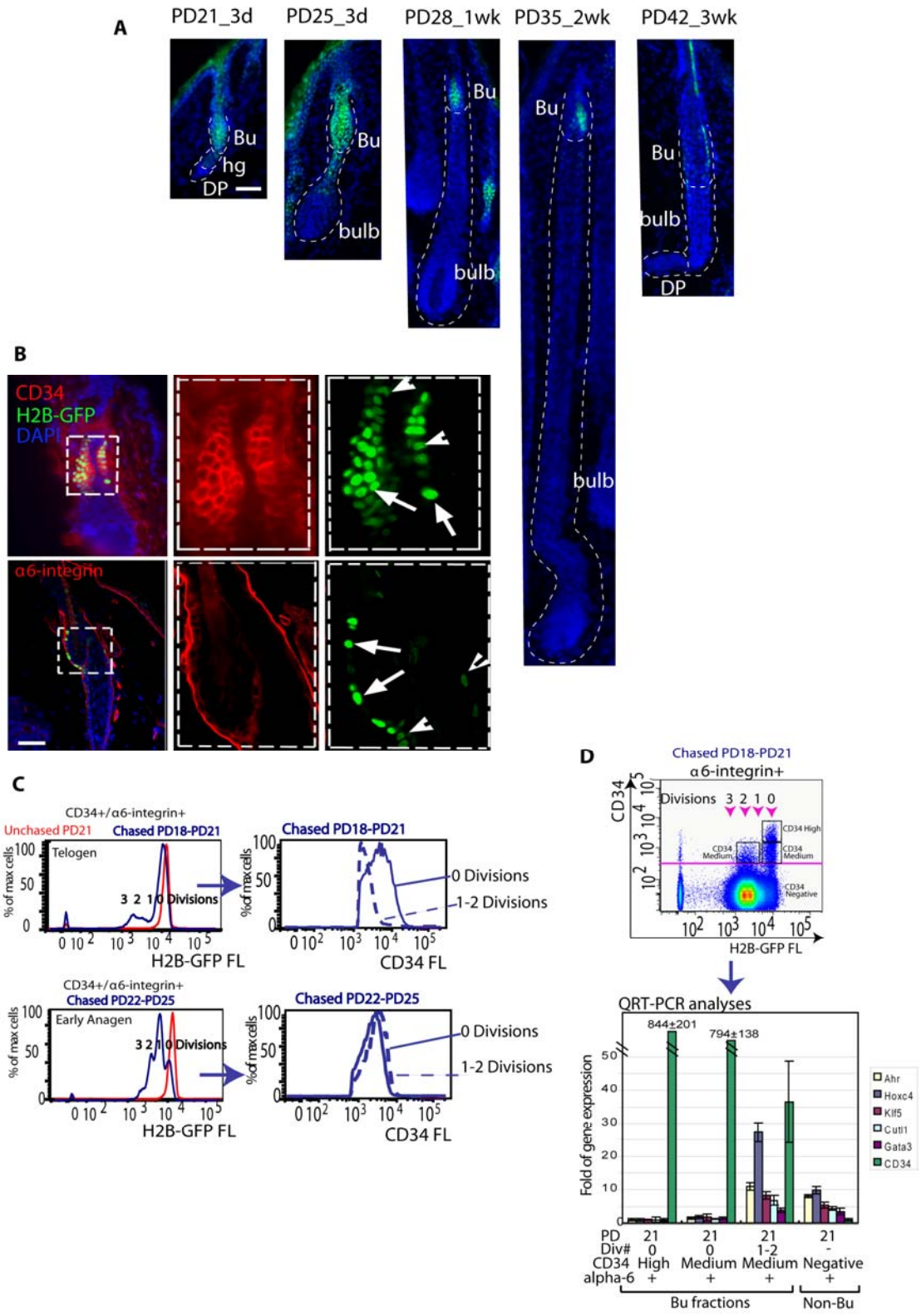
A
PD21_3d
PD25_3d
PD28_1wk
PD35_2wk
PD42_3wk
Bu
hg
DP
bulb
B
CD34
H2B-GFP
DAPI
α6-integrin
C
CD34+/α6-integrin+
Unchased PD21
Chased PD18-PD21
Telogen
3 2 1 0 Divisions
% of max cells
H2B-GFP FL
CD34 FL
0 Divisions
1-2 Divisions
CD34+/α6-integrin+
Chased PD22-PD25
Early Anagen
D
Chased PD18-PD21
α6-integrin+
Divisions 3 2 1 0
CD34 High
CD34 Medium
CD34 Negative
QRT-PCR analyses
844±201
794±138
Fold of gene expression
Ahr
Hoxc4
Klf5
Cutl1
Gata3
CD34
PD
Div#
CD34
alpha-6
21
0
High
+
21
0
Medium
+
21
1-2
Medium
+
21
-
Negative
+
Bu fractions
Non-Bu

were un-divided (Bu, 0 Division) or divided (Bu, 1-2 Divisions) and CD34-/α6+ non-bulge (Non-Bu) cells (Fig. 2.1E, right panels). We analyzed these cells by RT-PCR for mRNA expression of CD34 and other bulge-enriched factors (Tumbar et al., 2004), which appeared largely down-regulated in divided cells from PD18-PD21 but not from PD22-PD25 chases (Table 2.1; Fig. 2.1F). To find the divided CD34+/α6+ cells in situ we administered Bromodeoxyuridine (BrdU) together with doxy for 3 days (PD18-PD21 and PD22-PD25). In the PD18-PD21 experiment CD34+/BrdU+ cells localized exclusively at the bulge/germ transition zone, near the known region where Mx cells emerge and cells begin to proliferate first (Greco et al., 2009) (Fig. 2.1G, top). In contrast, in the PD22-PD25 experiment CD34+/BrdU+ cells were present inside the bulge (Fig. 2.1G, bottom). In conclusion, newly generated bulge cells, analyzed as CD34+/α6+ divided cells, seemed to divide at higher rates and show lower expression of bulge-enriched markers at PD18-PD21 relative to PD22-PD25.

Stage-dependent genomic expression signatures of newly generated CD34+/α6+ cells

To extract information about differentiation status of newly generated bulge cells at distinct hair cycle phases, we determined the gene expression signatures in subpopulations of HFs isolated from mice treated with doxy from PD18-PD21 and PD22-PD25 stages: telogen-anagen transition and anagen, respectively. We sorted CD34+/α6+ bulge cells as divided (Bu, 1-2 Div) and undivided (Bu, 0 Div) subpopulations and the CD34-/α6+ (non-bulge) subpopulation (N=3 mice per stage; Fig. 2.3A). We analyzed a total of 18 RNA samples by Affymetrix expression microarrays (Experimental Procedures). First, we extracted a set of 767 probes changed by ≥2 fold ($p \leq 0.05$; one-tailed student t test) in all 6 undivided CD34+/α6+ (bulge) populations relative to 6 CD34-/α6+ (non-bulge) populations (Table 2.2). This set constitutes the bulge and non-bulge signatures of genes that remain expressed

Table 2.1. Primers used for RT and QRT-PCR analysis

Gene symbol	Forward Primer 5'->3'	Reverse Primer 5'->3'
GAPDH	ACTGCCACCCAGAAGACTGT	GATGCAGGGATGATGTTCTG
CD34	AAGGCTGGGTGAAGACCCTTA	TGAATGGCCGTTTCTGGAAGT
Bmp6	TCCTTGAACCGCAAGAGTCTC	CTCACCCTCAGGAATCTGGG
Ltbp2	AACAGCACCAACCACTGTATC	CCTGGCATTCTGAGGGTCAAA
Gas1	CCATCTGCGAATCGGTCAAAG	GCTCGTCGTCATATTCTTCGTC
Ctgf	GGGCCTCTTCTGCGATTTC	ATCCAGGCAAGTGCATTGGTA
Nck2	AGGACAGGCTACGTGCCTT	GTACTCCGCATCAGTGCTTGG
Macf1	GCTCAAGTGCTAGTCAGAGTAAC	ACCAGGGTTTGTCATAACATCG
Gata3	CTTTGCAATGCCTGCGGACTC	ATTAGCGTTCCTCCTCCAGAG
Hoxc4	GCAACCCATAGTCTACCCTTGG	CTCTCAGAGAGGCACAGCGAGT
Cutl1	CCTTCATCCGGATGCAGCTCT	GCTGGCAGAGGTCTTTGGAGT
Klf5	GAGCTGGTCCAGACAAGATGT	GATGCTGTAAGGTATGCCTTC
Ocln	GACCCTGACCACTATGAAACA	TCCAGCTCTTTATCTAGACGA
Notch3	CACTGGGCTGCAGCTGTGAAC	CAACCGCACAATGTCCTGGTG
Bmp4	CAGAGCCAGGGAACCGGGCTT	GTCCACCTGCTCCCGAAAGAG
WNT4	CTTCACAACAACGAGGCTGGC	GCTTGAACTGTGCATTCCGAG
Tnfrsf19	CCACTGTGCCCATAGAGCATG	CAGACCCGAAGAAGGCTGGCA
Ahr	GTCAGTCCTCAGGCATACTAT	GCTCAAGTCGGACGAATAGGT
Lgr5	CCAATGGAATAAAGACGACGGCAACA	GGGCCTTCAGGTCTTCCTCAAAGTCA

preferentially in each subpopulation at both PD18-PD21 and PD22-PD25 stages. Log2 of signal/average values from this set (and an inclusive 9450 probe set) yielded expression dendograms with two major clusters: one for the 6 undivided CD34+/α6+ bulge subpopulations (triplicate per each of the two stages) and another for the 6 CD34-/α6+ non-bulge subpopulations (Fig. 2.3B; 2.4A). Strikingly, the divided CD34+/α6+ cells (Bu, 1-2 Div) from the PD18-PD21 chase, but not from the PD22-PD25 chase, clustered together with the CD34-/α6+ non-bulge subpopulation (Fig. 2.3B). At PD22-PD25, the divided CD34+/α6+ cells showed little changes in gene expression relative to undivided CD34+/α6+ cells (Fig. 2.3C), and these changes were likely related to the differences in their proliferative status. In contrast, at PD18-PD21 the divided CD34+/α6+ cells showed down-regulation of most (~95%) bulge-enriched mRNAs or "bulge signature genes" relative to undivided CD34+/α6+ cells and up-regulation of some previously reported Mx signature genes ((Rendl et al., 2005) Fig. 2.3C). QRT-PCR for 5 transcription factors previously implicated in keratinocyte or HF differentiation and for 5 reported Mx signature genes (Chen et al., 2006; Jones and Reiners, 1997; Luong et al., 2002; Rendl et al., 2005; Rieger et al., 1994; Sur et al., 2006) confirmed the microarray expressions. These mRNAs were high in divided CD34+/α6+ cells from PD18-PD21 chases, but not from PD22-PD25 chases (Fig. 2.3D). This high expression was not found in undivided α6+/CD34+ cells at PD18-PD21, even when we sorted them into CD34-medium and CD34-high cells (Fig. 2.2D). The PD18-PD21 divided CD34+/α6+ cell, although clustered with CD34-/a6+ cells in the expression dendograms, displayed their own subset of enriched mRNAs attesting to their distinct identity (Table 2.3). LGR5, a recently reported lower bulge/HG marker (Jaks et al., 2008), was higher in all PD18-PD21 CD34+/α6+ cell fractions relative to CD34-/α6+ non-bulge cells or relative to PD22-PD25 CD34+/α6+ bulge fractions (Fig. 2.3E and 2.4B,C), as expected (Jaks et al., 2008).

Figure 2.3. Expression profiling at 2-hair cycle stages.

(A) Cell subpopulations sorted and profiled by expression microarrays. (B) Gene (top), and cell population (left) dendogram heat map shows 2 main population clusters (blue star). Newly divided CD34+/a6+ cells (Bu 1-2 Div) cluster with a different group at each stage. (C) Genes changed in Bu (1-2 Div) cell populations relative to Bu (0 Div) are shown as percent of 4 hair lineages gene signatures: CD34+/a6+ bulge (Bu). CD34-/a6+ non-bulge (NonBu), matrix (Mx), dermal papillae (DP) (Table S2). Note down-regulation of bulge signature genes and higher up-regulation of Mx genes at PD18-PD21. DP was a negative control as an un-related lineage and showed low and similar representation in both populations. (D). QRT-PCR (relative to GAPDH) of several Non-Bu or Matrix signature genes found up-regulated in our microarray in Bu (1-2 Div) relative to Bu (0 Div) shown with SEM. N=2 mice per stage (triplicate wells). Regular RT-PCR performed for 4 additional mice per stage is not shown. (E) Same QRT-PCR analysis for LGR5; a second experiment with another set of mice at each stage is shown in Fig. 2.4.

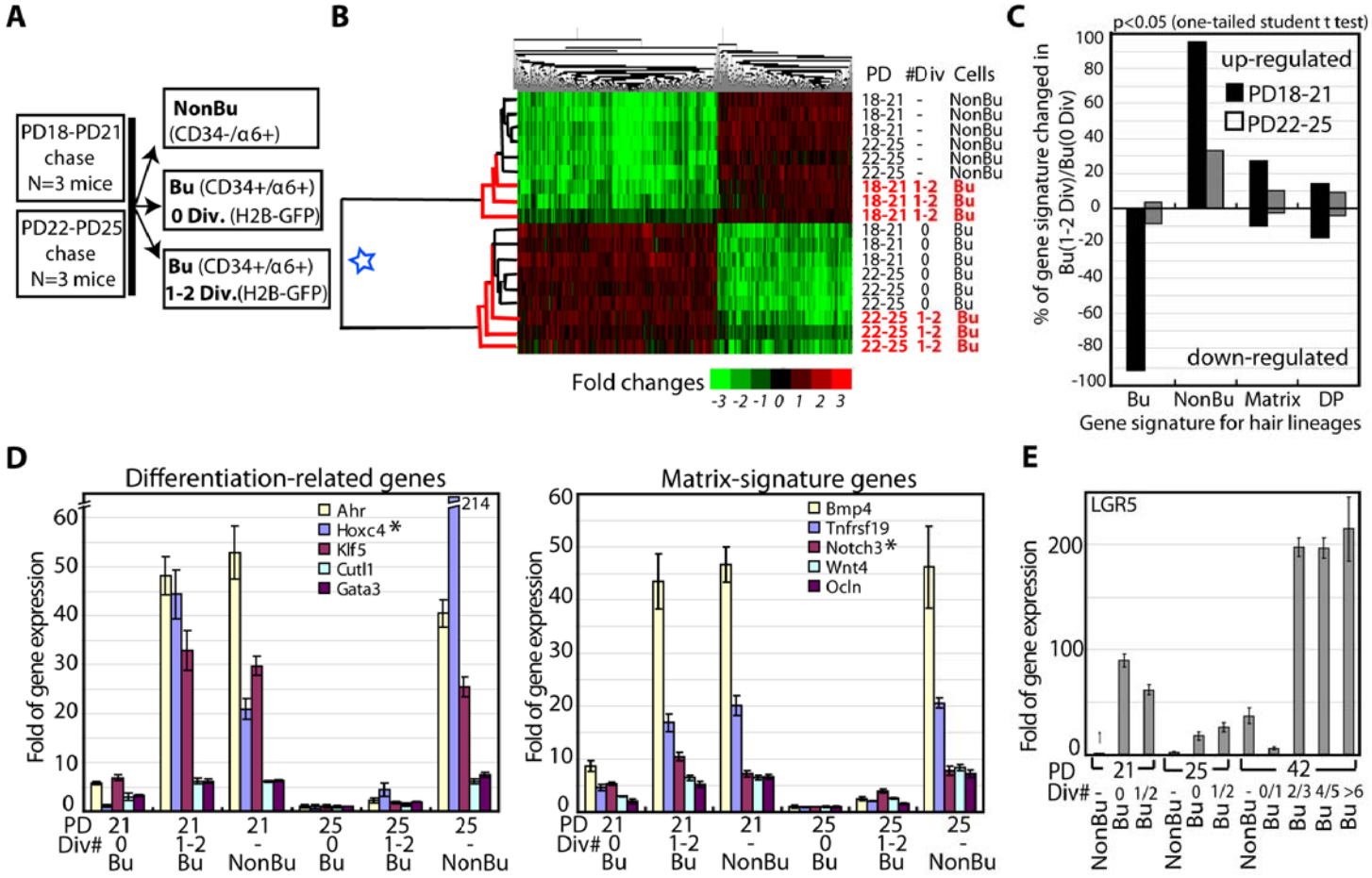
A
PD18-PD21 chase N=3 mice
PD22-PD25 chase N=3 mice
NonBu (CD34-/α6+)
Bu (CD34+/α6+) 0 Div. (H2B-GFP)
Bu (CD34+/α6+) 1-2 Div.(H2B-GFP)
B
PD #Div Cells
18-21 - NonBu
22-25 - NonBu
18-21 1-2 Bu
22-25 1-2 Bu
18-21 0 Bu
22-25 0 Bu
Fold changes
-3 -2 -1 0 1 2 3
C
p<0.05 (one-tailed student t test)
% of gene signature changed in Bu(1-2 Div)/Bu(0 Div)
up-regulated
PD18-21
PD22-25
down-regulated
Bu NonBu Matrix DP
Gene signature for hair lineages
D
Differentiation-related genes
Ahr
Hoxc4 *
Klf5
Cutl1
Gata3
Fold of gene expression
PD 21 21 21 25 25 25
Div# 0 1-2 - 0 1-2 -
Bu Bu NonBu Bu Bu NonBu
Matrix-signature genes
Bmp4
Tnfrsf19
Notch3*
Wnt4
Ocln
E
LGR5
Fold of gene expression
PD 21 25 42
Div# - 0 1/2 - 0 1/2 - 0/1 2/3 4/5 >6
NonBu Bu Bu NonBu Bu Bu NonBu Bu Bu Bu Bu

Figure 2.4. Microarray and QRT-PCR analysis of bulge cells with distinct divisions at different hair cycle stages.

(A) Heat map of all 18 microarray databases generated from sorted cells at PD21 and PD25 confirms cell population clustering in 2 major groups when utilizing expanded data set. Statistical data analysis was first performed using R statistical package (http://www.r-project.org/). The signals were log2-transformed after offset by 64, and normalized log ratios were obtained by LOESS fitting to the median of each probe set across all arrays in the data set. Gene filtering was applied to include only 9540 probe sets having at least 1 Present call and standard deviation of 0.5 or greater in normalized log ratio. To look for differential genes between any 2 conditions, two-sample t test was applied on the normalized log ratio of each probe set, with value cutoff set at 0.001 and 0.05. The normalized data matrix was visualized using GeneMaths 2.0 software (Applied Maths, Austin, TX), in which hierarchical clustering was performed using complete linkage algorithm. (B) LGR5, a hair germ and bulge marker showed microarray signals that were higher in both of the bulge fractions relative to non-bulge, at both telogen and anagen. (C) QRT-PCR in a second set of samples isolated from individual mice confirms LGR5 expression by microarray shown in (B). First set is shown in Fig. 2.3E.

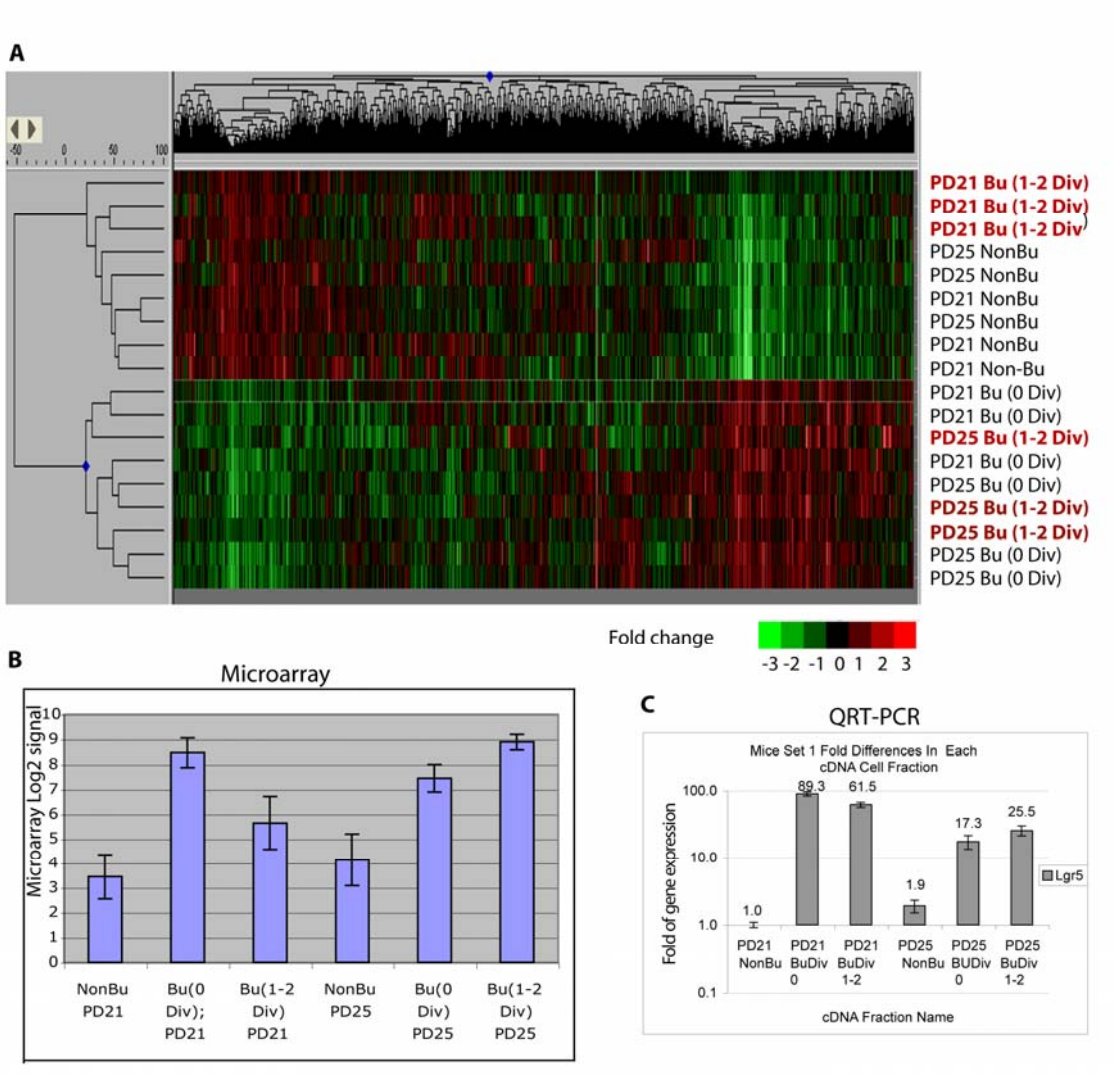
A
PD21 Bu (1-2 Div)
PD21 Bu (1-2 Div)
PD21 Bu (1-2 Div)
PD25 NonBu
PD25 NonBu
PD21 NonBu
PD25 NonBu
PD21 NonBu
PD21 Non-Bu
PD21 Bu (0 Div)
PD21 Bu (0 Div)
PD25 Bu (1-2 Div)
PD21 Bu (0 Div)
PD25 Bu (0 Div)
PD25 Bu (1-2 Div)
PD25 Bu (1-2 Div)
PD25 Bu (0 Div)
PD25 Bu (0 Div)
Fold change
-3 -2 -1 0 1 2 3
B
Microarray
Microarray Log2 signal
NonBu PD21
Bu(0 Div); PD21
Bu(1-2 Div) PD21
NonBu PD25
Bu(0 Div) PD25
Bu(1-2 Div) PD25
C
QRT-PCR
Mice Set 1 Fold Differences In Each cDNA Cell Fraction
Fold of gene expression
89.3
61.5
17.3
25.5
1.9
1.0
Lgr5
PD21 NonBu
PD21 BuDiv 0
PD21 BuDiv 1-2
PD25 NonBu
PD25 BUDiv 0
PD25 BuDiv 1-2
cDNA Fraction Name

Table 2.2. Signals detected in all samples analyzed by microarray from PD18-PD21 and PD22-PD25 stages, in each of the 4 cell lineage gene expression signature: CD34+/a6+ (bulge, Bu) and CD34-/a6+ (non-bulge, NonBu) defined from our data (see text); matrix and dermal papillae from (Rendl, et al., 2005). Bulge signature encompasses genes increased by >2 fold in each of the 6 mice total analyzed at PD18-PD21 and PD22-PD25 when comparing undivided CD34+/a6+ (Bu, 0 Div) versus CD34-/a6+ (NonBu) subpopulations ($p<0.05$). Non-bulge signature is the reversed comparison.

Table 2.2.1. Bulge signatures

462 genes up-regulated >2 fold in Undivided Bu (0div) cells relative to Non-Bulge cells at PD21 and PD25.

Probe Set ID	Gene Symbol	Probe Set ID	Gene Symbol	Probe Set ID	Gene Symbol
1417869_s_at	Ctsz	1445296_at	D7Ertd715e	1418455_at	Copz2
1455795_at	Dse	1441974_at	Camk4	1421733_a_at	Tpst1
1423341_at	Cspg4	1424701_at	Pcdh20	1419276_at	Enpp1
1439373_x_at	WNT5b	1417356_at	Peg3	1441629_at	---
1450988_at	Lgr5	1460187_at	Sfrp1	1437284_at	Fzd1
1426639_a_at	Tcf7l2	1450700_at	Cdc42ep3	1418608_at	Calml3
1448323_a_at	Bgn	1455090_at	Angptl2	1437197_at	Sorbs2
1424099_at	2310016C16Rik	1426301_at	Alcam	1450124_a_at	Atp2a3
1449688_at	D10Ertd610e	1448877_at	Dlx2	1455418_at	---
1425733_a_at	Eps8	1426300_at	Alcam	1431691_a_at	Rab31
1420726_x_at	Tmlhe	1420924_at	Timp2	1448606_at	Lpar1
1460559_at	Kank2	1451538_at	Sox9	1431072_a_at	Ccdc50
1430011_at	2610317O13Rik	1450767_at	Nedd9	1450040_at	Timp2
1427391_a_at	Col12a1	1450944_at	Cspg4	1423259_at	Id4
1423669_at	Col1a1	1434286_at	Trps1	1432936_at	5330433J24Rik
1439852_at	---	1460619_at	Mfsd9	1447640_s_at	Pbx3
1458806_at	---	1453267_at	Zfhx3	1451737_at	Pik3r1
1458409_at	C86595	1426640_s_at	Trib2	1427450_x_at	Myo1b

Table 2.2.1 (continued)

1435772_at	Kif21b	1439713_at	Itga1	1455531_at	Mfsd4
1417929_at	Slc7a8	1426167_a_at	Camk4	1456481_at	D9Ertd280e
1415780_a_at	Armcx2	1454824_s_at	Mtus1	1438666_at	Ldlrad3
1424407_s_at	Cbx6	1441391_at	---	1456609_at	Camk2n1
1422824_s_at	Eps8	1420731_a_at	Csrp2	1421063_s_at	Snrpn
1448426_at	Sardh	1450509_at	Chst11	1454890_at	Amot
1456020_at	Sh3tc2	1450044_at	Fzd7	1439887_at	---
1455018_at	Lmtk2	1448117_at	Kitl	1424768_at	Cald1
1430392_at	9530086O07Rik	1434369_a_at	Cryab	1422540_at	Fbln1
1448664_a_at	Speg	1419108_at	Ophn1	1436356_at	Lgals7
1416405_at	Bgn	1460294_at	Atp8a2	1422550_a_at	Mtap6
1419573_a_at	Lgals1	1416221_at	Fstl1	1450869_at	Fgf1
1417011_at	Sdc2	1424050_s_at	Fgfr1	1417673_at	Grb14
1435260_at	Akt3	1416474_at	Nope	1423389_at	Smad7
1455494_at	Col1a1	1438214_at	Trps1	1444432_at	D330040H18Rik
1441972_at	6230424C14Rik	1452572_at	Camk4	1460307_at	Akt3
1452250_a_at	Col6a2	1419442_at	Matn2	1418929_at	Ift57
1451983_at	Irx1	1439843_at	Camk4	1436188_a_at	Ndrg4
1459522_s_at	Gyg	1426152_a_at	Kitl	1428540_at	3321401G04Rik
1434180_at	Fermt2	1448669_at	Dkk3	1427385_s_at	Actn1
1435394_s_at	Rhoc	1416778_at	Sdpr	1435399_at	Synpo2
1448990_a_at	Myo1b	1432464_a_at	2310057J16Rik	1416630_at	Id3
1437154_at	Cep170	1430521_s_at	Cpne8	1437528_x_at	A730017C20Rik
1432591_at	Pappa	1438620_x_at	Sfrp1	1459259_at	EG328264
1448519_at	Tead2	1425779_a_at	Tbx1	1416257_at	Capn2
1418317_at	Lhx2	1434642_at	Hsd17b11	1448788_at	Cd200
1434797_at	6720469N11Rik	1444347_at	Mgat4a	1450809_at	Sval2
1436501_at	Mtus1	1416165_at	Rab31	1456603_at	1500005K14Rik
1443939_at	OTTMUSG00000008561	1424755_at	Hip1	1460337_at	Sh3kbp1
1455087_at	D7Ertd715e	1434943_at	BC023055	1450627_at	Ank

Table 2.2.1 (continued)

1419978_s_at	D10Ertd610e	1441787_at	---	1424367_a_at	Homer2
1418532_at	Fzd2	1455872_at	BC065085	1428585_at	Actn1
1426481_at	Klhl22	1418175_at	Vdr	1424542_at	S100a4
1422758_at	Chst2	1445148_at	---	1454332_at	6030442H21Rik
1450805_at	Sgcd	1448870_at	Ltbp1	1445328_at	Col4a4
1447040_at	---	1425906_a_at	Sema3e	1429693_at	Dab2
1436988_at	5430433G21Rik	1451932_a_at	Adamtsl4	1454867_at	Mn1
1424890_at	Bnc1	1449524_at	Eda	1422784_at	Krt6a
1437853_x_at	Ndn	1449751_at	Slc6a6	1434314_s_at	Rab11fip5
1438980_x_at	Pm20d1	1452833_at	Rapgef2	1422612_at	Hk2
1446133_at	D2Ertd295e	1448590_at	Col6a1	1449107_at	Nudt4
1437417_s_at	Gpc6	1435951_at	Grip1	1426231_at	Vit
1420725_at	Tmlhe	1448395_at	Sfrp1	1426869_at	Boc
1438861_at	Bnc2	1435360_at	Zfp651	1448021_at	---
1425090_s_at	Kcnc4	1459132_at	Bnc2	1427700_x_at	Krt6a
1427476_a_at	Trim32	1458226_at	Flnb	1425631_at	Ppp1r3c
1457333_at	Sdk2	1422985_at	Fzd1	1416613_at	Cyp1b1
1429896_at	5830408B19Rik	1455298_at	---	1422783_a_at	Krt6a
1455439_a_at	Lgals1	1457445_at	Trps1	1418397_at	Zfp275
1426973_at	Gpr153	1424770_at	Cald1	1424699_at	Ccdc136
1460359_at	Armcx3	1451310_a_at	Ctsl	1453916_at	4933431K23Rik
1447445_at	---	1454877_at	Sertad4	1421193_a_at	Pbx3
1426561_a_at	Npnt	1450928_at	LOC100045546	1427042_at	Mal2
1418534_at	Fzd2	1445095_at	---	1418456_a_at	Cxcl14
1422869_at	Mertk	1421941_at	Camk4	1423136_at	Fgf1
1436736_x_at	D0H4S114	1427673_a_at	Sema3e	1431099_at	Hoxd8
1423680_at	Fads1	1444646_at	8430420F16Rik	1438101_at	---
1437403_at	Samd5	1443974_at	Plcl1	1449178_at	Pdlim3
1421429_a_at	Npnt	1420753_at	Tll1	1444763_at	Ptprk
1420911_a_at	Mfge8	1436590_at	Ppp1r3b	1434667_at	Col8a2

Table 2.2.1 (continued)

1429097_at	C030044C12Rik	1449530_at	Trps1	1423352_at	Crispld1
1416473_a_at	Nope	1448052_at	Cgnl1	1448146_at	Wwp2
1455251_at	Itga1	1450625_at	Col5a2	1436167_at	Shf
1439073_at	Mllt4 /// Zfp160 /// LOC627912	1445723_at	Plcl1	1454734_at	Lefl
1444696_at	BC059841	1460287_at	Timp2	1416846_a_at	Pdzrn3
1435641_at	Mgat4a	1421346_a_at	Slc6a6	1451535_at	Il31ra
1415855_at	Kitl	1448145_at	Wwp2	1457276_at	Snf1lk2
1430388_a_at	Sulf2	1449621_s_at	Thsd1	1428663_at	5133401H06Rik
1443337_at	---	1417829_a_at	Rab15	1421891_at	St3gal2
1422818_at	Nedd9	1452207_at	Cited2	1434301_at	D330050I23Rik
1422983_at	Itgb6	1416211_a_at	Ptn	1423585_at	Igfbp7
1431033_x_at	Agl	1418061_at	Ltbp2	1418457_at	Cxcl14
1448259_at	Fstl1	1430520_at	Cpne8	1443832_s_at	Sdpr
1436987_at	5430433G21Rik	1428123_at	2610528K11Rik	1438891_at	---
1429543_at	6230424C14Rik	1420148_at	Slc6a6	1433638_s_at	Hoxd8
1450839_at	D0H4S114	1428136_at	Sfrp1	1444395_at	Dixdc1
1423278_at	Ptprk	1425514_at	Pik3r1	1430142_at	Tgm5
1450350_a_at	Jdp2	1439151_at	Msrb3	1459546_s_at	Enpp1
1422155_at	Hist2h3c2	1455188_at	Ephb1	1445534_at	Flnb
1450208_a_at	Elmo1	1437081_at	Timp2	1428902_at	Chst11
1449202_at	Sema4g	1421157_at	Fzd3	1426023_a_at	Rabep1
1453313_at	Sesn3	1453801_at	Them5	1453523_at	Krtap17-1
1428579_at	Fmnl2	1433691_at	Ppp1r3c	1451119_a_at	Fbln1
1422865_at	Runx1	1421908_a_at	Tcf12	1435261_at	Tmtc1
1440248_at	Casc4	1422592_at	Ctnnd2	1423584_at	Igfbp7
1425874_at	Hoxc13	1418205_at	Thsd1	1448710_at	Cxcr4
1421350_a_at	Grip1	1450085_at	Angptl2	1418643_at	Tspan13
1421158_at	Cgnl1	1437467_at	Alcam	1449730_s_at	Fzd3
1460167_at	Aldh7a1	1427516_a_at	Boc	1415877_at	Dpysl3
1448765_at	Fyn	1433924_at	---	1450781_at	Hmga2
1417355_at	Peg3	1432592_at	Pappa	1429764_at	1500005K14Rik

Table 2.2.1 (continued)

1420764_at	Scrg1	1438441_at	Id4	1418505_at	Nudt4
1423277_at	Ptprk	1419717_at	Sema3e	1425357_a_at	Grem1
1433662_s_at	Timp2	1428851_at	1300014I06Rik	1422169_a_at	Bdnf
1428861_at	4631422O05Rik	1424373_at	Armcx3	1422619_at	Ppap2a
1434639_at	Klhl29	1452415_at	Actn1	1422324_a_at	Pthlh
1416662_at	Sardh	1439849_at	OTTMUSG00000008561	1441624_at	Sorbs2
1416796_at	Nck2 /// LOC100044475	1415856_at	Emb	1443771_x_at	Smad7
1423852_at	Shisa2	1440444_at	Fads1	1427405_s_at	Rab11fip5
1421830_at	Ak3l1	1447878_s_at	Fgfrl1	1434581_at	2410066E13Rik
1442226_at	Sema3e	1424950_at	Sox9	1426615_s_at	Ndrg4
1426560_a_at	Npnt	1417393_a_at	C1qdc2	1452309_at	Cgnl1
1436799_at	Enox1	1435207_at	Dixdc1	1440070_at	Chat
1443047_at	---	1418484_at	Tekt2	1452114_s_at	Igfbp5
1420087_at	Fzd3	1420522_at	Ccdc50	1439422_a_at	C1qdc2
1426750_at	Flnb	1431680_a_at	Ptprk	1422168_a_at	Bdnf
1437466_at	Alcam	1443335_at	---	1420895_at	Tgfbr1
1457316_at	Mtap6	1444733_at	---	1422620_s_at	Ppap2a
1447602_x_at	Sulf2	1452264_at	Tenc1	1418849_x_at	Aqp7
1418187_at	Ramp2	1422537_a_at	Id2	1415857_at	Emb
1446245_at	---	1421011_at	Hsd17b11	1433583_at	Zfp365
1448989_a_at	Myo1b	1418835_at	Phlda1	1417526_at	Pcbp3
1424769_s_at	Cald1	1425911_a_at	Fgfr1	1455463_at	Phyhip
1443026_at	---	1415854_at	Kitl	1450135_at	Fzd3
1435452_at	Tmem20	1428547_at	Nt5e	1459850_x_at	Glrb
1430425_at	Sdk2	1460197_a_at	Steap4	1419332_at	Egfl6
1418309_at	Tnfrsf11b	1423353_at	Crispld1	1443957_at	Dixdc1
1454677_at	Timp2	1416740_at	Col5a1	1416953_at	Ctgf
1428808_at	Prickle2	1417312_at	Dkk3	1435176_a_at	Id2
1449303_at	Sesn3	1436551_at	Fgfr1	1416779_at	Sdpr
1458662_at	Daam1	1421267_a_at	Cited2	1422313_a_at	Igfbp5
1440250_at	Col4a4	1422974_at	Nt5e	1448613_at	Ecm1

Table 2.2.1 (continued)

1434557_at	Hip1	1435354_at	Kcnj15	1420498_a_at	Dab2
1443161_at	---	1436959_x_at	Nelf	1433944_at	Hectd2
1422864_at	Runx1	1436207_at	Tcf3	1418072_at	Hist1h2bc
1441843_s_at	5230400 M03Rik	1451453_at	Dapk2	1428284_at	8430427H 17Rik
1422670_at	Rnd2	1460513_a_at	Ednra	1422504_at	Glrb
1422437_at	Col5a2	1421129_a_at	Atp2a3	1454613_at	---
1456739_x_at	Armcx2	1428340_s_at	Atp13a2	1446681_at	BB086117
1416594_at	Sfrp1	1440339_at	Enpp1	1453327_at	Krt24
1423260_at	Id4	1422823_at	Eps8	1430604_a_at	Dab2
1416455_a_at	Cryab	1416072_at	Cd34	1437722_x_at	Pcbp3
1418932_at	Nfil3	1454997_at	Msrb3	1435672_at	3830612 M24
1423851_a_at	Shisa2	1439871_at	---	1423805_at	Dab2
1436303_at	Mllt4	1433525_at	Ednra	1431146_a_at	Cpne8
1437849_x_at	Armcx2	1436223_at	---	1448326_a_at	Crabp1

Table 2.2.2. Non-Bulge signatures

Non-Bulge signature made of 305 genes up-regulated >2 fold in each mouse analyzed at PD21 and PD25 in non-Bu cells relative to Bu (0 div).

Probe Set ID	Gene Symbol	Probe Set ID	Gene Symbol	Probe Set ID	Gene Symbol
1459747_at	---	1417853_at	Clca1	1426530_a_at	Klhl5
1453352_at	Atp10b	1427677_a_at	Sox6	1443602_at	---
1453304_s_at	Ly6e	1424831_at	Cpne2	1436182_at	---
1433795_at	Tgfbr3	1435436_at	Epas1	1418944_at	Cysltr1
1444587_at	AI481207	1460220_a_at	Csf1	1418872_at	Abcb1b
1459321_at	---	1435282_at	Gm967	1441342_at	Dpp4
1421398_at	Trim7	1459354_at	---	1416007_at	Satb1
1433977_at	Hs3st3b1	1419000_at	Cpxm2	1435040_at	Irak3
1451871_a_at	Ghr	1443814_x_at	Ctsh	1436591_at	BC023744
1438125_at	C230085N15Rik	1450276_a_at	Scin	1442449_at	Slc6a2
1451127_at	AW146242	1439675_at	Ppara	1416382_at	Ctsc
1435595_at	1810011O10Rik	1449079_s_at	St3gal6	1458438_at	Ccdc122
1417813_at	Ikbke	1456640_at	Sh3rf2	1458738_at	---
1427553_at	ENSMUSG00000058380	1418383_at	Apcdd1	1426397_at	Tgfbr2
1440607_at	---	1449070_x_at	Apcdd1	1441341_at	---
1456654_at	Paqr5	1449594_at	---	1435323_a_at	Mboat1
1450724_at	AB030242	1448904_at	D6Wsu176e	1422967_a_at	Tfrc
1436755_at	Itih5	1454777_at	Slco2b1	1423856_at	Popdc3
1450852_s_at	F2r	1423017_a_at	Il1rn	1429808_at	1110020C03Rik
1449994_at	Epgn	1425285_a_at	Rab27a	1455424_at	Wnk2
1440274_at	---	1450731_s_at	Tnfrsf21	1438953_at	Figf
1446244_at	Zyg11b	1452232_at	Galnt7	1426288_at	Lrp4
1441214_at	Exph5	1427138_at	Ccdc88c	1423570_at	Abcg1
1451348_at	Depdc6	1422474_at	Pde4b	1433501_at	Ctso

Table 2.2.2 (continued)

1419709_at	Stfa1 /// Stfa3	1450981_at	Cnn2	1425663_at	Il1rn
1438097_at	Rab20	1445938_at	5930427L02 Rik	1457780_at	Stx11
1450947_at	2610528J 11Rik	1427231_at	Robo1	1448558_a_at	Pla2g4a
1426708_at	Antxr2	1447791_s_a t	Gna14	1443553_at	---
1427183_at	Efemp1	1418382_at	Apcdd1	1438109_at	Clca5
1418930_at	Cxcl10	1438658_a_a t	Edg3	1446498_at	Il20ra
1451021_a_at	Klf5	1443906_at	Cd55	1454862_at	Phldb2
1435462_at	Plcxd2	1427600_at	---	1417962_s_at	Ghr
1443870_at	Abcc4	1452592_at	Mgst2	1416008_at	Satb1
1451593_at	H2-K1	1435777_at	E030018N1 1Rik	1425620_at	Tgfbr3
1437856_at	Ipmk	1460259_s_a t	Clca1 /// Clca2	1419532_at	Il1r2
1440465_at	---	1441242_at	---	1450507_at	Pou2f3
1459713_s_at	Tmem16a	1422631_at	Ahr	1451798_at	Il1rn
1440162_x_at	A630043P 06	1441926_x_a t	Tmie	1420913_at	Slco2a1
1452741_s_at	Gpd2	1441687_at	WNT4	1439150_x_at	Grtp1
1449528_at	Figf	1418791_at	Sh3gl2	1416452_at	Oat
1449815_a_at	Ssbp2	1441946_at	Itih5	1430255_at	Klf5
1435106_at	Limch1	1444723_at	6530418L21 Rik	1451501_a_at	Ghr
1451739_at	Klf5	1457948_at	---	1421643_at	Ikzf2
1452031_at	Slc1a3	1437699_at	E430014B0 2Rik	1460242_at	Cd55
1425264_s_at	Mbp	1424303_at	Depdc7	1435911_s_at	Slc2a12
1456956_at	Ikzf2	1424208_at	Ptger4	1452416_at	Il6ra
1420385_at	Gna14	1419523_at	Cyp3a13	1433769_at	Als2cl
1459601_at	Snf1lk	1416379_at	Panx1	1416200_at	Il33
1455263_at	9030625A 04Rik	1437059_at	Sox21	1421073_a_at	Ptger4
1424268_at	Smox	1451415_at	1810011O1 0Rik	1417185_at	Ly6a
1418203_at	Pmaip1	1418267_at	Mst1	1424968_at	2210023G 05Rik
1438570_at	---	1455501_at	Slc2a12	1437308_s_at	F2r
1437398_a_at	Aldh9a1	1445621_at	---	1421355_at	Tgm3

Table 2.2.2 (continued)

1429049_at	Nuak2	1435761_at	Stfa1 /// Stfa3	1436163_at	Kcnj16
1444242_at	Slco2a1	1430551_s_at	Lipm	1426914_at	Marveld2
1450763_x_at	WNT3	1452614_at	Bcl2l15	1415921_a_at	Tnfrsf19
1422870_at	Hoxc4	1429951_at	Ssbp2	1432666_at	---
1439449_at	Satb1	1442074_at	---	1418003_at	1190002H23Rik
1451835_at	Sox21	1433132_at	Edaradd	1439195_at	---
1444261_at	---	1418649_at	Egln3	1431057_a_at	Prss23
1455162_at	4922503N01Rik	1421817_at	Gsr	1426908_at	Galnt7
1453148_at	Sema3d	1429123_at	Rab27a	1435819_at	---
1460129_at	Slc6a2	1449078_at	St3gal6	1447299_at	---
1440802_at	Clasp2	1416930_at	Ly6d	1421223_a_at	Anxa4
1442389_at	Oas1f	1438671_at	Ppp2r2c	1418365_at	Ctsh
1455200_at	Pak6	1434683_at	---	1434877_at	Nptx1
1438279_at	Dpp4	1432018_at	Ascl2	1437578_at	Clca2
1421217_a_at	Lgals9	1436928_s_at	Adcy3	1437312_at	Bmpr1b
1453802_at	Limch1	1418025_at	Bhlhb2	1456200_at	Ipmk
1460248_at	Cpxm2	1434575_at	Epb4.1l1	1429159_at	Itih5
1418648_at	Egln3	1453511_at	2310007B03Rik	1425918_at	Egln3
1439352_at	Trim7	1451326_at	Abhd14b	1421571_a_at	Ly6c1
1421960_at	Adcy3	1426568_at	Slc2a9	1426018_a_at	Sox6
1429284_at	Mobkl2b	1434777_at	Mycl1	1424308_at	Slc24a3
1448786_at	1100001H23Rik	1456981_at	Tmc7	1425212_a_at	Tnfrsf19
1454438_at	Rab27a	1451375_at	Ehf	1450695_at	Ahr
1418937_at	Dio2	1448977_at	Tcfap2c	1435094_at	Kcnj16
1448918_at	Slco3a1	1422139_at	Plau	1438954_x_at	Figf
1420459_at	Ripply3	1448147_at	Tnfrsf19	1455689_at	Fzd10
1429566_a_at	Hipk2	1457140_s_at	Rassf10	1418030_at	Slco3a1
1437542_at	Ikzf2	1443639_at	Apcdd1	1418762_at	Cd55
1422571_at	Thbs2	1458653_at	---	1417639_at	Slc22a4
1450005_x_at	Dlk2	1427746_x_at	H2-K1	1419463_at	Clca2

Table 2.2.2 (continued)

1436689_a_at	Aldh9a1	1457656_s_at	C230085N15Rik	1421471_at	Npy1r
1457407_at	Robo1	1452092_at	4631426J05Rik	1424129_at	Mfsd1
1421185_at	Mettl7a1	1419188_s_at	Ccl27	1460038_at	Pou3f1
1421492_at	Ptgds2	1437671_x_at	Prss23	1430457_at	Daf2
1431382_a_at	Clip4 /// LOC100048376	1426454_at	Arhgdib	1419136_at	Akr1c18
1435842_at	Nat8l	1429262_at	Rassf6	1417150_at	Slc6a4
1426725_s_at	Ets1	1445625_at	---	1420630_at	8430419L09Rik
1425002_at	Sectm1a	1453202_at	E330016A19Rik	1428323_at	Gpd2
1449282_at	Cysltr1	1440363_at	---	1426850_a_at	Map2k6
1435203_at	Man2a2	1437665_at	Il22ra2	1417953_at	D6Wsu176e
1434918_at	Sox6	1432523_at	Hipk2	1449848_at	Gna14
1416697_at	Dpp4	1435321_at	Limch1	1437231_at	Slitrk6
1430191_at	9130004J05Rik	1417434_at	Gpd2	1431362_a_at	Smoc2
1429824_at	4930550C14Rik	1437604_x_at	Apcdd1	1436030_at	Cachd1
1423305_at	Extl1	1435693_at	Mall	1422912_at	Bmp4
1433933_s_at	Slco2b1	1419086_at	Fgfbp1	1434083_a_at	Elmod1
1440150_at	Tgm3	1421199_at	Dlg2	1440041_at	---
1417852_x_at	Clca1	1437800_at	Edaradd	1438301_at	---
				1439795_at	Gpr64

Table 2.3. Signals for genes increased in divided CD34+/ 6+ (Bu, 1-2 Div) at PD21 relative to all other populations attesting to a distinct identity of this subpopulation.

189 genes up-regulated in PD21 Bu (1-2 Div) relative to PD21 Bu (0 Div) in 3 mice with p-value<= 0.001.

Probe Set ID	Gene Symbol	Probe Set ID	Gene Symbol	Probe Set ID	Gene Symbol
1415921_a_at	Tnfrsf19	1424470_a_at	Rapgef3	1439795_at	Gpr64
1415935_at	Smoc2	1424572_a_at	H2afy	1440246_at	Lass6
1416008_at	Satb1	1424968_at	2210023G05Rik	1441384_at	---
1416123_at	Ccnd2	1425212_a_at	Tnfrsf19	1441926_x_at	Tmie
1416155_at	Hmgb3	1425345_at	Ccdc28a	1442019_at	---
1416200_at	Il33	1425620_at	Tgfbr3	1442389_at	Oas1f
1416452_at	Oat	1425663_at	Il1rn	1443284_at	---
1416749_at	Htra1	1425918_at	Egln3	1443870_at	Abcc4
1416988_at	Msh2	1426018_a_at	Sox6	1443991_at	Dock1
1417055_at	0610009D07Rik	1426288_at	Lrp4	1444273_at	AW555355
1417077_at	Bcap29	1426807_at	Lta4h	1445761_at	D4Ertd628e
1417122_at	Vav3	1426850_a_at	Map2k6	1446834_at	Ctsc
1417150_at	Slc6a4	1426908_at	Galnt7	1447937_a_at	4933409K07Rik
1417185_at	Ly6a	1426914_at	Marveld2	1448147_at	Tnfrsf19
1417483_at	Nfkbiz	1426933_at	Oxsr1	1448354_at	G6pdx
1417639_at	Slc22a4	1427005_at	Plk2	1448489_at	Pafah2
1417700_at	Rab38	1427165_at	Il13ra1	1448641_at	Mbtd1
1417749_a_at	Tjp1	1427185_at	Mef2a	1448651_at	Nudt5
1417771_a_at	Psmc6	1427390_at	Bloc1s3	1448803_at	Golga4
1417953_at	D6Wsu176e	1427462_at	E2f3	1448918_at	Slco3a1
1417962_s_at	Ghr	1427477_at	Tmprss13	1448936_at	Stx12
1418003_at	1190002H23Rik	1428323_at	Gpd2	1449078_at	St3gal6

Table 2.3 (continued)

1418030_at	Slco3a1	1429049_at	Nuak2	1449278_at	Eif2ak3
1418152_at	Nsbp1	1429159_at	Itih5	1449626_s_at	Acbd4
1418153_at	Lama1	1429564_at	Pcgf5	1449816_at	Sult5a1
1418365_at	Ctsh	1429811_at	4933424B01Rik	1449888_at	Epas1
1418762_at	Cd55	1429824_at	4930550C14Rik	1449968_s_at	Acot9 /// Acot10
1418823_at	Arf6	1430089_at	5830469G19Rik	1450187_a_at	Galt
1418971_x_at	Bcl10	1431057_a_at	Prss23	1450724_at	AB030242
1418991_at	Bak1	1431405_a_at	Cspp1	1450763_x_at	WNT3
1419136_at	Akr1c18	1431609_a_at	Acp5	1450852_s_at	F2r
1419463_at	Clca2	1434575_at	Epb4.1l1	1450885_at	Dffa
1419532_at	Il1r2	1434815_a_at	Mapkapk3	1450947_at	2610528J11Rik
1420226_x_at	Hoxa4	1435203_at	Man2a2	1451261_s_at	Stap2
1420630_at	8430419L09Rik	1435321_at	Limch1	1451415_at	1810011O10Rik
1420873_at	Twf1	1435323_a_at	Mboat1	1451501_a_at	Ghr
1420913_at	Slco2a1	1435531_at	Usp3	1451593_at	H2-K1
1421073_a_at	Ptger4	1435626_a_at	Herpud1	1451835_at	Sox21
1421223_a_at	Anxa4	1435917_at	Ociad2	1452482_at	Erbb3
1421355_at	Tgm3	1436023_at	Bclaf1	1452626_a_at	1810014F10Rik
1421471_at	Npy1r	1436122_at	Zfp667	1452661_at	Tfrc
1421571_a_at	Ly6c1	1436182_at	---	1453148_at	Sema3d
1421643_at	Ikzf2	1436421_s_at	Arpc5l	1453355_at	Wnk2
1421704_a_at	Pik3c2g	1436448_a_at	Ptgs1	1453511_at	2310007B03Rik
1422087_at	Mycl1	1436689_a_at	Aldh9a1	1454777_at	Slco2b1
1422397_a_at	Il15ra	1436893_a_at	7-Mar	1454817_at	Utp18

Table 2.3 (continued)

1422428_at	Acsbg1	1437059_at	Sox21	1455084_x_at	Shmt2
1422661_at	Lgals8	1437231_at	Slitrk6	1455162_at	4922503N01Rik
1422912_at	Bmp4	1437244_at	Gas2l3	1455424_at	Wnk2
1422967_a_at	Tfrc	1437458_x_at	Clu	1455435_s_at	Chdh
1423120_at	Ide	1437578_at	Clca2	1455590_at	Nqo2
1423236_at	Galnt1	1437671_x_at	Prss23	1455732_at	1700025G04Rik
1423570_at	Abcg1	1437868_at	BC023892	1456090_at	Pdhx
1423748_at	Pdk1	1438255_at	Foxn3	1456674_at	E130016E03Rik
1423856_at	Popdc3	1438401_at	Ubn1	1456911_at	Clasp2
1423946_at	Pdlim2	1438671_at	Ppp2r2c	1456956_at	Ikzf2
1424060_at	Neil3	1438699_at	Srd5a1	1459146_at	Mapk6
1424129_at	Mfsd1	1438784_at	Bcl11b	1459321_at	---
1424139_at	Rap1a	1438853_x_at	Ddx54	1459713_s_at	Tmem16a
1424148_a_at	Stap2	1438953_at	Figf	1460171_at	Cops5
1424308_at	Slc24a3	1438954_x_at	Figf	1460248_at	Cpxm2
1424358_at	Ube2e2	1439675_at	Ppara	1460259_s_at	Clca1 /// Clca2
1460737_at	Igbp1	AFFX-TransRecMur	Tfrc	1460599_at	Ermp1

169 genes up-regulated in PD21 Bu (1-2 Div) relative to PD21 NonBu cells in 3 mice with p-value<= 0.01

Probe Set ID	Gene Symbol	Probe Set ID	Gene Symbol	Probe Set ID	Gene Symbol
1415727_at	Apoa1bp	1424185_a_at	Morf4l1	1441391_at	---
1415739_at	Rbm42	1424367_a_at	Homer2	1441587_at	Plch2
1415909_at	Stip1	1424460_s_at	Lpcat1	1443842_at	Arfgef2
1416036_at	Fkbp1a	1424542_at	S100a4	1444078_at	Cd8a
1416048_at	Phc2	1424660_s_at	Crtc2	1444523_s_at	Ube2v1

Table 2.3 (continued)

1416072_at	Cd34	1424769_s_at	Cald1	1445204_at	---
1416256_a_at	Tubb5	1424919_at	Erbb2	1446055_at	---
1416285_at	Ndufc1	1424966_at	Tmem40	1446681_at	BB086117
1416331_a_at	Nfe2l1	1425068_a_at	Tex264	1447669_s_at	Gng4
1416438_at	Puf60	1425357_a_at	Grem1	1447860_x_at	Cog8
1416594_at	Sfrp1	1425418_at	Wfdc5	1448180_a_at	Hn1
1416813_at	Tia1	1425658_at	Cd109	1448185_at	Herpud1
1417138_s_at	Polr2e	1425779_a_at	Tbx1	1448325_at	Myd116
1417374_at	Tuba4a	1425874_at	Hoxc13	1448395_at	Sfrp1
1417393_a_at	C1qdc2	1426465_at	Dlgap4	1448519_at	Tead2
1417397_at	Slc9a1	1426724_at	Cnn3	1448580_at	Glg1
1417406_at	Sertad1	1426750_at	Flnb	1448760_at	Zfp68
1417408_at	F3	1426973_at	Gpr153	1448863_a_at	Tnfaip1
1417437_at	Xrcc6	1427567_a_at	Tpm3	1449096_at	Ccdc127
1417490_at	Ctsb	1428143_a_at	Pnpla2	1449202_at	Sema4g
1417738_at	Rab25	1428542_at	Eif1ad	1449256_a_at	Rab11a
1417783_at	Als2	1428750_at	Cdc42ep2	1449258_at	D11Wsu99e
1418089_at	Stx8	1428884_at	Tmem57	1449403_at	Pde9a
1418116_at	Ifrg15	1428966_at	2610204K14Rik	1449617_at	2900092E17Rik
1418317_at	Lhx2	1429187_at	---	1449713_at	Cbx7
1419006_s_at	Peli2	1429337_at	Tmem87b	1450044_at	Fzd7
1419573_a_at	Lgals1	1429693_at	Dab2	1450187_a_at	Galt
1420148_at	Slc6a6	1429742_at	Rcbtb2	1450434_s_at	Pcyt1a
1420350_at	Lce1a2	1430698_a_at	Pibf1	1450717_at	Ang
1420425_at	Prdm1	1431230_a_at	Btbd9	1450928_at	LOC100045546
1420504_at	Slc6a14	1431295_a_at	Stx18	1451072_a_at	Rnf4

Table 2.3 (continued)

1420536_at	Crybb2	1433583_at	Zfp365	1451187_at	0610037P05Rik
1420676_at	Lce1a1	1433801_at	9930012K11Rik	1451538_at	Sox9
1420677_x_at	Lce1a1	1434151_at	Mettl7a1	1451764_at	Marveld3
1420764_at	Scrg1	1434183_at	LOC546078	1452037_at	Mgat2
1420892_at	WNT7b	1434286_at	Trps1	1452138_a_at	Ace2
1420901_a_at	Hk1	1434541_x_at	Khdrbs1	1452351_at	C030027K23Rik
1421057_at	Dnase1l3	1435133_at	Ugcg	1452812_at	Lphn1
1421129_a_at	Atp2a3	1435341_at	Ppig	1453094_at	Foxn3
1421397_a_at	Lrdd	1435602_at	Sephs2	1453218_at	Lce1c
1421612_a_at	H2afy3 /// H2afy2	1435922_at	Fbxl19	1453523_at	Krtap17-1
1421997_s_at	Itga3	1436110_at	---	1454773_at	Rxra
1422087_at	Mycl1	1436395_at	Card6	1454877_at	Sertad4
1422563_at	Cr1l	1436448_a_at	Ptgs1	1455018_at	Lmtk2
1422783_a_at	Krt6a	1436454_x_at	Fen1	1455175_at	Phf13
1422864_at	Runx1	1436604_at	Ttll3	1455288_at	1110036O03Rik
1423259_at	Id4	1437849_x_at	Armcx2	1455298_at	---
1423260_at	Id4	1437868_at	BC023892	1455315_at	Trp53i13
1423425_at	1300012G16Rik	1437888_at	Wnk1	1455505_at	Gatad2a
1423726_at	Vat1	1438164_x_at	Flot2	1456194_a_at	Park7
1423774_a_at	Prc1	1438172_x_at	Exod1	1456585_x_at	E130309D02Rik
1423889_at	EG434402	1439073_at	Mllt4	1456633_at	Trpm3
1423986_a_at	Shisa5	1439151_at	Msrb3	1457834_at	Yy1
1424099_at	2310016C16Rik	1439852_at	---	1457921_at	1810037C20Rik
1424118_a_at	Spc25	1439887_at	---	1459711_at	Sdk1
1424168_a_at	Capzb	1440152_x_at	Edf1 /// LOC674653	1460287_at	Timp2
				1460359_at	Armcx3

Unlike the previous report (Jaks et al., 2008), in catagen (PD21-PD42 chase) we found consistently high levels of LGR5 mRNA expressed in most CD34+/α6+ cell fractions, including those that divided only 2-3x in one hair cycle (see Discussion). LGR5 expression was variable in cells with 0-1 divisions, consistent with previously reported rare association of LGR5+ cells with BrdU label-retaining cells (LRCs; Jaks et al., 2008). In summary, our gene expression data demonstrated divergence in expression profiles of divided CD34+/α6+ cells at the two hair cycles stages analyzed (PD18-PD21 and PD22-PD25).

The data thus far suggested that newly divided (1-2 divisions) CD34+/α6+ cells, which may represent newly generated bulge cells, were distinct in molecular makeup, proliferation rates, and localization at PD18-PD21 (telogen-anagen) with respect to PD22-PD25 (anagen). The CD34+/α6+ cells generated at the telogen-anagen stage displayed characteristics consistent with progenitor cell differentiation: more vigorous divisions; localization right outside the SC niche (bulge) in the tissue zone where Mx is first generated; high expression of differentiation and progenitor Mx markers; and lower expression levels of most bulge markers. In contrast, later in anagen, newly generated CD34+/α6+ divided less frequently, remained inside the SC niche (bulge), and maintained the bulge-enriched gene expression signature. Although it is unclear if the divided CD34+/α6+ cells isolated here at telogen-anagen transition were directly bulge-derived, this possibility is likely, given the earlier tracking of downward cellular displacements from bulge into germ (Cotsarelis, 2006; Ito et al., 2004; Tumbar et al., 2004). These data would then imply that newly generated bulge progeny differentiate near the niche exit during an early hair cycle stage while expanding their pool of bulge-like cells (self-renewing) inside the niche at the latter stage. To directly address this hypothesis we explored further the lineage relationship between bulge, HG, and Mx/bulb cells in hair cycle.

Bulge cells leave their niche prior to division

In vivo evidence based on short-term tracking of bulge LRCs, indicated that bulge progeny contribute differentiated cells to the HG/Mx formation (Cotsarelis, 2006; Ito et al., 2004; Tumbar et al., 2004). It remains unclear, however, if the cells divide/self-renew prior to their departure from the bulge. A model derived from transplantation of rat whisker cells suggested that bulge SCs migrate away from the niche during quiescence (Claudinot et al., 2005; Oshima et al., 2001). Here we recognized bulge cells due to higher levels of H2B-GFP retention after PD21-PD42 doxy chase, and subsequently tracked their location in HF compartments in the second telogen. Telogen morphology is defined by 3 molecularly distinct compartments: bulge, made of 2 concentric epithelial cell layers surrounding the club hair, with SCs in the outer CD34+ layer; hair germ (HG), an epithelial cell cluster underneath with little if any CD34; and the mesenchymal dermal papillae (DP) structure (Fig. 2.5A). In over 25 mice sacrificed between PD42-PD56, HF morphology indicated end of catagen at PD42, telogen with small HGs at PD43, somewhat larger HGs at or after ~PD47, and mostly anagen at PD56 (not shown). To examine if bulge cells directly contributed to HG size increase by first dividing in the niche, we counted number of HG cells at two telogen time points, and correlated it with H2B-GFP levels and BrdU incorporation over time. We removed dermal cells by collagenase treatment to release full HFs at PD43 and PD44 and imaged them by confocal optical sectioning (Rendl et al., 2005; Waghmare et al., 2008). Analysis of image stacks, maximal projections and rotations showed that HGs contained on average ~20 cells at PD43 and 35 cells at PD44 (Fig. 2.5C). Moreover the number of apparent bright H2B-GFP cells in the HGs also increased at PD44 relative to PD43 (Fig. 2.5B-E; 2.6). This semi-quantitative analysis was confirmed by quantitatively integrating the H2B-GFP intensity in a 3D cell volume for a smaller set of HFs (Fig. 2.5F,G). These data

demonstrated that bulge cells, including some cells with H2B-GFP levels consistent with only one division, contributed to an increase in HG size from PD43 to PD44. Moreover, this happened in the absence of divisions because we detected no proliferation in HFs from mice sacrificed 6 hrs after BrdU injection (Fig. 2.5H,I) or after continuous administration of BrdU for 3 days (PD41-PD44, N=3 mice, data not shown). At later stages BrdU appeared first in HGs and then in bulges (Fig. 2.5H,I), as expected (Greco et al., 2009), and as seen before in the first telogen (Fig. 2.1G). Catagen specific caspase staining to detect cell death was absent in all stages examined (Fig. 2.5H); PD40 was used as positive control for this staining. These data indicated that during telogen bulge cells, including some that divided rarely (~once in 3 weeks), leave their normal niche and go into the HG without a simultaneous bulge-replenishing division.

Retrospective view of single bulge cell fate: differentiation or self-renewal phases

To map bulge-cell fate *in vivo* we genetically labelled single cells at quiescence and examined progeny distribution in HF compartments during hair growth. We chose the first telogen for labelling because it precedes the most synchronous hair cycle. We employ transgenic mice with keratin 14 (K14) epithelial expression of the tamoxifen inducible Cre-ER (Vasioukhin et al., 1999) crossed with Rosa26R reporter mice (Soriano, 1999). Tamoxifen injection into mice turns on β-Galactosidase in epithelial cells. The expression remains on in all the cell lineages descending from the originally marked cell, and is detected by X-Gal staining in skin sections. To increase our chance of labelling single bulge cells per HF we utilized the more inefficient mouse line of the two previously generated (Vasioukhin et al., 1999). First, we maximized X-Gal staining efficiency in a strong constitutively expressed epithelial

Figure 2.5. Bulge-cell departure from the niche during the quiescent phase.

(A) Schematic of telogen HF structure, showing 2 layers of cells surrounding the shaft that make the bulge (Bu), and the hair germ (hg) underneath. DP, dermal papillae. (B) Confocal image from whole HFs in 100 m skin sections of pTRE H2B-GFP/K5tTA mice with doxy chase from PD21. Note increased number of hg cells by PD44, quantified in (C) and shown with SEM (N=39 HFs). (D) Confocal stack images of whole HF collected side by side from skin sections of pTRE-H2B-GFP/K5tTA mice at PD43 and PD44 (3-wks doxy chase; PD43 is shown in Fig. S3). Optical z-stacks are shown as tiled images. Numbers indicate actual optical slice and arrows point to a bright H2B-GFP cell throughout the stack located in hg at PD44, normally found in bulge at PD43. TOPRO-3 was used as DNA counterstain for revealing the hair follicle structures (not shown). (E) Stacks in (D) are shown as maximal projection through the slices on XY, ZY, and XZ plane. Arrow points to the same cells as in (D). (F) Total intensity after background subtraction (Int) in each optical z-section for cell indicated by arrow in (D&E) used to obtain total 3D intensity, which was then used to generate the plot in G. (G) H2B-GFP intensity/hg cell volume shows more bright cells at PD44 relative to PD43 (see Fig. S3); brightest (0 divisions) and dimmest bulge cells are shown for comparison. There are only 1-2 cells with 0 division, and they were localized in the bulge at PD43&PD44. (H) Skin section for mice fed doxy and BrdU for 3 days at stages indicated, and stained for BrdU (top) or caspase (bottom). (I) Frequencies of BrdU+ HFs (N at top) averaged in 3 mice/stage, with SEM. Scale bars, 10 um.

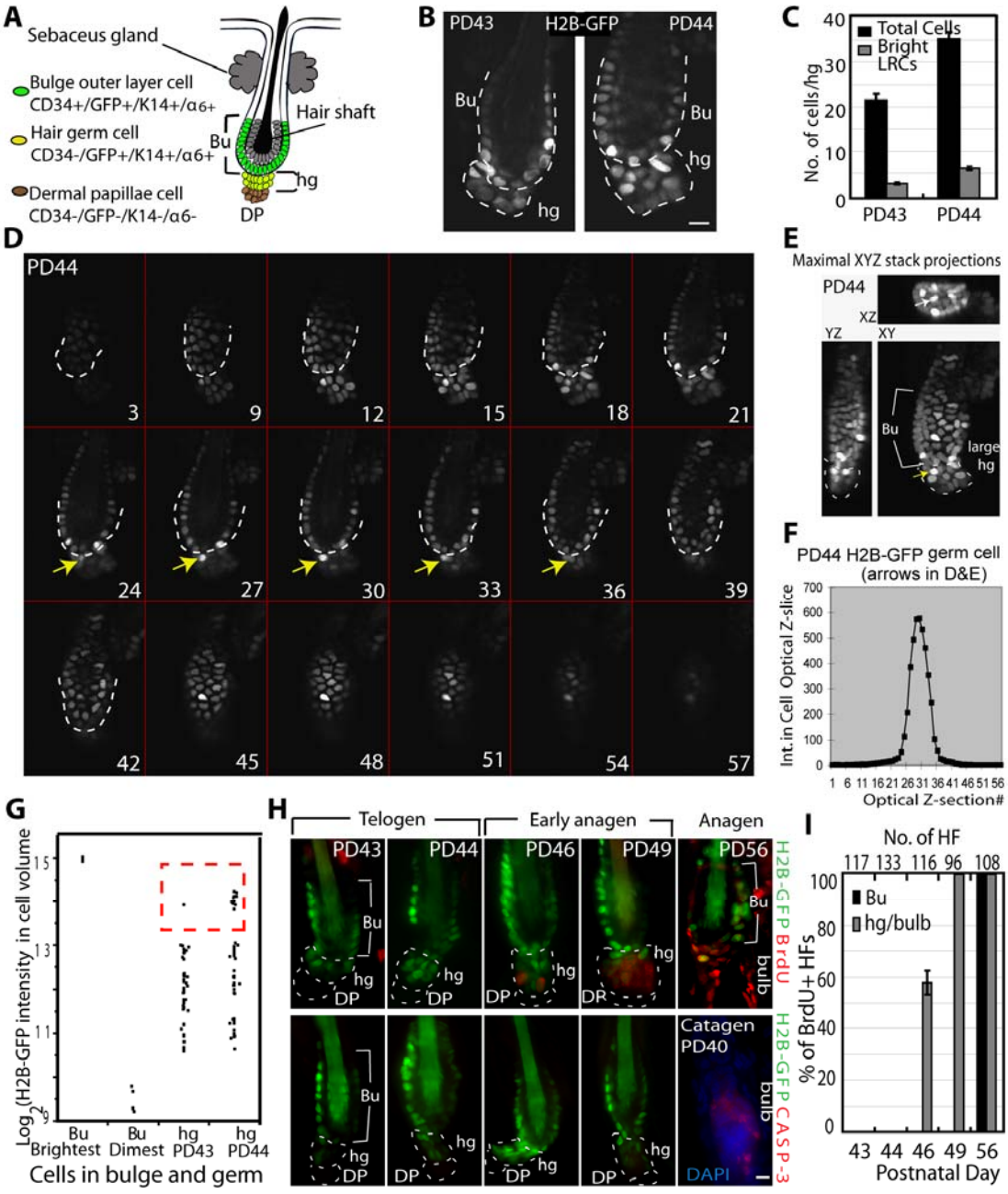
A
Sebaceus gland
Bulge outer layer cell
CD34+/GFP+/K14+/α6+
Hair germ cell
CD34-/GFP+/K14+/α6+
Dermal papillae cell
CD34-/GFP-/K14-/α6-
Hair shaft
Bu
hg
DP
B
PD43
H2B-GFP
PD44
Bu
hg
C
Total Cells
Bright LRCs
No. of cells/hg
PD43
PD44
D
PD44
E
Maximal XYZ stack projections
PD44
XZ
YZ
XY
Bu
large hg
F
PD44 H2B-GFP germ cell
(arrows in D&E)
Int. in Cell Optical Z-slice
Optical Z-section#
G
Log2 (H2B-GFP intensity in cell volume
Bu Brightest
Bu Dimest
hg PD43
hg PD44
Cells in bulge and germ
H
Telogen
Early anagen
Anagen
PD43
PD44
PD46
PD49
PD56
H2B-GFP BrdU
bulb
Catagen
PD40
H2B-GFP CASP-3
DAPI
I
No. of HF
117 133 116 96 108
Bu
hg/bulb
% of BrdU+ HFs
Postnatal Day

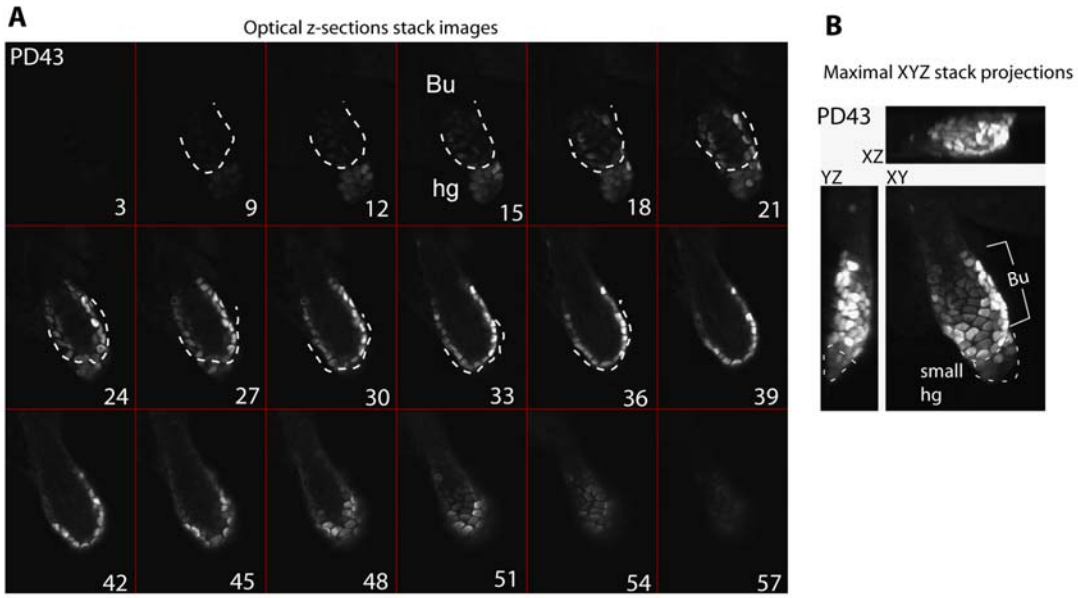

Figure 2.6. Confocal analysis of whole hair follicles with quantification of H2B-GFP in a cell volume.

(A) Confocal stack images as collected in Fig. 3D-F showing an example of a skin section from pTRE-H2B-GFP/K5tTA mice from PD21-PD43 doxy chase; Telogen). These images were collected side by side with those from PD21-PD44 chases (shown in Fig. 2.5D-F). (B) Stacks in (A) are shown as maximal projection through the slices on XY, ZY, and XZ plane.

K14-Cre line (Fig. 2.7C). Second, we established the appropriate dose of tamoxifen (Fig. 2.7A), the precise timing of hair cycle stages in this new mouse genetic background (Fig. S4B), and the minimum chase time (4 days) for reaching X-Gal labelling plateau during a prolonged quiescence phase to eliminate confounding proliferation effects (Fig. 2.7D). Finally, we injected mice with tamoxifen at the catagen/telogen transition (PD17), sacrificed them at different stages and analyzed skin tissue at telogen (PD17-PD21 chase), early anagen (PD17-PD25 chase) and late anagen (PD17-PD35 chase; Fig. 2.7E). Since the K14 promoter was active in several skin epithelium compartments in their basal cells, X-Gal+ cells were found in HFs, inter-follicular epidermis, and sebaceous glands. The latter, located above the bulge, do not contribute cells to normal HFs homeostasis (Horsley et al., 2006). X-Gal staining was undetectable in skin sections analyzed from 10 K14-CreER x Rosa26R mice injected with oil only (no tamoxifen control) at PD17 and sacrificed at PD25, 35, 90 and over 1 year (Fig. 2.7H). Moreover, the tamoxifen induced X-Gal labelling was highly inefficient (~20% of all HFs), and occurred as rare patches dispersed throughout the mouse back skin (Fig. 2.7H). To examine X-Gal distribution in full HFs, we used thick skin sections (60-90μm thick). We imaged them by phase contrast or bright field microscopy in skin sections with or without hematoxylin staining, which adds contrast to the tissue (Fig. 2.8A-D, 2.7F-H). To emphasize the X-Gal labelling, images are shown with little contrast. The K14 promoter is active in both bulge and HG cells, but given a cell ratio of bulge to HG cells of roughly 10:1, by random chance we expected ~90% X-Gal+ HFs with bulge-only labelling. In fact, we found ~99% of PD17-PD21 X-Gal+ HFs with bulge-only staining (76% as single and 23% as multiple cells; Fig. 2.8B,E). Some unexplained bias against HG marking by the CreER might have also contributed to specificity of labelling to the bulge.

Figure 2.7 A-D. Optimization of single bulge-cell labeling scheme.

(A) Frequencies of hair follicle (HF) labeling patterns shown with SEM as percent of total hair follicles at PD25 4 days after 1 or 2 injections of tamoxifen at 100 g/g body weight. Note lower labeling efficiency with one injection and a high relative frequency of single bulge cell labeled HFs. (N= 3 mice for each stage.) (B) Images of skin sections collected from mice at ages indicated, 6 hrs after BrdU injection, and immunostained for BrdU (red). Blue is DNA DAPI staining, and appears diffuse due to denaturing of double strands with HCl, to expose the BrdU antigen. Note proliferation in the bulge area until postnatal day PD14, with rare BrdU+ cells at PD15-16, and lack of BrdU+ bulge cells thereafter. (C) Images of 20um skin sections collected from K14Cre X Rosa26R mice at indicated stages after staining for X-gal. Continuous staining was found on hair follicle cells, shown here with focus at the bulge area. (D) Frequencies of hair labeling patterns and total labeling efficiency is shown with SEM during the long quiescent phase after 4 (PD51) and 10 (PD57) days of tamoxifen (TM) induction at PD47. At equal tamoxifen dose the efficiency of labeling is maximal 4 days post-injection, and does not increase further after 6 additional days of chase. This validates the ability to mark cells at different developmental stages separated by at least 4 days, without interferences from prolonged tamoxifen activity in the skin cells. N is number of X-Gal+ hair follicles for each time point; number of mice are shown in brackets.

Figure 2.7 E-H. Optimization of single bulge-cell labeling scheme.

(E) Labeling efficiency of induced (X-Gal+ HFs) in skin sections at times indicated shows similar frequency of total follicles counted across the stages analyzed (N=3 mice/stage; > 1000 total HF/stage. TM, tamoxifen). These data, along with additional time points are re-shown in Fig 2.11. (D&G) Phase contrast (F) and hematoxylin (G) bright-field images of thin skin sections stained with X-gal show relevant X-Gal patterns at 2 critical stages. (H) Low magnification (4x) images of thick skin sections (60-90 um) X-Gal stained at stages indicated with or without tamoxifen injection. Additional No-Tamoxifen oil only controls were collected from 2nd anagen (N=2) and 1-year old mice (N=2). No labeling was observed without tamoxifen injection . TM was injected at PD17. Arrows indicate single cell labeled bulges at top, and bulb versus bulge labeling pattern at bottom.

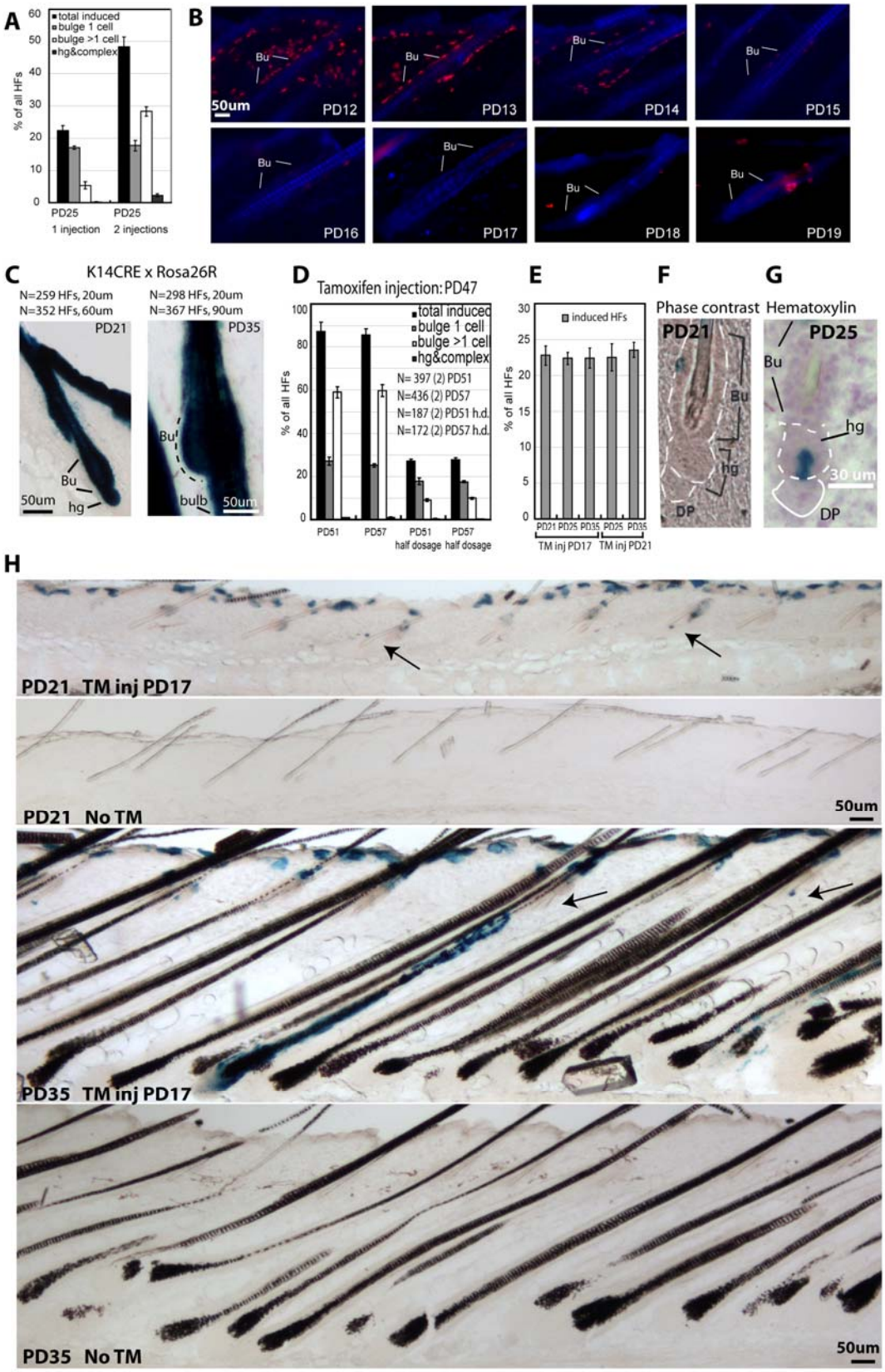
A
total induced
bulge 1 cell
bulge >1 cell
hg&complex
% of all HFs
PD25
1 injection
PD25
2 injections
B
Bu
50um
PD12
PD13
PD14
PD15
PD16
PD17
PD18
PD19
C
K14CRE x Rosa26R
N=259 HFs, 20um
N=352 HFs, 60um
N=298 HFs, 20um
N=367 HFs, 90um
PD21
PD35
Bu
hg
bulb
50um
D
Tamoxifen injection: PD47
total induced
bulge 1 cell
bulge >1 cell
hg&complex
N= 397 (2) PD51
N=436 (2) PD57
N=187 (2) PD51 h.d.
N=172 (2) PD57 h.d.
% of all HFs
PD51
PD57
PD51 half dosage
PD57 half dosage
E
induced HFs
% of all HFs
PD21 PD25 PD35 PD25 PD35
TM inj PD17
TM inj PD21
F
Phase contrast
PD21
Bu
hg
DP
G
Hematoxylin
PD25
Bu
hg
30 um
DP
H
PD21 TM inj PD17
PD21 No TM
50um
PD35 TM inj PD17
PD35 No TM
50um

If bulge-cell daughters followed a simple model of asymmetric fate decisions with respect to their niche, they would replenish the bulge (SC) pool (self-renew) and simultaneously generate the progenitor cell (differentiate), which would be expelled from the bulge and differentiate further into the bulb. Thus, after a growth period the X-Gal+ progeny of the original single-labeled bulge cell should be always detectable in both the bulge (stem cell) and the bulb (differentiated) compartments (complex labeling pattern). Strikingly, skin from PD17-PD25 chases showed only 6% HFs with a complex pattern, likely attributable to noise in the system due to 23% of the original labeled HFs with multiple X-Gal+ cells (PD17-PD21). The remaining 94% of labeled HFs had X-Gal+ cells exclusively in either one of the two HF compartments: 80% HFs with bulge-only X-Gal labeling pattern and 14% HFs with HG-only pattern (Fig. 2.8C,E). The bulge-resident cells remained largely undivided in the PD17-PD25 chase, as shown by ~60% of labeled HFs with a single X-Gal+ cell/bulge. In contrast X-Gal+ HG cells were found single or in pairs (indicative of divisions), sometimes in direct contact with the DP (Fig. 2.8C and 2.7G). These patterns detected in thick skin sections could be reconstituted from a random pool of 36-labelled HFs in serial thin (20μm) sections, ruling out potential issues of X-Gal penetration (Fig. 2.9A-C). Moreover, the fraction of labeled HFs in PD17-PD21, PD17-PD25, PD17-PD35 chases remained constant (Fig. 2.11D). This rules out the possibility that a significant fraction of single labeled bulge cells were missed in our analysis, or that the labeling may take longer to reveal in the HG or hair bulb cells. These data indicated that bulge cells exited their bulge residency without simultaneous division inside the niche, consistent with our previous H2B-GFP tracking data (Fig. 2.5). We also examined the distribution of single X-Gal+ cells within the bulge in PD17-PD21 chase and PD17-PD25 chase in >100 HFs. The X-Gal+ cells marked preferentially the middle bulge at PD21 and the lower bulge at PD25, suggesting a generalized downwards bulge

Figure 2.8. Single-bulge cells lineage tracing during 1st adult hair cycle.

(A-D) X-Gal stained skin sections (60-90 um) from K14CreER x Rosa26R mice tamoxifen injected at PD17 and sacrificed at times indicated. Dotted lines delineate the bulge (Bu) and hair germ (hg) or bulb compartments. Scale bar, 50 um. (E) Frequencies of X-Gal patterns shown as average with SEM (N.3 mice/stage). DP, dermal papillae. (F) Scheme of chases PD17-PD21 or PD21-PD25, and X-Gal patterns in HFs at PD35 in anagen (G), re-shown as fold changes (H).

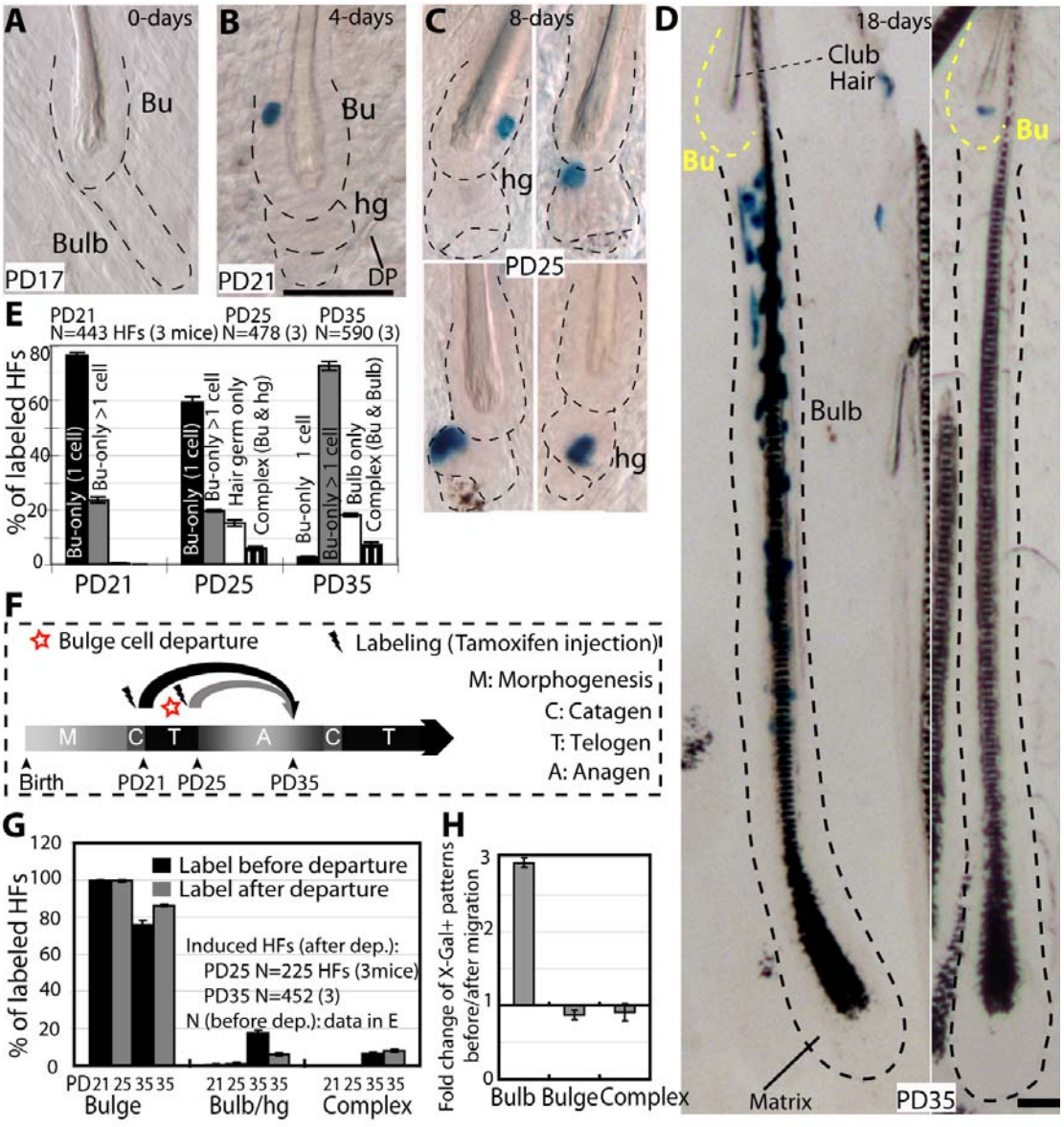
A
0-days
Bu
Bulb
PD17
B
4-days
Bu
hg
PD21
DP
C
8-days
hg
PD25
hg
D
18-days
Club
Hair
Bu
Bu
Bulb
Matrix
PD35
E
PD21
N=443 HFs (3 mice)
PD25 N=478 (3)
PD35 N=590 (3)
% of labeled HFs
Bu-only (1 cell)
Bu-only >1 cell
Bu-only (1 cell)
Bu-only >1 cell
Hair germ only
Complex (Bu & hg)
Bu-only 1 cell
Bu-only >1 cell
Bulb only
Complex (Bu & Bulb)
PD21
PD25
PD35
F
Bulge cell departure
Labeling (Tamoxifen injection)
M: Morphogenesis
C: Catagen
T: Telogen
A: Anagen
M
C
T
A
C
T
Birth
PD21
PD25
PD35
G
% of labeled HFs
Label before departure
Label after departure
Induced HFs (after dep.):
PD25 N=225 HFs (3mice)
PD35 N=452 (3)
N (before dep.): data in E
PD21 25 35 35
Bulge
21 25 35 35
Bulb/hg
21 25 35 35
Complex
H
Fold change of X-Gal+ patterns before/after migration
Bulb
Bulge
Complex

cellular displacement (Fig. 2.9D). Simple upward motion of the hair shaft can potentially explain these data, but might not account for the presence of bulge X-Gal+ cells away from the bulge base onto the DP (Fig. 2.8D&2.7G). This latter observation suggests a possible active migration for the X-Gal+ ulge-cell through the pre-existing HG cells (which were X-Gal-) to reach the DP.

X-Gal+ cells at full anagen (PD35) remained segregated in either bulb or bulge compartments in 93% of the labeled HFs (Fig. 2.8D). HFs with bulb-only labelling pattern, represented 17% of all HFs labelled at PD35, and contained numerous X-Gal+ cells in all the differentiated hair lineages in thick sections and cross-sections, and in thin serial sections (Fig. 2.8D and Fig. 2.10). These data were consistent with previous transplantation and skin dermabrasion experiments (Blanpain et al., 2004; Claudinot et al., 2005; Ghazizadeh and Taichman, 2001), and indicated frequent division of the bulge-progeny in the bulb. The data also demonstrated multipotency *in vivo* of the originally marked single bulge-cells (Fig. 2.10). Bulbs showed sectors of labelling as expected from their known polyclonal origin (Claudinot et al., 2005; Ghazizadeh and Taichman, 2001; Kopan et al., 2002). Only a fraction of the bulb-labelled follicles displayed X-Gal+ Mx cells, most likely due to the cessation of self-renewal of this progenitor/transit amplifying cell population by the end of anagen at PD35, as expected (Legue and Nicolas, 2005). The bulge zone around the old hair shaft (club hair) completely lacked X-Gal staining in the bulb-only patterns (Fig. 2.8D and 2.7H), while the zone adjacent to it rarely displayed few X-Gal+ cells (~2% of the total labelled HFs) mostly in inner (differentiated) layers around the new hair shaft.

HFs with bulge-only labelling patterns at PD35, represented 76% of total labelled HFs, and contained 2-5 X-Gal+ cells clustered around the club hair (Fig. 2.8D and 2.7H). These data were consistent with rare cell divisions (mostly 1-3) within the

Figure 2.9. Patterns of X-Gal staining in hair follicles in PD17-PD25 (early anagen), and position change of labelled cell in the bulge in PD17-PD21 chase to PD17-PD25 chase.

(A) Serial skin sections, 20 um thick, stained with hematoxylin (for contrast) and with X-gal, illustrate reconstruction of full HFs. HFs numbered 1-4 show different patterns, and are indicated by arrows in consecutive sections. (B) The 4 HFs indicated by arrows in A were shown at higher resolution. (C) Distribution of X-Gal patterns among a randomly selected pool of 36 HF reconstructed from serial sections. (D) A random pool of labelled hair follicles from PD17-PD21 and PD17-PD25 chases were analyzed for X-Gal patterns in 20mm skin sections. The HFs that showed only one bulge (Bu) X-Gal+ cell were analyzed for the position of the X-Gal+ cell in the bulge using the club hair and bottom of bulge as reference. The frequency of HFs with a X-Gal+ cell at a certain position was plotted for PD17-PD21 and PD17-PD25 respectively. The data demonstrates that all the X-Gal+ cells within the bulge undergo downward motions between PD21 and PD25. The presence of X-Gal+ cells on top of the DP in some HFs (Fig. 2.8G) suggests that the bulge cells somehow slide through the pre-existing X-Gal- cells to reach the DP, an observation that we attributed to active migration (see also text).

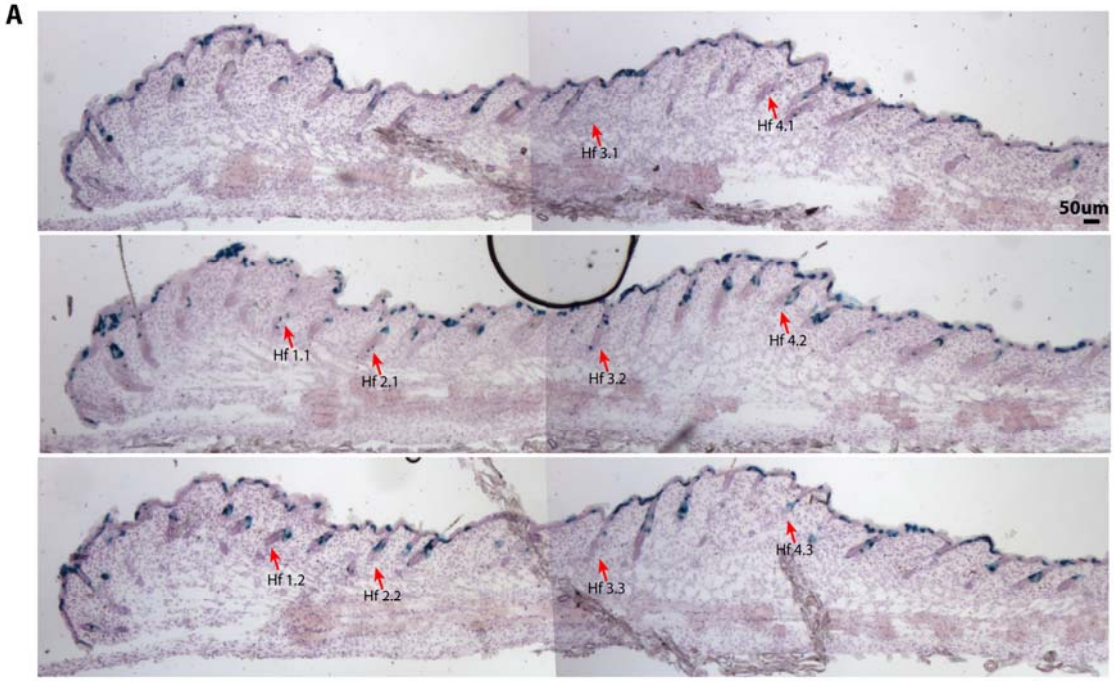

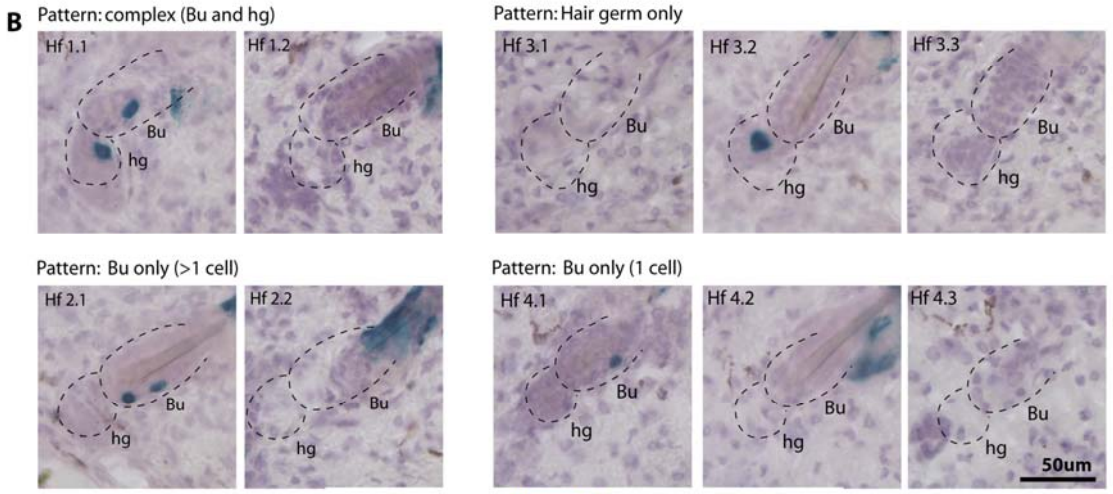

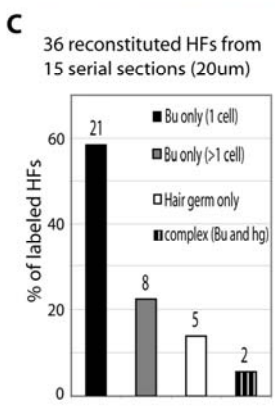

D

	Total Labelled HFs	Bu only (1 Cell)	Bu only (>1 Cell)	hair germ only	complex
PD21_TM17	132	102	29	0	1
PD25_TM17	211	122	35	39	15

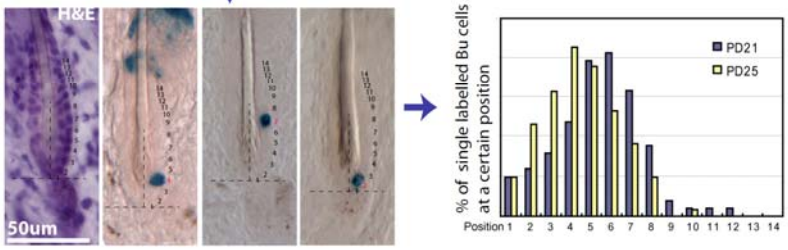

Figure 2.10. Multipotency of bulge cells *in vivo.*

(A) Hair bulb with indicated differentiated lineages. Outer root sheath (ORS); IRS (inner root sheath made of cuticle (C), Huxley (Hu), and Henle (He) cell layers); hair shaft "core" made of 3 cell layers: (Cu) cuticle, (Co) cortex, (Me) medulla. Cp is ORS companion layer, included with the IRS category for simplification. (B) Quantification of PD35 labelling patterns in mice injected with tamoxifen at PD17. Lineages containing X-Gal+ cells are indicated at bottom, shown with SEM in 3 mice (>60 labelled HFs/mouse). (C&D) X-Gal bulb-only patterns in thick (90mm) or thin (20mm) serial sections. Scale bar, 50mm. (E) Cross-sectional images of X-gal stained skin from PD17-PD35 chase 20mm shows multiple differentiated layers in a majority of HFs. Scale bar, 10 mm. (F) Patterns of labelling, with SEM shown as % of a defined pattern from total labelled HFs (N= 3 mice, > 200 labelled HFs/mouse).

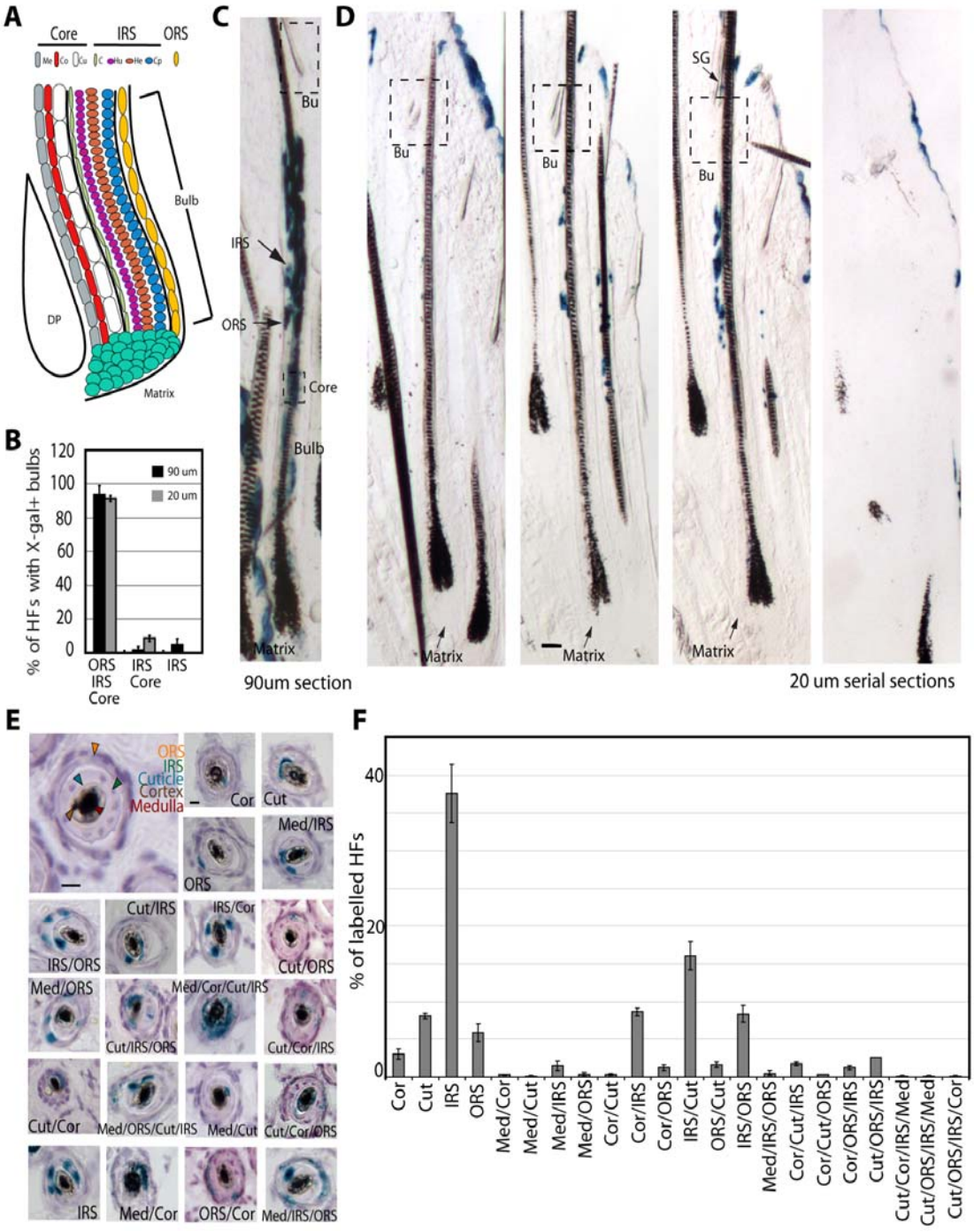
A
Core
IRS
ORS
Me Co Cu
C Hu He Cp
Bulb
DP
Matrix
B
% of HFs with X-gal+ bulbs
120
100
80
60
40
20
0
90 um
20 um
ORS
IRS
Core
IRS
Core
IRS
C
Bu
IRS
ORS
Core
Bulb
Matrix
90um section
D
Bu
Bu
Bu
SG
Matrix
Matrix
Matrix
20 um serial sections
E
ORS
IRS
Cuticle
Cortex
Medulla
Cor
Cut
Med/IRS
ORS
Cut/IRS
IRS/Cor
IRS/ORS
Cut/ORS
Med/ORS
Med/Cor/Cut/IRS
Cut/IRS/ORS
Cut/Cor/IRS
Cut/Cor
Med/ORS/Cut/IRS
Med/Cut
Cut/Cor/ORS
IRS
Med/Cor
ORS/Cor
Med/IRS/ORS
F
% of labelled HFs
40
20
0
Cor
Cut
IRS
ORS
Med/Cor
Med/Cut
Med/IRS
Med/ORS
Cor/Cut
Cor/IRS
Cor/ORS
IRS/Cut
ORS/Cut
IRS/ORS
Med/IRS/ORS
Cor/Cut/IRS
Cor/Cut/ORS
Cor/ORS/IRS
Cut/ORS/IRS
Cut/Cor/IRS/Med
Cut/ORS/IRS/Med
Cut/ORS/IRS/Cor

niche, in line with previous results from quantitative proliferation history (Fig. 2.1 and (Waghmare et al., 2008). The presence of multiple X-Gal+ cells confined to the bulge indicated that bulge cells divided within the niche and generated more bulge-cell progeny, but none of them left the niche within the first hair cycle. These data collectively provides evidence for divergent fate of individual bulge cells within one hair cycle to either: a) leave the niche, proliferate vigorously to generate many differentiated bulb cells at an earlier stage; b) remain in the SC niche (bulge), divide infrequently, generate more bulge cells and replenish the bulge pool (self-renew) at a later stage.

To further define these differentiation and self-renewal stages, we marked cells in the bulge before or after some of them departed the bulge (Fig. 2.8F). To do this we injected tamoxifen at PD21, after the bulge cell migrated into the HG, and examined HF labelling in PD21-PD25 and PD21-PD35 chases. We found comparable labelling efficiency with that obtained from previous chases (PD17-PD21 and PD17-PD35; Fig. 2.7E). Moreover, 99% of the PD21-PD25 labelled HFs displayed bulge-only patterns, 76% as single cells (Fig. 2.8G). Importantly, the bulge-only (self-renewal) pattern was more prominent in PD21-PD35 chase than in previous PD17-PD35 chase, while the bulb-only (differentiation) pattern was diminished by 3-fold (Fig. 2.8H). These results indicated reduction in bulge-cell differentiation fate choice by the time of early anagen onset and supported a temporal segregation of differentiation and self-renewal phases of bulge cells in telogen/anagen transition versus anagen.

Differentiation or self-renewal of long-term bulge residents throughout life

Our data thus far suggested a spatial and temporal divergent fate of bulge resident cells to either differentiate or self-renew. However, the bulb-only pattern,

indicative of unidirectional differentiation fate, might arise from direct X-Gal labelling of a putative short-lived progenitor cell temporarily residing in the bulge rather than from the SC itself. These progenitors could be generated in anagen by the asymmetric divisions of the true long-lived SCs, and could remain confined to the bulge until the next telogen-anagen transition. In this scenario, the true SCs might only exist among the X-Gal+ cells that self-renewed in anagen by divisions and survived in HFs through at least one hair cycle. If these SCs behaved by an asymmetric cell fate decision model, then we should always detect complex patterns in the subsequent hair cycles. However, if the SCs undergo unidirectional or symmetric fate decisions, we may still detect bulb-only patterns in which the originally labelled cell, and all of its bulge-progeny altogether decide to leave the bulge pool, without maintaining any replenishing descendants behind in the niche.

To follow the fate of bulge-derived cells in long-term we analyzed X-Gal patterns in mice sacrificed at different time points after the first hair cycle, up to 1 year of life (Fig. 2.11A). We first checked skin sections at PD49 in early telogen, which follows the massive bulb apoptosis that occurred in catagen. When we compared the overall frequency of marked HFs before catagen (PD35) and after catagen (PD49), we found a 4% overall drop, accounting for a loss of ~17% of the labelled HFs (Fig. 2.11D). Since at PD35 17% of HFs showed bulb-only labelling patterns, these data suggested that all X-Gal+ bulb cells died in the massive apoptosis detected in the bulb in catagen. If some X-Gal+ bulb cells in each HF survived catagen to make a new HG, as previously proposed (Jaks et al, 2008), we would expect a substantial fraction of HFs (17% of the PD35 bulb-only labelled follicles) to show exclusive X-Gal labelling in HGs at PD49. However, we found no HFs with exclusive HG labelling pattern (Fig. 2.11C). Furthermore, at PD49 the surviving X-Gal+ cells were found exclusively in the bulge in ~99% of labelled HFs and in bulge and HGs in the

Figure 2.11. Long-term single-bulge cell lineage tracing.

(A) Scheme of 1st telogen labelling and long-term chases. (B,E&H) Illustrative images from thick (60-90 um) skin sections show X-Gal staining in bulge (Bu) (yellow line) and bulb/germ (white line) compartments. Image in (E) shows a rare patch of frequent HF induction illustrating the coexistence of all 3 staining patterns in one skin region. Image in H shows bulb-only and bulge-only patterns after one year and at least 3 hair cycles post-labelling. The predominant patterns were complex (see counts in F). Scale bars, 50 um. (C&F) Quantification with SEM of X-Gal patterns at stages indicated. (D&G) Frequency of all labelled follicles counted at each stage (from data in Fig 2.8&2.11) show significant decline from one hair cycle to another.

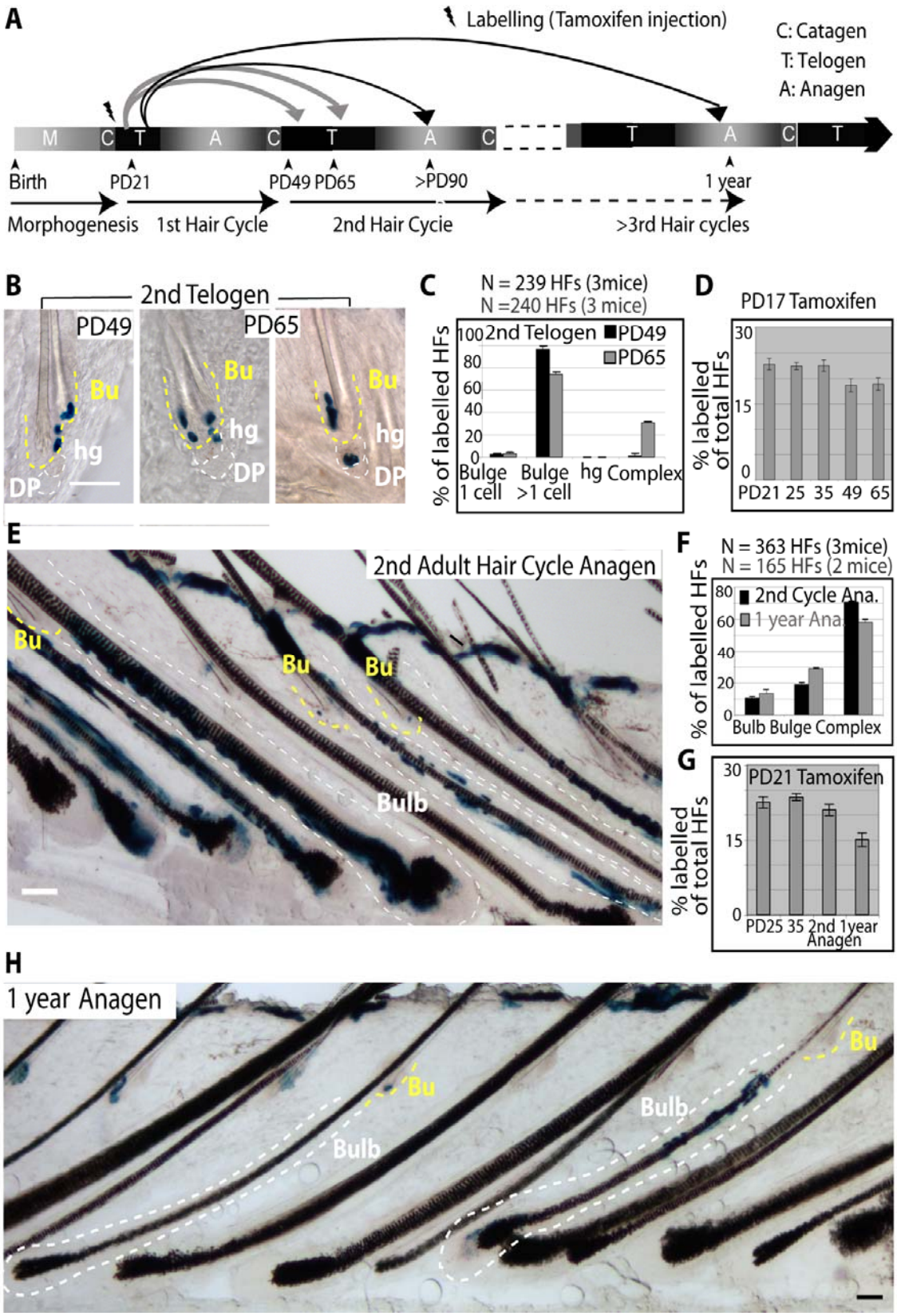
A
Labelling (Tamoxifen injection)
C: Catagen
T: Telogen
A: Anagen
M C T A C T A C T A C T
Birth
PD21
PD49 PD65
>PD90
1 year
Morphogenesis
1st Hair Cycle
2nd Hair Cycie
>3rd Hair cycles
B
2nd Telogen
PD49
PD65
Bu
hg
DP
C
N = 239 HFs (3mice)
N =240 HFs (3 mice)
% of labelled HFs
2nd Telogen
PD49
PD65
Bulge 1 cell
Bulge >1 cell
hg
Complex
D
PD17 Tamoxifen
% labelled of total HFs
PD21 25 35 49 65
E
2nd Adult Hair Cycle Anagen
Bu
Bulb
F
N = 363 HFs (3mice)
N = 165 HFs (2 mice)
2nd Cycle Ana.
1 year Ana.
Bulb Bulge Complex
G
PD21 Tamoxifen
PD25 35 2nd 1year Anagen
H
1 year Anagen

remaining ~1% (Fig. 2.11B,C). The X-Gal+ bulge clone size was on average ~ 4 cells (N=61 HFs) roughly comparable with the bulge clone size at PD35. By PD65, in late second telogen when bulge cells are still in divisional quiescence, we detected X-Gal+ cells in both bulge and HGs in ~24% of labelled HFs (complex pattern; Fig. 2.11B,C). The bulge-only pattern decreased proportionally at PD65 relative to PD49 to 74% of the labelled HFs. These results indicated that bulge-cells left the niche again in quiescence during the second telogen, re-iterating their earlier behaviour.

In second anagen (PD90) or after 1-year, ~70% of labelled HFs showed mainly complex patterns (Fig. 2.11E-H). These results demonstrated the contribution of the originally single labelled bulge cells to all hair compartments including their own, after repeated cycles of regeneration, a hallmark of SCs. The remaining HFs showed bulge-only (19-29%) or bulb-only (11-13%) labelling patterns, in thick (90μm) or thin serial sections (Fig. 2.11E,F,H; 2.12). The bulb-only pattern is indicative of unidirectional fate decision for the long-lived self-renewing bulge cells to leave their niche and differentiated into the bulb. The bulge-departed cells were likely lost in the bulb by differentiation and apoptosis as supported by the incremental decline in frequency of labelled HFs from one hair cycle to another (Fig. 2.11G).

Figure 2.12. Patterns of X-Gal staining in hair follicles after long-term chases.

(A) Bulge and bulb only patterns in 1 year anagen shown in thick (90um sections) within the same skin area. (B) Thin 20 mm serial sections stained with hematoxylin and X-gal staining in 1-year in anagen, illustrates bulge and bulb-only patterns. These patterns could be reconstructed in 3 serial sections from a random pool of ~25 labelled HFs localized near the edge of the sections, which served as a landmark (not shown). Asterisk in B, bottom left panels, indicates X-Gal staining in the upper region of the club hair, outside the bulge area.

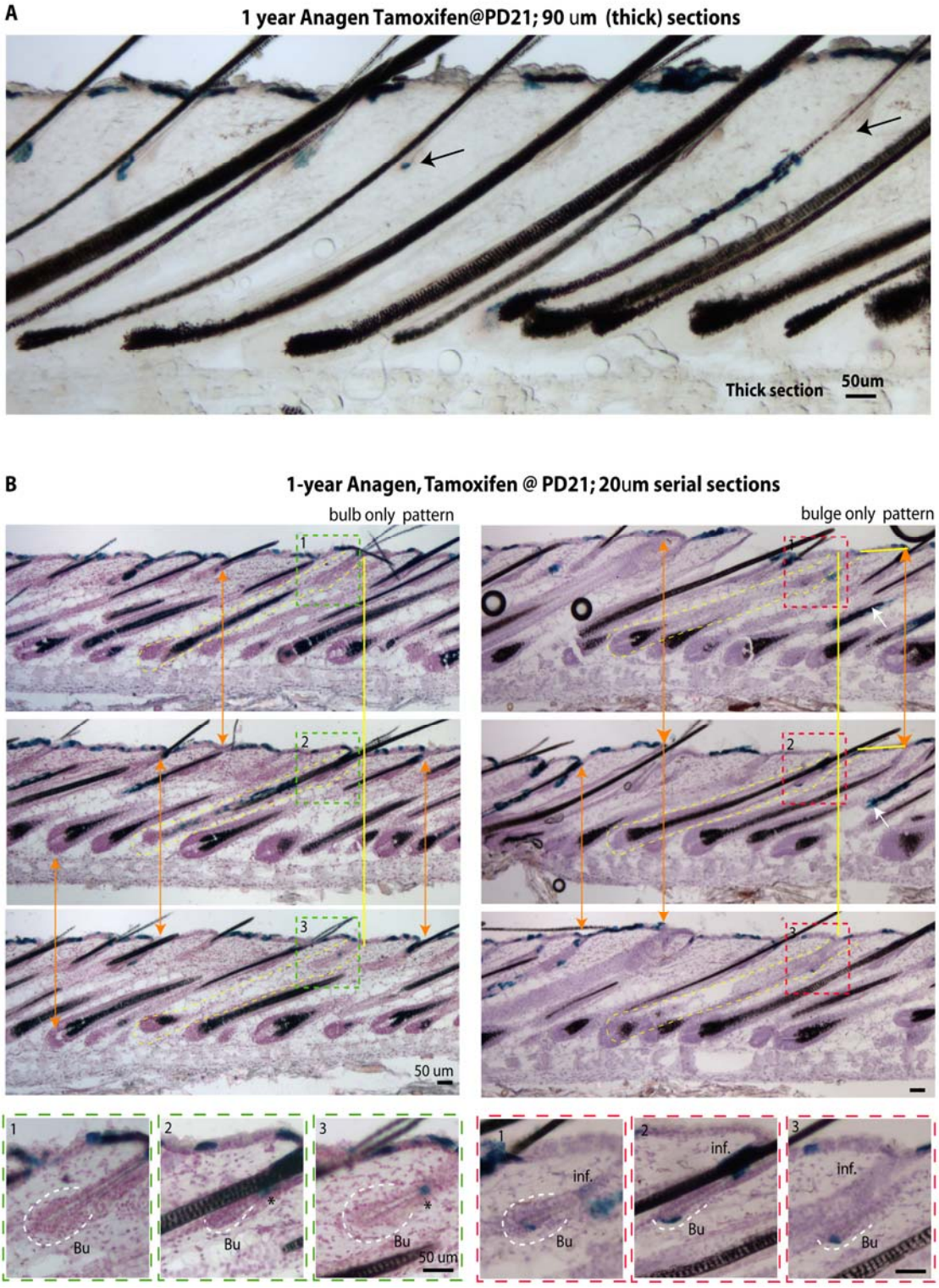
A
1 year Anagen Tamoxifen@PD21; 90 um (thick) sections
Thick section
50um
B
1-year Anagen, Tamoxifen @ PD21; 20um serial sections
bulb only pattern
bulge only pattern
1
2
3
50 um
Bu
inf.
*

Discussion

Single-cell fate tracing in intact vertebrate tissue confirms the "slow-cycling" SC model

The "slow-cycling" SC model states that cells with infrequent divisions contribute to normal homeostasis of adult tissues. Most evidence at the single cell supporting this model comes from blood and hair follicle *in vitro* transplantation assays (Blanpain et al., 2004; Foudi et al., 2009; Wilson et al., 2008). Recent evidence from unperturbed tissue employing lineage tracing in epidermis, hair follicle, and intestine seemed to challenge this model (Barker et al., 2007; Clayton et al., 2007; Jaks et al., 2008). Here we provide evidence from an intact vertebrate tissue, at the single cell level and in long-term assays, for the infrequent division model in hair follicle bulge stem cells.

We employed mice with repressible H2B-GFP expression (Tumbar et al., 2004) to determine proliferation kinetics, gene expression, and cell identity data. Furthermore, we used epithelial driven inducible K14-CreER transgenic mice (Vasioukhin et al., 1999) to genetically mark single bulge cells and follow their fate during adult hair regeneration. We found that in the bulge, single X-Gal+ cells generated ~2-5 progeny during anagen, which remained confined to the bulge in ~70% of labeled HFs, and were not exported in the bulb during that same anagen. This suggested infrequent (mostly 1-3) anagen divisions, in line with our H2B-GFP division counts (Fig. 2.1 and (Waghmare et al., 2008). The newly generated bulge cells at anagen preserved the known bulge characteristics, as shown by location, kinetics of divisions, and gene expression profiles, therefore self-renewing and expanding their own pool. In the next two anagen phases analyzed here, ~70% of

these cells generated progeny which contributed to all differentiated bulb lineages, while maintaining long-term progeny as bulge residents (complex X-Gal patterns; Fig. 2.11E,F). Thus, we conclude that a majority of these long-lived infrequently dividing (bulge) cells differentiate and self-renew (although not necessarily by asymmetric division; see below), a hallmark of multipotent SCs. In the bulb, bulge-derived progeny behaved as bona fide multipotent progenitor (transit amplifying) cells, generating large clones of hundreds of X-Gal+ cells in only 2 weeks (PD21-PD35). Finally, the bulb cells derived from the bulge did not survive in the bulb past the apoptotic (catagen) phase to make the hair germ (HG). This was suggested by lack of exclusive HG labelling patterns and little (<1%) HFs with complex bulge and HG labelling in the second telogen, and by the incremental decrease in overall labelled HFs from one hair cycle to another by a fraction numerically consistent with the frequency of bulb-only patterns detected in the previous cycle.

LGR5 was reported as a germ-specific gene in catagen, presumably marking preferentially frequently cycling cells (Jaks et al., 2008). However, we detected LGR5 mRNA expression in CD34+/α6+ bulge cells at all hair cycle stages, although the levels were lower in anagen. In catagen, expression was variable in cells with 0-1 divisions, but strong in cells with only 2-3 divisions after one complete anagen (Fig. 2.3E). These observations confound the interpretation of recently published lineage-tracing data. That said, the bulge cells fate-mapped in our present study via Cre recombination contributed to Mx and inner hair lineages but not to the early telogen HG, suggesting that unlike the Mx, the HG might be a bulge-independent lineage. These data might suggest a possible direct lineage relationship of HG to make most of the ORS, and of bulge to make Mx and some ORS. ORS and Mx cells were maintained as independent progenitors as shown by lineage tracing in anagen (Legue et al., 2005). This possibility requires further experimental testing via a germ specific

Cre-driven recombinase. Importantly, the majority of lower ORS cells dilute rapidly BrdU or H2B-GFP label, while surviving bulge and some germ cells retain significant label after one hair cycle (Cotsarelis, 2006; Greco et al., 2009; Ito et al., 2004; Tumbar et al., 2004). We quantified that here (Fig. 2.2A; Fig. 2.5B-G) and found that all HG cells divided in fact infrequently, only 2-5x during one hair cycle (Fig. 2.5G). Thus, if a putative lower bulb traveling HG "cycling" population existed (Greco et al., 2009; Jaks et al., 2008), would differ from a "dormant" bulge population by a mere 1-2 divisions, since bulge cells divide on average ~ 3x (Waghmare et al., 2008). Our previous experiments utilizing BrdU and H2B-GFP pulse-chase demonstrated that a few extra divisions are sufficient to dilute BrdU beyond detection (Waghmare et al., 2008), which can lead to miss-interpretation of the results from BrdU label retention experiments. We conclude that all the surviving cells in the permanent HG segment are in fact infrequently dividing. Given an estimate of ~ 10 hair cycles in a lifetime they divide altogether ~30-50 times, while some of them divided much fewer times.

Intriguingly, our H2B-GFP chases documented that most bulge divisions occur over a short period of only several days and bright H2B-GFP LRCs group on one side of the bulge (examples in Fig. 2.5). These data suggested a potentially short-lived inductive polarized signal, which may awaken bulge cells to rapidly proliferate for a few days and then return to quiescence. The activation signal has been proposed to travel as a wave across the body (Plikus et al., 2008) and may be relayed from follicle to follicle. It is possible that a few bulge cells, potentially similar to the BMI-1 expressing cells at the +4 position in the intestine, may remain relatively unused in normal tissue growth (Jaks et al., 2008; Morris and Potten, 1999), and may account for a fraction of the bulge-only patterns detected in our long-term assays. These cells need not represent a distinct population and do not remain quiescent, but may simply

divide fewer times due to their farther position relative to some diffusible activation and migration signals.

The HFSC niche displays distinct differentiation and self-renewal stages

During telogen-anagen transition HG cells divide first while bulge cells follow later in anagen (Cotsarelis, 2006; Greco et al., 2009). However, data have been lacking as to whether bulge cells would constantly export the newly generated putative progenitor cells into the bulb upon each division. Such export would be expected from a simple relationship of the stem and progenitor cells with the resident niche (bulge), as predicted from an asymmetric fate decision documented by early work in *Drosophila* (Morrison and Kimble, 2006). Our data clearly showed that upon division in anagen bulge-cell progeny were not immediately exported into the bulb, but rather remained confined to the niche (70% bulge-only patterns in first anagen) where they retained the bulge-specific characteristics, and finally returned to quiescence. Therefore in anagen the bulge cells divided and produced more of their kind, self-renewing their pool. To replenish the tissue, the bulge cells departed the niche at a different stage (telogen), in quiescence, and did not simultaneous self-renew the bulge pool by divisions. Once outside the niche the bulge-derived cells subsided to a fate of proliferation, differentiation, and death in the bulb as suggested collectively by all of our data including lineage-tracing experiments. From early anagen (PD25) to late anagen (PD35) the frequency of HFs with any germ/bulb labelling remained nearly constant, another indication that in anagen bulge cell divisions did not significantly contribute differentiated progeny cells to the bulb (Fig. 2.8E). Moreover, telogen resident bulge cells showed 3x higher propensity to depart the niche and differentiate than early anagen bulge cells (Fig. 2.8F-H). These data collectively suggest that individual cells within the HFSC niche, the bulge, are assigned distinct fates to either

leave the niche and differentiate, or stay in the bulge and self-renew the pool at different time points in homeostasis (Fig. 2.13A). The HFSC niche displays distinct stages of differentiation and self-renewal, which occur in telogen and telogen/anagen transition and in anagen, respectively. Progenitor cell differentiation takes place at distinct times and tissue location from the self-renewal of SCs. This model is consistent with the previous results from long-term *in vitro* assays on whisker bulge cells (Claudinot et al., 2005; Oshima et al., 2001). We speculate that the spatial-temporal segregation of self-renewal and differentiation may ensure protection of the SC niche from penetration of cell differentiation tissue signals.

Symmetric fate decisions for stem cell daughters: Future lessons for SCs dynamics throughout life

Our data provide information on the long-term dynamics and interplay of fate decision that SCs face in a complex tissue in adult life. Let us assume a rigid model of asymmetric bulge SC fate decisions during adult homeostasis (Morrison and Kimble, 2006), in which the SC is permanently retained inside the niche (bulge) and the progenitor is eventually (after a lag period in our system) exported outside the niche. Then, marked bulge cells, which previously self-renewed in the niche in the first anagen and survived catagen death, qualifying as SCs, should always replenish the bulge with cell progeny in the later hair cycles. Therefore we should not detect patterns in which all bulge SC descendants left the bulge niche to differentiate into the bulb. However, in our experiments we detected a significant fraction of bulb-only labelling patterns (11-13%) in the second anagen and even one year post-labelling. Since the original labelling was nearly 100% bulge specific, this indicated that a substantial fraction of self-renewing, long-lived bulge cells exited the niche and differentiated into the bulb without leaving any surviving descendants behind in the

Figure 2.13. Dynamics of hair follicle bulge stem cells during tissue homeostasis.

(A) The bulge cells undergo distinct phases of differentiation and self-renewal. First, at the telogen-anagen transition bulge cells depart the niche, proliferate and begin to differentiate to matrix progenitors of inner hair lineages. Second, bulge cells replenish their pool by divisions in anagen (self-renew), when newly generated bulge cells remain in the niche during the same hair cycle. (B) Models for adult SC renewal by illustrating symmetric (top) and asymmetric (bottom) divisions, and the predicted organization and dynamic of stem/progenitor cells in the niche in each scenario. Loss of SC identity may occur outside the niche (bulge) before or after the first differentiating division.

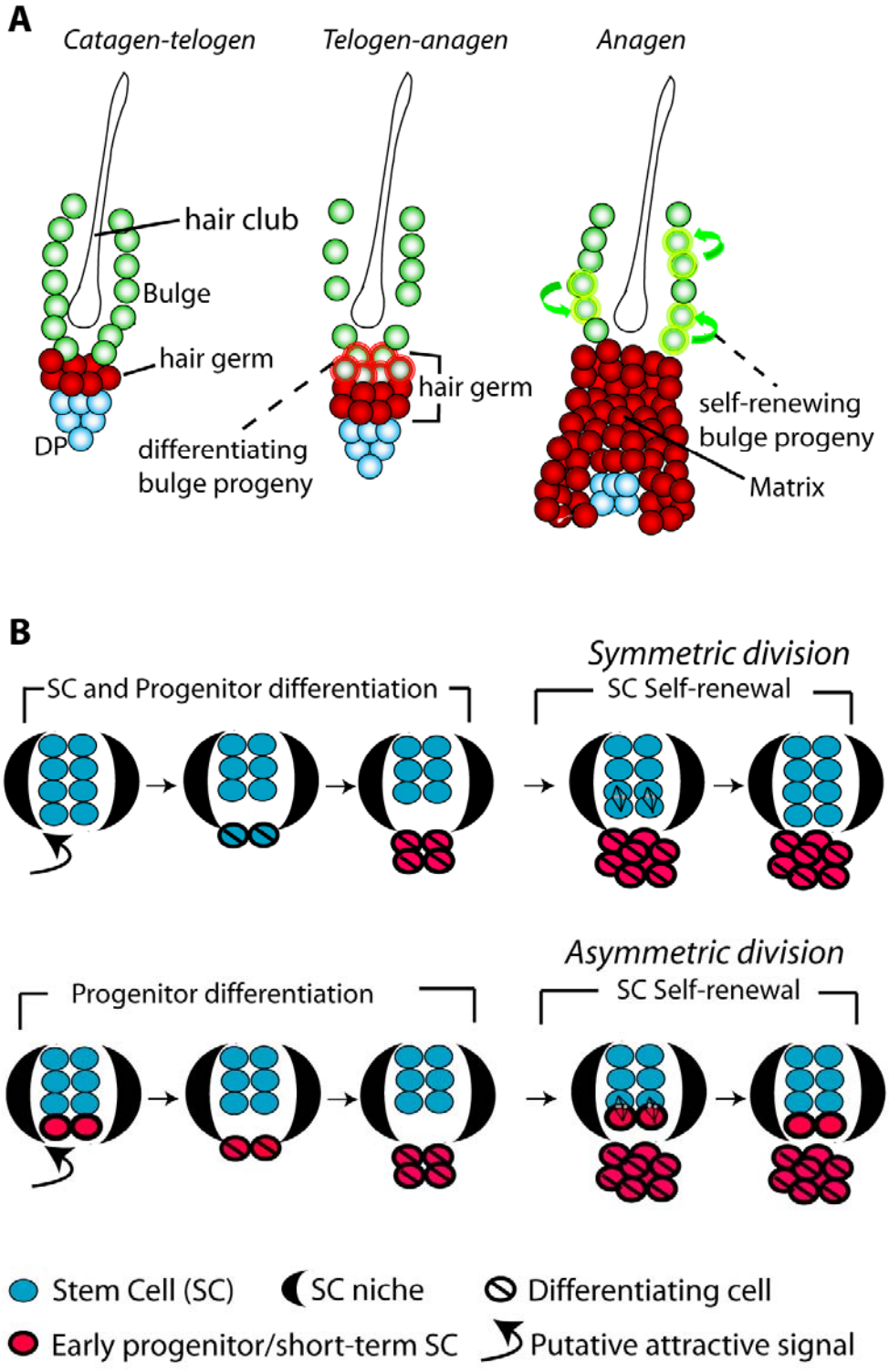
A
Catagen-telogen
Telogen-anagen
Anagen
hair club
Bulge
hair germ
DP
differentiating
bulge progeny
hair germ
self-renewing
bulge progeny
Matrix
B
Symmetric division
SC and Progenitor differentiation
SC Self-renewal
Asymmetric division
Progenitor differentiation
SC Self-renewal
Stem Cell (SC)
SC niche
Differentiating cell
Early progenitor/short-term SC
Putative attractive signal

niche (Fig. 2.11). Bulb descendants of these cells most likely did not survive in the follicles to make the new HGs, as explained above. Bulge cell death in catagen (Cotsarelis, 2006) may also contribute indirectly in the long-term to the overall loss of labelled HFs, by reducing the frequency of X-Gal+ cells per bulge. Why would infrequently dividing bulge cells divide a few more times to generate more progeny than needed to repopulate the new bulge just to die later on? The explanation may be in a safety mechanism that insures enough bulge cells were generated prior to their return to quiescence. These cells would re-organize around the additional hair club in catagen, while the surplus cells would die. The collective loss of bulge cells by migration and differentiation documented here potentially combined with some apoptosis accounted for approximately one third of the original labelling by one year of chase. This suggested a massive loss of SCs from the pool via a unidirectional, or symmetric fate decision of SC daughters towards a non self-renewing fate. Given the magnitude of this loss, if the SC pool size were to be grossly maintained over lifetime, then a compensation mechanism for this incremental SC decline would be required.

First, the simplest compensation mechanism that best fits our data would implicate in part or entirely symmetric self-renewing SC daughter fates in adult homeostasis (Fig. 2.13B, top). Such a mechanism was also suggested for at least a fraction of adult inter-follicular epidermis SCs (Clayton et al., 2007), and for other SCs in embryogenesis or in injury (Morrison and Kimble, 2006). Our data are consistent with a population model for tissue homeostasis, similar with that proposed for the *C. elegans* germ line (Morrison and Kimble, 2006), another system besides HF with a cluster of relatively many SCs. In a population model individual HFSCs have equal potential to replenish the pool through symmetric division in the niche (in anagen) or to be exported (in telogen), proliferate, differentiate, and eventually die. Assignment to one of these two fates would likely depend upon the distance of

individual SCs from the signalling centre (in this case the DP). In contrast, in systems where only few SCs are found in a niche, such as the *Drosophila* germ line, the tissue must insure that self-renewal occurs before a SC may leave the niche compartment to be lost in the differentiating region. The applicability of this model to other adult vertebrate tissues with clustering SCs will have to be addressed experimentally in the future.

Second, if asymmetric divisions were strictly imposed onto SCs in adult homeostasis (Fig. 2.13B, bottom), in light of our data, progenitors would be constantly required to de-differentiate at each regenerative cycle to compensate for the substantial incremental SC loss documented here. In this scenario, mutual interchange between progenitor and SC populations could be more extensive than previously recognized, potentially obscuring the distinction between these predicted cell types.

Conclusions

Here we provide evidence from an intact adult vertebrate tissue, at the single cell level and in long-term for the infrequently dividing "slow-cycling" stem cell model. In addition, we showed that differentiation and self-renewal in the hair follicle stem cell niche are spatially and temporally segregated during hair cycle. Finally, our data are consistent with a stem cell population fate deterministic model involving, at least in part, unidirectional fate decisions of stem cell daughters upon divisions.

CHAPTER 3

STEM CELL DYNAMICS IN MOUSE HAIR FOLLICLES: A STORY FROM CELL DIVISION COUNTING AND SINGLE CELL LINEAGE TRACING

Summary

Understanding tissue stem cells behavior is a prerequisite for elucidating the mechanisms that govern their self-renewal and differentiation. Previously, we provided single cell lineage tracing and proliferation history data (based on H2B-GFP label dilution over time) in mouse hair follicles. We proposed a population deterministic model with symmetric stem cell fate decisions throughout life. Here we provide data suggesting that in hair follicle stem cells the self-renewing divisions within the niche (bulge) are symmetric with respect to localization of daughter cells near the basement membrane, an important niche component. In contrast, when cells migrate from the niche to the differentiating zone where they become short-lived progenitors, their daughter cells can adopt asymmetric orientation relative to the basement membrane. Furthermore, we document the dynamic re-localization of cells within the bulge to accommodate the hair follicle morphological changes through hair cycle. In addition, we provide a method to compute the change in number of minimum cell loss encountered when the fold change can be experimentally determined. We computed a minimum of 42% of bulge cell loss during one hair cycle, a massive rate

---

This chapter has been published in Cell Cycle (Zhang, Y.V., White, B.S., Shalloway, D.I., and Tumbar, T. (2010).Cell Cycle 9, 1504-1510.), and is reprinted with permission. The following is detailed contribution of authors: Tumbar T and Zhang YV designed the experiments and analyzed the data. Zhang YV performed the experiments presented in Fig. 3.1-4. White BS and Shalloway DI performed the mathematically modeling, made Fig. 3.5, and wrote the modeling section of the text. Zhang YV and Tumbar T made the Fig. 3.1-4 and wrote the rest of the paper.

of loss previously unrecognized. Finally, we showed that a multipotent population of cells found at the junction zone between hair follicle and epidermis, known to express Lrig1, cycle more rapidly than some other hair follicle compartments.

Introduction: Symmetric daughter-cell fate decisions for infrequently dividing hair follicle stem cells

Regenerative tissues contain stem cells (SCs) that self-renew and differentiate for an extended period of time. In normal tissue homeostasis SC division is thought to be infrequent and to involve an asymmetric daughter-cell-fate decision, in which one daughter remains a SC while the second partially differentiates into a progenitor cell with short-term growth potential (Dor and Melton, 2004; Fuchs, 2009; Morrison and Kimble, 2006). This model was recently challenged by lineage tracing data in the undisturbed mouse epidermis, hair follicle, and small intestine (Barker et al., 2007; Clayton et al., 2007; Jaks et al., 2008).

In mouse skin, adult hair follicles undergo synchronous and periodic regeneration during the hair cycle, which consists of three morphologically distinct stages: quiescence (telogen), growth (anagen), and apoptotic regression (catagen) (Cotsarelis, 2006). The hair is composed of a temporary differentiated region known as the bulb and a permanent un-differentiated region known as the bulge. The bulb contains progenitor matrix cells that differentiate into inner layers, including the hair shaft, and that undergo apoptosis during catagen. The bulge contains most of the hair follicle's infrequently dividing cells (Ito et al., 2004; Taylor et al., 2000), and its residents contribute to hair growth in transplantation assays (Blanpain et al., 2004; Claudinot et al., 2005; Hoffman, 2006; Morris et al., 2004). The hair germ is thought

to at least temporarily contain SCs (Greco et al., 2009; Jaks et al., 2008), and seems to arise from the bulge when its cells collapse around the hair club at the end of catagen (Ito et al., 2004). Lineage tracing marking of bulge and germ cells also indicates that this region contains SCs (Jaks et al., 2008; Morris et al., 2004).

In a recent study we employed two experimental approaches to elucidate SC dynamics, the fate decision mechanism, and division rates in mouse hair follicles (Zhang et al., 2009). First, we used double transgenic K5tTA x pTRE-H2B-GFP mice (Tumbar et al., 2004) to identify and trace H2B-GFP label-retaining cells in the bulge and hair germ at distinct stages of tissue homeostasis. We found that upon feeding mice doxycycline (chase) to shut off H2B-GFP expression, the protein is diluted 2-fold following each division (Tumbar et al., 2004; Waghmare et al., 2008). By a series of chase experiments across all stages of the first hair cycle and a combination of Fluorescence Activated Cell Sorting (FACS) and confocal microscopy, we quantified bulge cell proliferation at different stages and confirmed the infrequently dividing nature of both bulge and hair germ cells (Zhang et al., 2009). Moreover, we employed single bulge-cell lineage tracing using inducible K14CreER transgenic mice crossed with a Rosa26R reporter line (Vasioukhin et al., 1999). Tamoxifen injection induces Cre recombinase to enter the nucleus where it initiates production of β-galactosidase (LacZ), which turns the cell blue upon X-gal staining (Soriano, 1999). We found that singly labeled bulge cells either leave their niche to differentiate and eventually die or stay in the niche to self-renew (Zhang et al., 2009). Collectively our findings are consistent with a population deterministic model that involves a symmetric daughter-cell-fate decision for bulge SC descendants. We proposed that, to avoid exhausting the small (1-2 cell) pool of SCs comprising a "simple" niche, as defined by Spradling et al. (Spradling et al., 2001), a SC cannot leave it without first dividing to replenish and self-renew the remaining SC population (Fig. 3.1). A

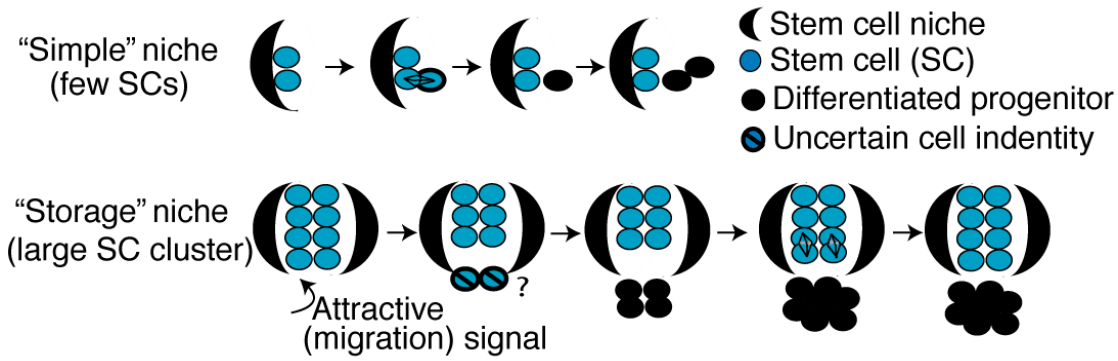

Figure 3.1. Stem cell niche models.

In "simple" niches stem cells divide asymmetrically to make one stem cell daughter and a committed progenitor daughter. In "storage" niches stem cells near the niche boundary respond to the attractive signal by migrating out of the niche and subsequently differentiating. Remaining stem cells divide symmetrically to replenish the stem cell pool.

"storage" niche (Spradling et al., 2001), such as the hair follicle, is instead supported by large groups of clustered SCs, with residents behaving as a population in a manner similar to that proposed for the *C. elegans* germ line (Morrison and Kimble, 2006). Individual SCs have equal potential to replenish the pool through division in the niche or to migrate away, proliferate, differentiate, and eventually die. Assignment to one of these two fates is likely dependent upon the distance of individual SCs from the signaling center (Fig. 3.1), which in the hair follicle is likely the dermal papilla (a mesenchymal structure at the base of the epithelial portion of the hair follicle).

Here we explore in more depth the nature of bulge cell division and the proliferation dynamics for a recently described multipotent cell population in the upper hair follicle (Jensen et al., 2009). Moreover, we provide a mathematical approach for estimating the expansion in number of bulge cells due to division based on H2B-GFP dilution data.

Materials and Methods

Transgenic mice

All experiments were approved by Cornell IACUC and carried out using standard procedure, as described (Waghmare et al, 2008). We generated Tet-off H2B-GFP mice by crossing hemizygous pTRE–H2B–GFP (Tumbar et al., 2004) (CD1) and K5tTA (FVB1) mice and identified GFP-expressing animals with an ultraviolet-based portable lamp (BLS Ltd). Mice were fed with 1 g doxy/kg mouse chow (Bio-serv), and sacrificed at various time points. For lineage tracing, we crossed K14-CreER (Vasioukhin et al., 1999) or K14CreERT2 (Li et al., 2000) and Rosa26R (Soriano, 1999) mice, and genotyped with PCR using CRE primers (5'-GCG GTC TGG CAG TAA AAA CTA TC-3', 5'-GTG AAA CAG CAT TGC TGT CAC TT-3'). Tamoxifen

delivered intraperitoneally to induce labelling (100 ug/g body weight) was dissolved in corn oil.

Tissue Staining and Microscopy

Staining procedure for immunofluorescence and Hematoxylin and Eosin (H&E) were as described previously (Tudorita Tumbar and Fuchs, 2006). Nuclei were labeled by 4',6'-diamidino-2-phenylindole (DAPI). Primary antibodies: α6 integrin (1:100, BD Pharmingen), CD34 (1:150, BD Pharmingen) and BrdU (1:300, Abcam), active capase 3 (1:500, R&D Systems), Ki67 (1:100, Novocastra), Secondary antibodies were coupled to the following fluorophores: FITC, Texas-Red or Cy5 (Jackson Laboratories). For X-gal staining, frozen skin sections were fixed 1 hr in 4% paraformaldehyde at 4°C, PBS washed 3x30 min., stained 24hrs at 37°C with X-gal buffer (Osorio et al., 2008), and incubated 3 hrs in 1M Na2CO3 to maximize sensitivity (Tanahashi and Tabira, 2000). For immuno-fluorescence and X-gal staining, images were acquired using the IP-Lab software (MVI) on a light fluorescence microscope (Nikon) equipped with a CCD 12-bit digital camera (Retiga EXi, QImaging). For confocal microscopy, frozen tissue sections (100 um) were fixed for 1 h in 4% paraformaldehyde and stained overnight with TOPRO3 (1:2000 dilution; Invitrogen). Confocal Z-sections were collected using a Leica microscope with details described in (Osorio et al., 2008; Waghmare et al., 2008).

Results

Divisions with respect to the basement membrane are largely asymmetric in the hair germ and symmetric in the bulge

Skin epithelium SCs are found among the basal layer cells, which express α6 /β4 integrins and contact the basement membrane (BM) (Fuchs and Raghavan, 2002), a location important for SC maintenance (Hynes, 2009). When the mitotic spindle of a basal layer cell orients perpendicularly to the BM the distal daughter cell differentiates (Lechler and Fuchs, 2005). Here we examined the placement of two bulge or germ daughter cells with respect to the BM.

Previously, we found that in K14CReER x Rosa26R mice 76% of labeled hair follicles had single cell labeling in a postnatal day (PD)17-21 chase (Zhang et al., 2009). Thus, we assume that most cell doublets found in the hair follicle at later stages are the two daughters descending from one cell division. We analyzed 53 hair follicles at PD25 with doublets in the hair germ and found that ~41% of the doublets showed perpendicular orientation to the BM (Fig. 3.2A). Assuming hair follicle cells differentiate after losing contact with the BM, as in the epidermis (Fuchs, 2009; Lechler and Fuchs, 2005), we speculate that a bulge cell entering the hair germ can either divide symmetrically along the BM to expand the outer root sheath, or asymmetrically to produce a differentiating inner layer cell along with a renewed hair germ/matrix progenitor. We also analyzed 74 hair follicles containing X-Gal+ doublets in the bulge at PD35 (during full anagen, following bulge cell division) and found ~81% of them parallel to the BM (Fig. 3.2B). These results suggest a strong bias for symmetric bulge cell division with respect to BM orientation of daughter cells (see Discussion).

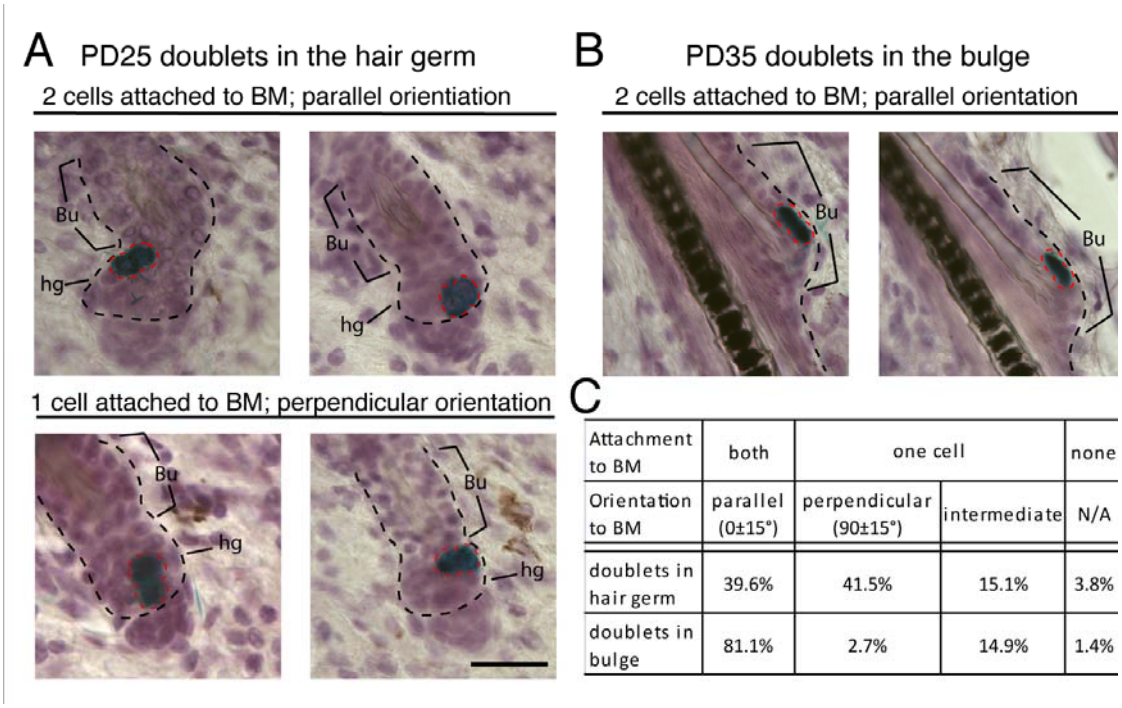

Attachment to BM	both	one cell		none
Orientation to BM	parallel (0±15°)	perpendicular (90±15°)	intermediate	N/A
doublets in hair germ	39.6%	41.5%	15.1%	3.8%
doublets in bulge	81.1%	2.7%	14.9%	1.4%

Figure 3.2. Placement of two bulge daughter cells with respect to the niche.

Skin sections (20 μm) from K14CreER x Rosa26R mice (injected with tamoxifen at PD17 and stained for X-Gal and hematoxylin at days indicated) show doublet orientation with respect to the basement membrane (BM) and in two distinct compartmets: the differentiating zone (hair germ) and the stem cell niche (bulge). (A) Bulge cells exported in the germ divided both parallel (top) and perpendicular (bottom) with respect to the BM. (B) Bulge cells that continue to reside in the niche divided parallel to the BM. (C) Quantification of data in (A&B). BM, black dotted lines; Bu, bulge; hg, hair germ. Scale bar, 50 μm. N=127 hair follicles.

The bias towards bulge-cell labeling is Cre transgenic line dependent

Single cell lineage tracing is a powerful approach for studying SCs *in vivo*, but appropriate tools are lacking in most systems. Lineage tracing was possible in hair follicles because K14CreER labeling in our transgenic line occurs with low efficiency and, in telogen, is biased towards the bulge over the hair germ, despite the expected activity of the K14 promoter in both compartments and the demonstrated activity of the Rosa26 promoter in the hair germ of constitutively active K14Cre mice (Vasioukhin et al., 1999). To test whether germ cells are less responsive to tamoxifen, we examined a second K14CreER mouse transgenic line (a gift from Dr. Pierre Chambon) referred to as K14CreERT2 (Li et al., 2000). We found that in K14CreERT2 x Rosa26R mice, all skin epithelium compartments including the hair germ, were fully induced after 4 days (Fig. 3.3) throughout most of the skin. This suggests that the preference for bulge labeling is transgenic line dependent. We again found preferential bulge labeling in a third transgenic line, in which Cre is not driven by the K14 promoter and is expected to be expressed at low levels in the bulge and germ (unpublished data). We speculate that at low levels of Cre recombinase expression the bulge cells are more easily marked, possibly due to a more open chromatin structure in these cells relative to hair germ cells. Future studies on selected transgene insertions should facilitate single cell lineage tracing in other SC systems.

Proliferation dynamics at the hair follicle junctional zone reveals higher activity when compared to the bulge

Using the H2B-GFP inducible expression system, we previously quantified the proliferation history of a CD34+/a6-integrin+ bulge cell population by flow cytometry, and of single bulge and germ cells in situ by confocal optical sectioning of thick skin sections (Waghmare et al., 2008; Zhang et al., 2009). These data confirmed

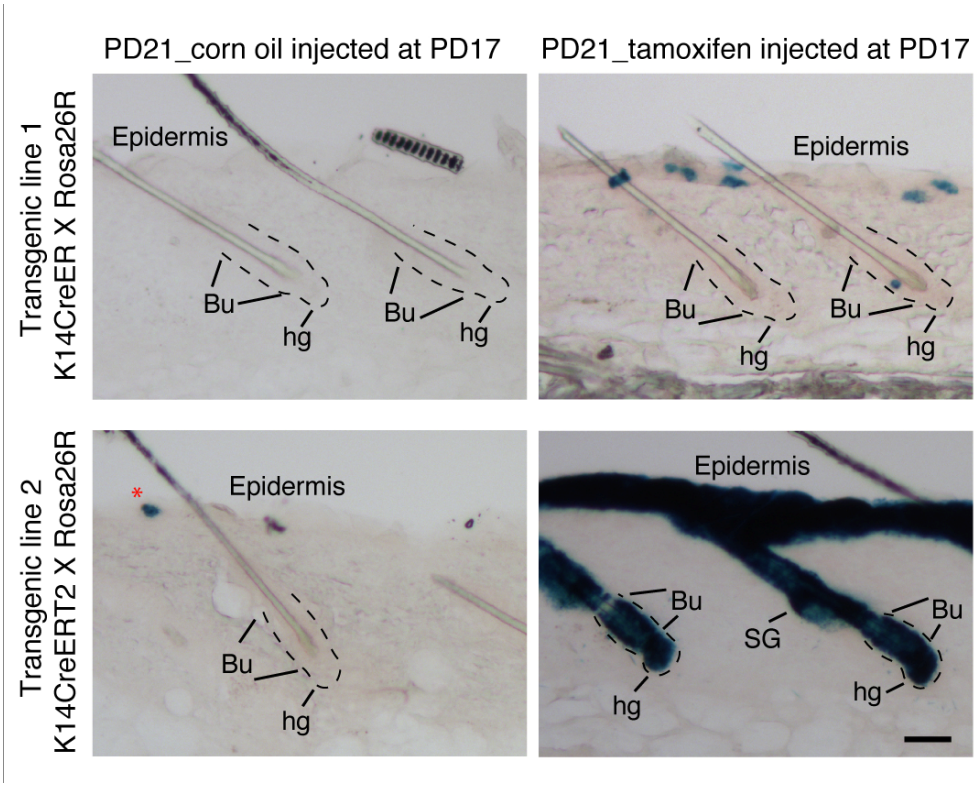

Figure 3.3. Distinct transgene activation in two K14CreER mouse lines.

Skin sections (60 μm) from two mouse lines (as indicated at the left of the panel) injected with tamoxifen (100 μg/g body) or corn oil (carrier) at PD17 and sacrificed at PD21 were stained for X-Gal (blue). Note single-cell bulge labeling in hair follicles from the K14-CreER line with no leaky expression in the absence of tamoxifen (top). In contrast, the K14CreERT2 line showed robust induction in all hair compartment including hair germ, as well as some leaky expression (bottom). Basement membrane around the bulge and hair germ marked with dotted lines. Bu, bulge; hg, hair germ; SG, sebaceous gland. Scale bar, 50 μm. N=3 mice per transgenic line.

the slow cycling nature of bulge and hair germ cells, most of which divided 2-5 times in one hair cycle. Insofar as infrequent division is a "stemness" marker, it is of interest to relate bulge proliferation to that of other multipotent cell populations, such as that expressing Leucine-rich repeats and immunoglobulin-like domain protein 1 (Lrig1) at the hair follicle junctional zone adjacent to the sebaceous gland and infundibulum (Jensen et al., 2009). Lrig1+ cells can give rise to all of the epidermal lineages, including the hair follicle, upon transplantation (Jensen et al., 2009). To quantify the proliferation of this newly characterized population, we applied the single cell division counting method to hair follicle junctional zone cells through the first adult hair cycle.

We fed the tet-off H2B-GFP expression mice doxycycline starting at telogen (PD21), and collected tissue at early anagen (PD28), full anagen (PD35) and the telogen of the next hair cycle (PD44). Thick cryo-sections of skin (100 μm) were stained with TOPRO3 DNA dye and imaged by confocal optical sectioning (detailed experimental procedure in Ref. 15). We found that cells at the junctional zone in general possessed less H2B-GFP than bulge cells, suggesting more vigorous proliferation activity (Fig 3.4A). Next, we summed the H2B-GFP fluorescent intensity at each sectioning plane to calculate the total volume intensity of randomly selected cells. From PD21 to PD28, bulge cells divided 0-3 times, whereas cells in the junctional zone divided 3-5 times (Fig. 3.4B). By full anagen at PD35, we showed previously that bulge cells divided 1-5 times (Zhang et al., 2009). Here we find that most cells in the junctional zone divided 5 or more times by PD35 with rare incidence of 4 divisions (Fig. 3.4B). At the next telogen (PD44), the proliferation profile of junctional zone cells remained similar to that of PD35, suggesting a quiescent stage around catagen, in line with Ki67 and short term BrdU labeling (not shown). This pause in proliferation coincides with the limited proliferation in the bulge and hair

Figure 3.4. Proliferation at the junctional zone and lateral movement of bulge cells in catagen.

(A) A single optical confocal slice from image stacks illustrates H2B-GFP retention in the bulge (Bu) as compared to the junctional zone (JZ) after each experiment. (B) Quantification of volume H2B-GFP intensity by integration through the optical stack for individual cells located in different hair follicle compartments defined by morphology. Cell divisions numbers were assigned to cells based on 2-fold dilution of H2B-GFP intensity per division, and the estimate that the brightest cells did not divide (Ref. (Waghmare et al., 2008) for details). (C) Top view sum projection of the bulge region stacks highlighted in (A) with yellow dotted box revealing active re-localization of bright H2B-GFP cells from the old club hair shaft (red asterisks) to the new bulge region (indicated by white arrow). hg, hair germ; SG, sebaceous gland; DP, dermal papilla. All skin sections were 100 μm thick and stained with TOPRO3 DNA dye. Scale bars, 20 μm. N=10 hair follicles per stage.

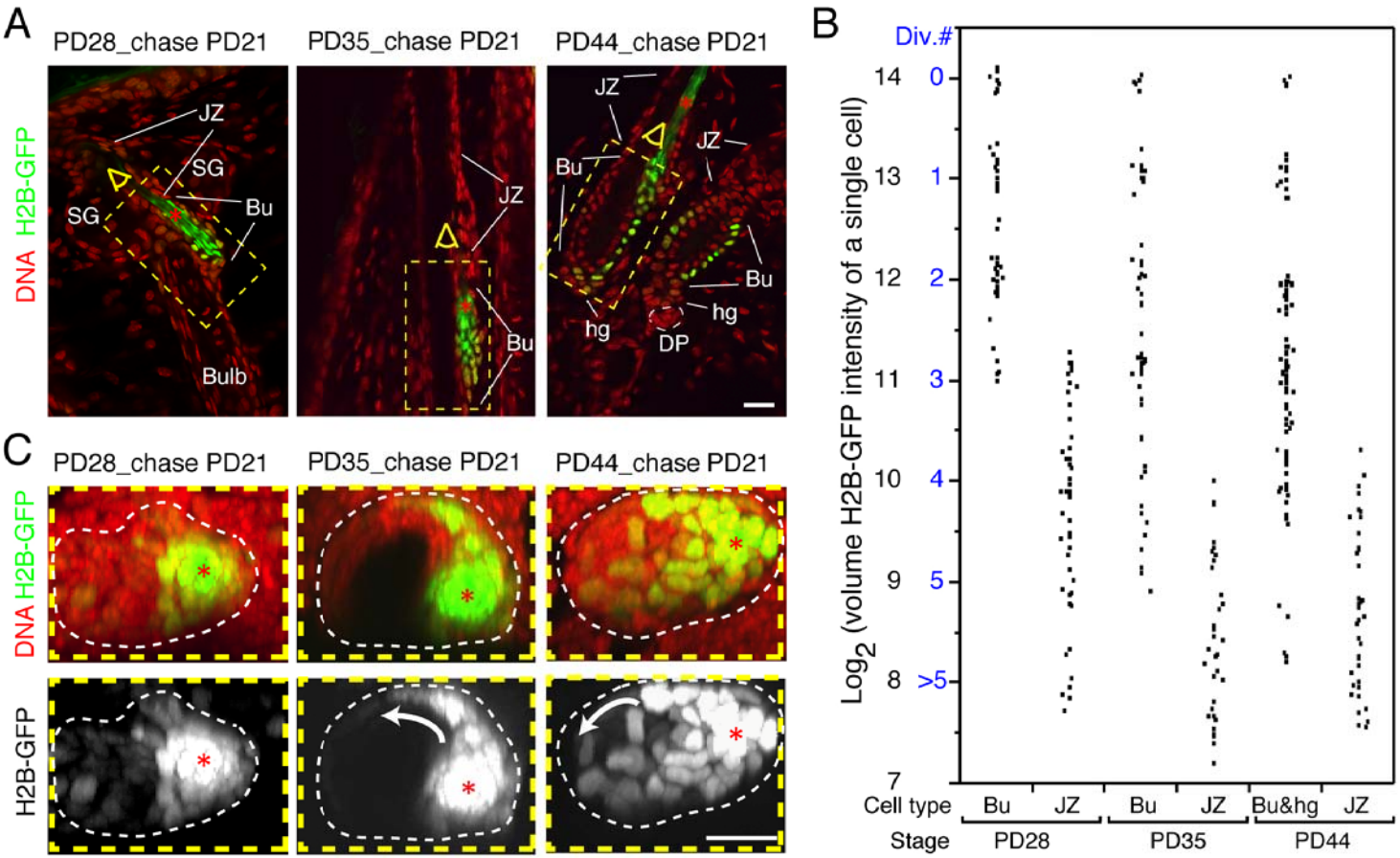
A
PD28_chase PD21
PD35_chase PD21
PD44_chase PD21
DNA H2B-GFP
JZ
SG
Bu
Bulb
hg
DP
C
H2B-GFP
B
Div.#
Log2 (volume H2B-GFP intensity of a single cell)
Cell type
Stage
PD28
PD35
PD44

germ at the same stage (Fig. 3.4B, Quantification section below, and Ref. 15). Thus, we conclude that cells in the junctional zone proliferate nearly twice as much as bulge and hair germ cells. The slow-cycling cells identified by DNA label retention in the junctional zone (Braun et al., 2003), are probably the few we identified that divide 4-5 times in one hair cycle.

Lateral migration of bulge cells in catagen in the newly generated club hair re-creates the niche

The fraction of CD34+/α6-integrin+ in the skin detected by flow cytometry although variable appears to increase from first to second telogen, which is in line with bulge cell divisions in >90% of bulge cells within this hair cycle (Osorio et al., 2008; Waghmare et al., 2008; Zhang et al., 2009). Since CD34+/α6-integrin+ bulge cells cluster around the old club hair site (old bulge site) during first telogen but are found in the new club site (new bulge site) by second telogen (Blanpain et al., 2004), it seems possible that these cells migrate laterally during catagen, when non-bulge outer root sheath cells found at the (future) new bulge site undergo apoptosis. To test the hypothesis that cells re-localize to the new bulge site, we used confocal microscopy to track the brightest H2B-GFP bulge cells during one hair cycle in sum projections through the z (longitudinal view) and y (cross-sectional) axes. We found trails of bright cells emanating from the old bulge site towards the new bulge site by PD35, and a re-localization of some of the bright cells in the new club hair site and into the hair germ by PD44 (late catagen/telogen) (Fig. 3.4C). These lateral movements are likely driven first by apoptosis of non-bulge cells at the new bulge site, and second by overcrowding of cells at the old bulge site.

Quantification of H2B-GFP pulse-chase data provides a model-independent measure of cell-population size increase and of minimum cell loss

An important indicator of tissue dynamics and growth is the fold change (*fc*) in its population size between an initial time t_0 and a final time t_1, e.g., the number of cells N_1^b found in the bulge at t_1 relative to the number of initial bulge cells N_0^b at t_0: $fc = \frac{N_1^b}{N_0^b}$.

Here we provide a method for calculating the fold change due to division based on H2B-GFP chase FACS data, and, in particular, on the fraction $p_{t_0 \to t_1, n}$ $(n \geq 0)$ of H2B-GFP-labeled cells that have divided n times and that are derived from the corresponding peaks of the FACS histograms of CD34+/α6-integrin+ bulge cells at the end of the chase (t_1) (Supplement). Significantly, the calculation makes assumptions neither about the mechanism of bulge replication (e.g., it is independent of the proliferative history that lead to the $p_{t_0 \to t_1, n}$) nor about the absolute number of cells within the population of interest. The key assumption is that the total H2B-GFP content (summed across all labeled bulge cells) decays due to protein degradation (Waghmare et al., 2008), but does not depend on the number of replications since H2B-GFP is distributed, while being conserved, between cells at division.

The *fc* calculation balances total H2B-GFP content at t_1 under two situations: a hypothetical one in which none of the initial N_0^b bulge divide and an experimentally-realized situation yielding N_1^{tot} cells at t_1 that are the progeny of the original cells. N_1^b of these remain in the bulge and N_1^l are lost from the bulge (e.g., due to apoptosis, export to the hair germ, or other downregulation of bulge markers), so that $N_1^{tot} = N_1^b + N_1^l$. Consider the H2B-GFP content of the cells in each histogram peak at t_1: The fraction $p_{t_0 \to t_1, 0}$ of cells in the $n = 0$ division peak constitute $N_1^b \cdot p_{t_0 \to t_1, 0}$ cells,

each with a fluorescence of 1 (in arbitrary dimensionless units), for a total contribution of $N_1^b \cdot p_{t_0 \to t_1, 0} \cdot 1$. Owing to the 2-fold dilution following division, each of the $N_1^b \cdot p_{t_0 \to t_1, 1}$ cells in the $n = 1$ peak have fluorescence $\frac{1}{2}$, for an aggregate contribution of $N_1^b \cdot p_{t_0 \to t_1, 1} \cdot \frac{1}{2}$. By extension, each of the $N_1^b \cdot p_{t_0 \to t_1, n}$ cells in peak n have fluorescence $\left(\frac{1}{2}\right)^n$, for an aggregate contribution of $N_1^b \cdot p_{t_0 \to t_1, n} \cdot \left(\frac{1}{2}\right)^n$. Summing these contributions across peaks gives the total H2B-GFP content in the bulge at the end of chase (t_1):

$$N_1^b \cdot p_{t_0 \to t_1, 0} \cdot 1 + N_1^b \cdot p_{t_0 \to t_1, 1} \cdot \frac{1}{2} + N_1^b \cdot p_{t_0 \to t_1, 2} \cdot \left(\frac{1}{2}\right)^2 + \ldots = N_1^b \cdot \sum p_{t_0 \to t_1, n} \cdot \left(\frac{1}{2}\right)^n .$$

By a similar argument, the total H2B-GFP content lost from the bulge by t_1, defined in terms of the (unknown) probabilities $p^l_{t_0 \to t_1, n}$ that a lost cell has divided n times, is $N_1^l \cdot \sum p^l_{t_0 \to t_1, n} \cdot \left(\frac{1}{2}\right)^n$. The sum of the H2B-GFP content across all N_1^{tot} cells must equal the total fluorescence $N_0^b \cdot 1$ in the bulge had the bulge cells not divided at all, which implies

$$N_0^b \cdot 1 = N_1^b \cdot \sum p_{t_0 \to t_1, n} \cdot \left(\frac{1}{2}\right)^n + N_1^l \cdot \sum p^l_{t_0 \to t_1, n} \cdot \left(\frac{1}{2}\right)^n \quad (1)$$

and, after rearranging,

$$fc = \frac{N_1^b}{N_0^b} = \frac{1 - \left(N_1^l / N_0^b\right) \cdot \sum_n p^l_{t_0 \to t_1, n} \cdot \left(\frac{1}{2}\right)^n}{\sum_n p_{t_0 \to t_1, n} \cdot \left(\frac{1}{2}\right)^n} . \quad (2)$$

$$fc_{no\ loss} = \frac{1}{\sum_n p_{t_0 \to t_1, n} \cdot \left(\frac{1}{2}\right)^n} > \frac{1 - \left(N_1^l / N_0^b\right) \cdot \sum_n p^l_{t_0 \to t_1, n} \cdot \left(\frac{1}{2}\right)^n}{\sum_n p_{t_0 \to t_1, n} \cdot \left(\frac{1}{2}\right)^n} = fc. \qquad (3)$$

Although applying Eq. (2) may be impractical since it depends on unknown parameters for cell loss $p^l_{t_0 \to t_1, n}$ that would be challenging to determine experimentally, it may be bounded by $fc_{no\ loss}$, the fold change calculated under the hypothesis of no cell loss (i.e., with $N_1^l = 0$).

The inequality holds because of the non-negativity of the second term in the numerator.

$fc_{no\ loss}$ can be calculated from H2B-GFP division data peaks (Fig. 1E in Ref. (Zhang et al., 2009)) to bound tissue expansion across different postnatal periods (Fig. 3.5). For example, the number of bulge cells increases by an $fc_{no\ loss}^{PD22-25}$ of ~1.9 in the first 3 days of chase and an $fc_{no\ loss}^{PD21-28}$ of ~2.7 across a seven day chase in early anagen. The results assume that any small fraction of bulge cells with H2B-GFP fluorescence below the detection limit (i.e., a "dim" peak) is comprised entirely of cells unlabeled due to mosaicism (Waghmare et al., 2008). The dim peak might also contain highly proliferative cells with diluted H2B-GFP fluorescence indistinguishable from that of unlabeled cells. A more conservative calculation accounts for such highly proliferative cells and shows that our assumption leads to a slight underestimation of *fc*, though the underestimation of average number of divisions (also shown in Fig. 3.5) may be more extreme.

To characterize the growth during anagen we calculated an $fc_{no\ loss}^{PD21-35}$ of ~3.4. However, when we counted the number of cells in the outer layer of the bulge, as defined morphologically in 20 μm skin sections at the first and second telogen, we found an ~2-fold increase. This was likely due to the generation during the interval of

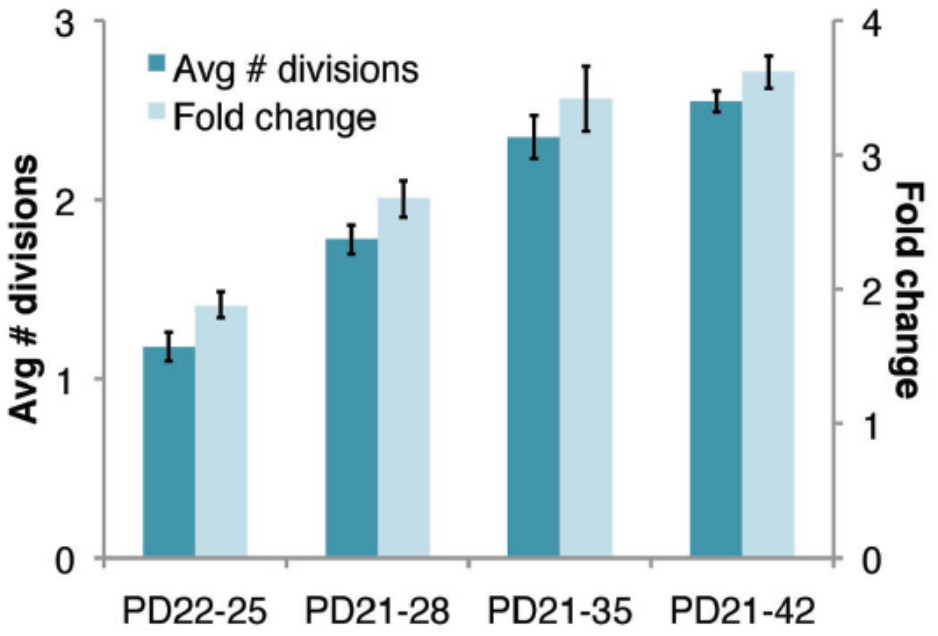

Figure 3.5. Average number of divisions and bulge population size fold change based on H2B-GFP-division tracking data calculated at indicated time periods assuming H2B-GFP cells with fluorescence below the background are unlabelled due to mosaicism. This provides an underestimate for average divisions but not for the fold change. Error bars are 90% credible sets.

a second club hair present in the bulge area. This gross discrepancy between the calculated and expected results led us to reject the hypothesis of no cell loss. However, we can rearrange Eq. (2) and use it to establish a minimum bound on the ratio of cells lost to those initially in the bulge N_1^l / N_0^b

$$\frac{N_1^l}{N_0^b} \geq 1 - \left(N_1^b / N_0^b\right) \cdot \sum_n p_{t_0 \to t_1, n} \cdot \left(\frac{1}{2}\right)^n . \quad (4)$$

Substituting the expected fold change between PD21 and PD35, $N_1^b / N_0^b = 2$, allows us to estimate the minimum fractional cell loss: $N_1^l / N_0^b > 0.42$. Assuming that the fractional cell loss, derived from the many bulges analyzed in a skin sample, is indicative of an individual bulge, we may multiply it by the ~150 cells expected to constitute a single bulge at PD21 to determine that more than ~63 bulge cells must be lost in one hair cycle.

Discussion

Here we provided a detailed analysis of the dynamics of tissue growth and of cell fate decisions in the hair follicle. Using our H2B-GFP division counting tools in situ we characterized the proliferation activity of a newly-identified multipotent cell population in the hair follicle junctional zone (Jensen et al., 2009), and found that these cells cycle more actively than bulge cells. These data should be useful in future experiments aimed at characterizing the role of this population in the skin and hair follicle.

Second, we analyzed the placement of two daughter cells descending from one cell division with respect to an important component of the stem cell niche, the basement membrane. Our data suggest that when a bulge cell moves into the differentiation zone – the hair germ– it either divides symmetrically along the BM to

expand the hair germ/outer root sheath pool, or asymmetrically likely to simultaneously produce a differentiating inner layer and a renewed progenitor/matrix cell contacting the BM. However, although these matrix precursor cells divide asymmetrically they do not fulfill the accepted definition of a stem cell, since they fail to self-renew after a short period of activity, as shown by lineage tracing data (Legue and Nicolas, 2005; Zhang et al., 2009), and instead best qualify as transit-amplifying or progenitor cells. In contrast, the permanent cells of the bulge divide symmetrically with respect to the basement membrane during anagen. This was predicted by our model (Fig. 3.1), in which loss of SCs from the pool by downward movement is compensated by symmetric SC expansion in the niche to replenish the pool throughout life. It is important to note that orientation with respect to the BM is only one aspect of asymmetric cell division and additional components of the fate determinant cellular distribution machinery should be explored in the future. Our attempt to examine the distribution of Numb (antibody a gift from Dr. W. Zhang (Yale U.)) and Par3 (antibody a gift from Dr. I. Macara (U. Virginia)) revealed ubiquitous distribution in interphase, and did not provide reliable signal in mitosis (as defined by phospho H3 staining) with our current methods.

Our previous model (Ref. (Zhang et al., 2009), and Fig. 1) implicates symmetric fate decision for bulge cell daughters without reference to the symmetric or asymmetric nature of the bulge cell division itself. In principle, cells that result from an asymmetric division might still adopt symmetric fates given a system sufficiently robust and flexible to adopt influences from the environment or given reversible differentiation cellular states. A simple interpretation of the data presented here predicts that in a relatively long-lived animal, such as the mouse, the progenitor cells divide asymmetrically for defined periods of time during which they actively sustain tissue growth, while the true long-lived stem cells behave as a reservoir that

periodically sacrifices a fraction of its residents to be expelled from the niche, become progenitors, differentiate, and eventually die. The SC pool would be replenished by symmetric expansion subsequent to loss due to active migration or passive downward movement. This two-gear system would permit the stem cell to remain relatively infrequently dividing over long-periods of time to reduce the rate of cancer, a challenge that a short-lived animal would not have to encounter. In other words, the progenitor cells in a mouse might behave as stem cells in a short-lived animal such as *Drosophila*.

Previously we noted that the amount of proliferation detected in the bulge during one hair cycle is incompatible with a previously adopted model in which only little bulge cellular turnover might take place in one hair cycle (Waghmare et al., 2008). The extent of bulge-cell proliferation suggested that more cellular export from the bulge into the bulb must occur than previously recognized (Legue and Nicolas, 2005), or else a significant fraction of bulge cells generated in anagen must die. Here we provided an approach for calculating an upper bound on the expansion of a cell population (fold change) based of H2B-GFP pulse chase data, which is insensitive to a particular replication model, for future use by the Developmental Biology community. When the actual number of cells can be experimentally determined, this upper bound can be used to estimate the minimum amount of cell loss, a measure that cannot be easily derived from experimental data. Our calculations indicated massive (42%) bulge cell loss in one hair cycle. We are currently in the process of modeling the number of cells exported from the bulge to contribute to bulb.

According to our H2B-GFP chases, proliferation occurs continuously during anagen (up to PD35) in a majority of the bulge cells and results in near doubling in the number of bulge cells by the end of the first hair cycle. Intriguingly, these cells remain confined around the old club hair site until early catagen, as suggested by lack

of re-distribution in X-Gal labeling among hair follicles from PD25-35 (Fig. 3.4 in (Zhang et al., 2009)) and by CD34 staining (data not shown). Therefore it is tempting to speculate that upon division in anagen an increase in bulge cell density could lead to contact inhibition which would eventually result in cessation of proliferation (Lien et al., 2006). Over-crowding of bulge cells around the old club hair site might therefore force the cells to re-organize and spread into adjacent areas towards the new club hair site to relieve the presumed contact inhibition. This hypothesis is in line with our detection of lateral movements in the H2B-GFP label-retaining bulge cells from the old club hair towards the newly generated club hair in catagen (Fig. 3.4). This step might be necessary to prepare the niche for a new cycle of proliferation and expansion in the next anagen. The control of stem cell pool size by a feed-back inhibition loop due to cell-cell contact is an area of future exploration.

CHAPTER 4

PHENOTYPIC ANALYSES OF *GATA6* KNOCKOUT IN SKIN EPITHELIUM

Introduction

Regenerative tissues contain stem cells that self-renew and differentiate for extended period of time. Various proliferation mechanisms have been adopted by stem cells to regulate their differentiation and self-renewal functions. In invertebrate tissues, a stem cell usually divides asymmetrically to generate a stem cell daughter that will remain in the stem cell niche and a progenitor daughter that will leave the niche to differentiate. In mammalian tissues, some stem cells utilize the evolutionarily conserved asymmetric cell division mechanism to achieve differentiation and self-renewal simultaneously, while others adopt more flexible regulation that switch between symmetric and asymmetric divisions upon the specific condition of the regenerating tissue (Morrison and Kimble, 2006; Spradling et al., 2008). In most stem cell systems, the stem cell – niche interactions prove crucial for the maintenance of stem cell property and the initiation of differentiation in progenitor cells. Niche attachment mediated signaling pathways, including BMP, JAK/STAT, and WNT, have been identified to stimulate stem cells to self-renew and inhibits the differentiation regulatory mechanisms (Morrison and Spradling, 2008).

In mouse hair follicles, the infrequently dividing bulges stem cells seem to have adopted a unique temporal-spatial stem cell proliferation regulatory mechanism where in the early differentiation phase stem cells migrate out of the niche becoming progenitors, and in the later self-renewal stage the remaining stem cells proliferate to replenish the stem cell pool (Zhang et al., 2009; Zhang et al., 2010). The divisions

within the storage niche appear symmetric with respect to the underlying basement membrane, whereas divisions within the progenitor zone are either symmetric or asymmetric. Single bulge cell lineage tracing studies show that bulge cells migrate out of the stem cell niche without prior division (Zhang et al., 2009; Zhang et al., 2010), and their cellular property immediately change toward differentiation characterized by gene expression profiling (Greco et al., 2009; Zhang et al., 2009). However, little is known regarding how this process takes place and which genetic regulatory mechanisms are responsible for the differentiation fate.

Transcription factors are known master regulators for cellular fate determination. From our previous arrays, we found the transcription factor GATA bind protein 6 (*GATA6*) to be preferentially expressed in differentiating hair follicle stem cells compared to quiescent or self-renewing stem cells (Zhang et al., 2009). *GATA6* belongs to a family of six transcription factors, which contain a double Zn-finger DNA binding domain and are important for cell differentiation and embryonic morphogenesis (Bresnick et al., 2005). *Gata6* regulates early differentiation steps in embryonic stem cells toward endoderm, testis, and ovary (Morrisey et al., 1998; Viger et al., 2008), and is essential for liver morphogenesis (Zhao et al., 2005). At the adult stage, *GATA6* is essential for the airway differentiation of tissue stem cells in the developing and adult lung (Zhang et al., 2008; Zhang et al., 2007), the cardiac inflow tract development and the specification of cardiomyocytes (Holtzinger and Evans, 2007; Tian et al., 2010). Other GATA transcription factors have also been implicated in stem cell functions: Gata1-3 are required for hematopoietic stem cell differentiation (Orkin, 1992), and Gata3 is crucial for the generation of the inner root sheath layer of the hair follicle (Kaufman et al., 2003). Here I explore in depth the function of *GATA6* in hair follicle stem cell differentiation. My data suggest *Gata6* is required for the proliferation, survival, and proper differentiation of progenitor cells in the hair.

While *Gata6* is not required for stem cell maintenance in the niche in the short-term, degeneration of all the support structures of the hair in the absence of *Gata6* results in complete demolition of the stem cell niche and loss of the bugle cells.

Materials and Methods

Transgenic mice

All experiments were done according to Cornell IACUC guidelines and carried out using standard procedure, as described (Waghmare et al, 2008). We generated Tet-off H2B-GFP mice by crossing hemizygous *pTRE–H2B–GFP* (Tumbar et al., 2004) (CD1) and *K5tTA* (FVB1) mice and identified GFP-expressing animals with an ultraviolet-based portable lamp (BLS Ltd). Mice were fed with 1 g doxy/kg mouse chow (Bio-serv), and sacrificed at various time points. We generated the *Gata6* inducible knockout mice by first crossing homozygous *Gata6* flox/flox mice (Sodhi et al., 2006) with the heterozygous K14CreERT2 line (Li et al., 2000) to generate *K14CreERT2 het : Gata6 flox/+*, then mated these mice back to *Gata6* flox/flox line and selected for *K14CreERT2 het : Gata6 flox/flox* mice as inducible knockout mice. Additionally, we introduced the BAT-GAL transgene to the inducible knockout line by first mating *BAT-GAL* mice (Maretto et al., 2003) with *Gata6 flox/flox* mice to generate *BAT-GAL het : Gata6 flox/flox* mice, then used those to mate with *K14CreERT2 het : Gata6 flox/flox* line, and subsequently selected for *K14CreERT2 het : BAT-GAL het : Gata6 flox/flox* offspring. *Gata6* genotyping was done using primers as described (Sodhi et al., 2006). *K14CreERT2* genotyping was done using *CRE* primers as described (Zhang et al., 2009). *BAT-GAL* genotyping was done using *LacZ* primers as described (Maretto et al., 2003). Tamoxifen delivered intraperitoneally to induce knockout (100 ug/g body weight) was dissolved in corn oil.

FACS analysis

We used SPHERO Rainbow particles, 3.0–3.4 um (Spherotech), to calibrate the FACS machine. All experiments were performed on a FACS Aria (BD Biosciences) in the Cornell University Flow Cytometry Facility and analyzed with FlowJo software. Skin cells were isolated from fresh tissue using trypsin digestion (0.25%) and stained with biotin-labelled CD34 antibody (eBioscience) and phycoerythrin-labelled a6-integrin (CD49f) antibody (BD Pharmingen). CD34 secondary antibody was Streptavidin-APC (BD Pharmingen). Live cells were those not stained by propidium iodide (PI; Sigma).

Tissue Staining and Microscopy

Staining procedure for immunofluorescence and Hematoxylin and Eosin (H&E) were as described previously (Tumbar et al., 2006). Nuclei were labeled by 4',6'-diamidino-2-phenylindole (DAPI). Primary and secondary antibody information was previously described in (Osorio et al., 2008) except for *Gata6* monoclonal antibody (1:50, Santa Cruz Inc.). For X-gal staining, frozen skin sections were fixed for 1 hr in 4% paraformaldehyde at 4°C, PBS washed 3x30 min., stained for 24hrs at 37°C with X-gal buffer (Osorio et al., 2008), and incubated for 3 hrs in 1M Na_2CO3 to maximize sensitivity (Tanahashi and Tabira, 2000). For immuno-fluorescence and X-gal staining, images were acquired using the IP-Lab software (MVI) on a light fluorescence microscope (Nikon) equipped with a CCD 12-bit digital camera (Retiga EXi, QImaging). For confocal microscopy, frozen tissue sections (100 um) were fixed for 1 h in 4% paraformaldehyde and stained overnight with TOPRO3 (1:2000 dilution; Invitrogen). Confocal Z-sections were collected using a Leica microscope with details described in (Osorio et al., 2008; Waghmare et al., 2008).

QRT–PCR

RNA isolation, cDNA generation and RT-PCR were described in (Osorio et al., 2008; Waghmare et al., 2008). Quantitative (Q) RT-PCR was performed on MyiQ thermocycler (Bio-Rad), as the manufacturer instructed. Signals from triplicate wells per primer pair were normalized to GAPDH. *GATA6* QRT-PCR primers: 5'-GTC CTG TGC CAA CTG TCA CAC-3' and 5'-CTG CTG TTA CCG GAG CAA GCT-3'.

Cell Culture and Grafting Assays

Primary keratinocytes were isolated from newborn mice as previously described (Tudorita Tumbar and Fuchs, 2006). Briefly, the back skin was dissected from the mice and treated with 0.25% dispase (Life Technologies, Inc., Mississauga, Ontario, Canada) at 4°C overnight. The epidermis was separated from the dermis with forceps and trypsinized for 15 minutes. The suspended keratinocytes were collected and cultured in low-Ca2+ keratinocyte E medium by plating in triplicate 200,000 live (not staining with trypan blue) cells on irradiated mouse embryonic fibroblasts (passage 4). Keratinocyte colonies in dishes were counted using phase-contrast microscopy or H&E staining. In grafting assays, pieces of ~2 x 2 cm full-thickness skin from postnatal day 3 mice were grafted onto immune-deficient nude mice (Segre et al., 1995). Donor skin was oriented in according direction (head to tail) on a wound created by removing a piece of full-thickness skin from the nude mice. After skin surgery, the skin graft on recipient mouse was wrapped under elastic bandages for two weeks. Mice were then observed regularly to determine hair growth.

Results

Gata6 expression in the hair follicle and inter-follicular epidermis

Gata6 mRNA expression in the hair follicle was first documented in our previous study where we isolated and expression profiled the differentiating stem cell progeny, self-renewing stem cell progeny, and quiescent stem cells from either early differentiation stage at postnatal day (PD)21 or later self-renewal stage at PD25 (Zhang et al., 2009). The microarray signals showed that differentiating stem cell up-regulated *Gata6* mRNA level compared to quiescent and self-renewing stem cells (Table 2.3). In order to confirm this microarray result, I extracted mRNA from different cell populations (Fig. 2.1) and performed QRT-PCR with *Gata6* specific primers (Fig. 4.1A). I found that *Gata6* expression level was indeed highest in the differentiating stem cell progeny located in the hair germ at PD21, while both proliferating and quiescent stem cells from the self-renewal stage at PD25 expressed *Gata6* at a minimum level. Another interesting observation was that the quiescent stem cells from the differentiation stage exhibited higher *Gata6* expression level than those from the self-renewal stage, which suggest the overall status of the niche might be regulated by the distance from the putative hair growth signaling center dermal papillae. Next, I used a monoclonal *Gata6* specific antibody to detect the *Gata6* protein level in the skin epithelium at both the quiescence stage of hair cycle (telogen) and the growth stage (anagen). At PD21 telogen, I detected bright nuclear *Gata6* immuno-staining in cells at the hair germ, the bottom of the bulge, the sebaceous gland, and the basal layer of inter-follicular epidermis (Fig. 4.1B). At PD35 full anagen, I found *Gata6* protein expressed in the matrix/progenitor compartment of the

Figure 4.1. *Gata6* expression in the skin epithelial.

(A) QRT-PCR analysis of *Gata6* mRNA level in different cell populations isolated from telogen and anagen (See Fig. 2.1; 2.3 for detailed description of cell populations). (B) Immuno-microscopy images for 20um skin sections stained with *Gata6* specific antibody and DAPI DNA dye. Skin was collected from PD21 telogen wild-type mice. Strong nuclear staining of *Gata6* was found in the epidermis, sebaceous gland, hair germ, and the bottom of the bulge compartment. (C) Immuno-microscopy images for 20um skin sections stained with *Gata6* specific antibody and DAPI DNA dye. Skin was collected from PD35 anagen wild-type mice. In the hair follicle, only matrix cells showed strong GATA6 signal (yellow dotted box with magnification in the lower panel). Bulge cells did not express *Gata6* at this stage of hair cycle (green dotted box). N>= 3 mice/stage. Scale bars, 50 um.

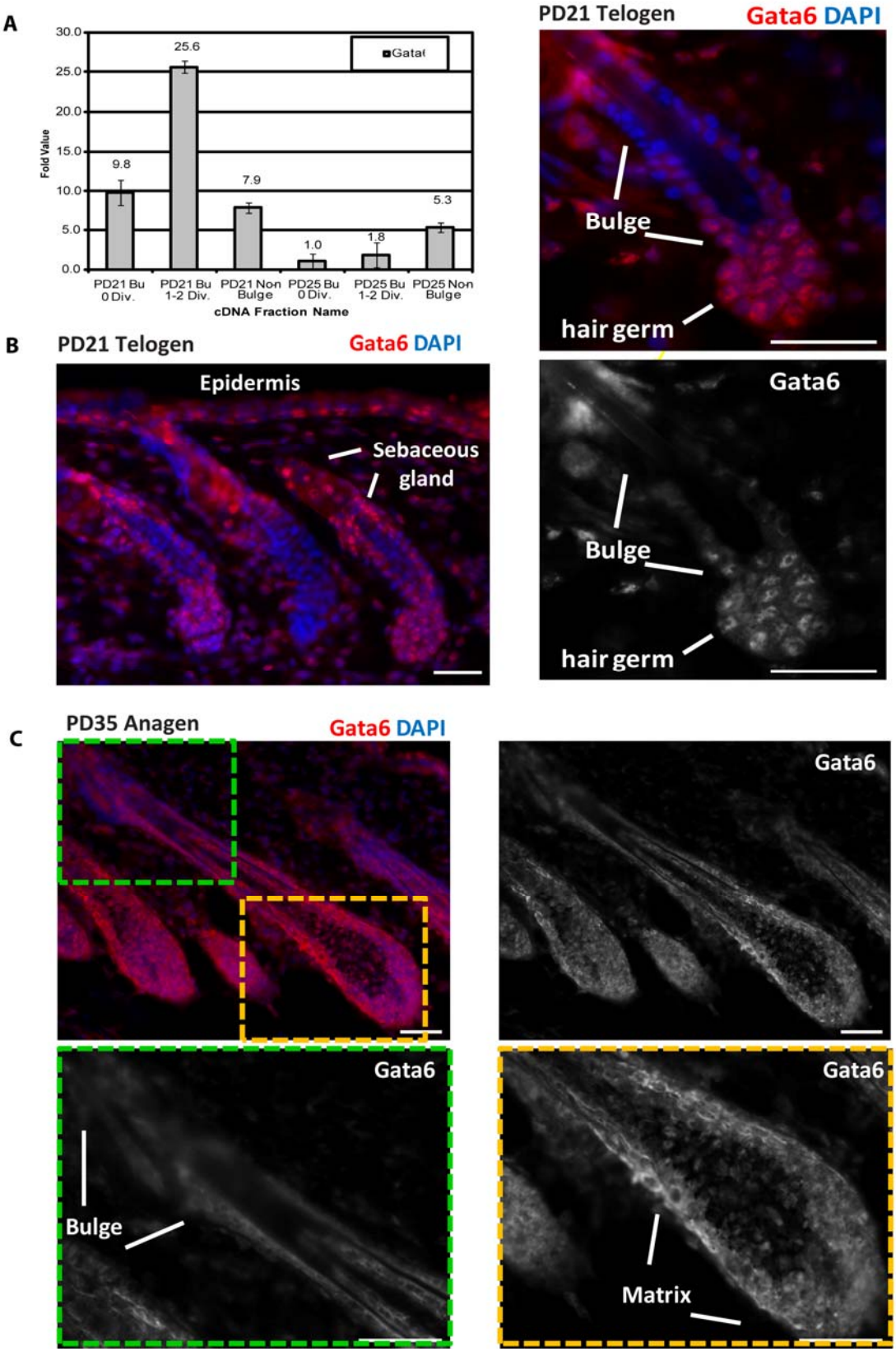
A
30.0
25.0
20.0
15.0
10.0
5.0
0.0
Fold Value
Gata6
9.8
25.6
7.9
1.0
1.8
5.3
PD21 Bu 0 Div.
PD21 Bu 1-2 Div.
PD21 Non Bulge
PD25 Bu 0 Div.
PD25 Bu 1-2 Div.
PD25 Non Bulge
cDNA Fraction Name
PD21 Telogen
Gata6 DAPI
Bulge
hair germ
B
PD21 Telogen
Gata6 DAPI
Epidermis
Sebaceous gland
Gata6
Bulge
hair germ
C
PD35 Anagen
Gata6 DAPI
Gata6
Gata6
Bulge
Gata6
Matrix

hair, but not in the stem cell niche – the bulge (Fig. 4.1C). Expression of *Gata6* in the sebaceous gland and the epidermis remained high at this stage (data not shown). These results confirmed our previous microarray data that *Gata6* expression is up-regulated in the differentiating hair progenitors but not in the stem cells in their niche during the self-renewing stage. In addition, I identified high *Gata6* expression in the epidermis basal layer and the sebaceous gland where specific progenitor populations reside to maintain tissue homeostasis.

Gata6 is required for progenitor cell maintenance during hair regeneration

To knockout *Gata6* in the skin epithelium, I generated *K14CreERT2 het : Gata6 flox/flox* mice (see methods). Previous study has shown that the *K14CreERT2* inducible line is very efficiently activated in all skin epithelium lineages upon tamoxifen injection (Li et al., 2000; Zhang et al., 2010). Given *Gata6*'s different expression patterns at quiescence and growth stage, I induced the knockout by tamoxifen injection at corresponding telogen (PD21) and early anagen (PD28) phases of the hair cycle (Fig. 4.2A). Tamoxifen injection efficiently excised the floxed exon, as shown by our PCR analysis and lack of nuclear *GATA6* signal in immuno-fluorescence (data not shown). In this chapter, control mice refer to wild type mice with or without tamoxifen injection, *K14CreERT2 het : Gata6 flox/flox* mice with corn oil injection, and *Gata6 flox/flox* mice with tamoxifen injection. These control mice behaved similarly in all the experiments. The knockout mice refer to *K14CreERT2 het : Gata6 flox/flox* mice with tamoxifen injection.

When I shaved the mice at PD21 and induced the knockout of *Gata6*, after 10 days, the control mice had grown back hair on the skin while the *Gata6* knockout mice failed to grow any new hair (Fig. 4.2B). Histological analyses of the skin sections

Figure 4.2. Loss of *Gata6* leads to hair regeneration defects.

(A) Scheme of knockout experiments at telogen PD21 or anagen at PD28. (B) Mice picture and corresponding 30um skin sections stained with hematoxylin. At PD21, hair follicles were at telogen before shaving and tamoxifen injections. The hair germ structure (arrow) contains ~15 cells in a section. At PD31, control mice grew new hair on the back skin, and the hair follicles are in full anagen stage. The *Gata6* knockout mice didn't grow any hair with arrested telogen hair follicles. The hair germ structure (arrow) were missing for most hair follicles in the knockout mice. Same analyses were done at anagen (C). *Gata6* knockout in anagen leads to degeneration of differentiated layers in the hair follicles and mis-organized melanin segregates. N>=3 at each stage for control and knockout mice. Scale bars, 50 um.

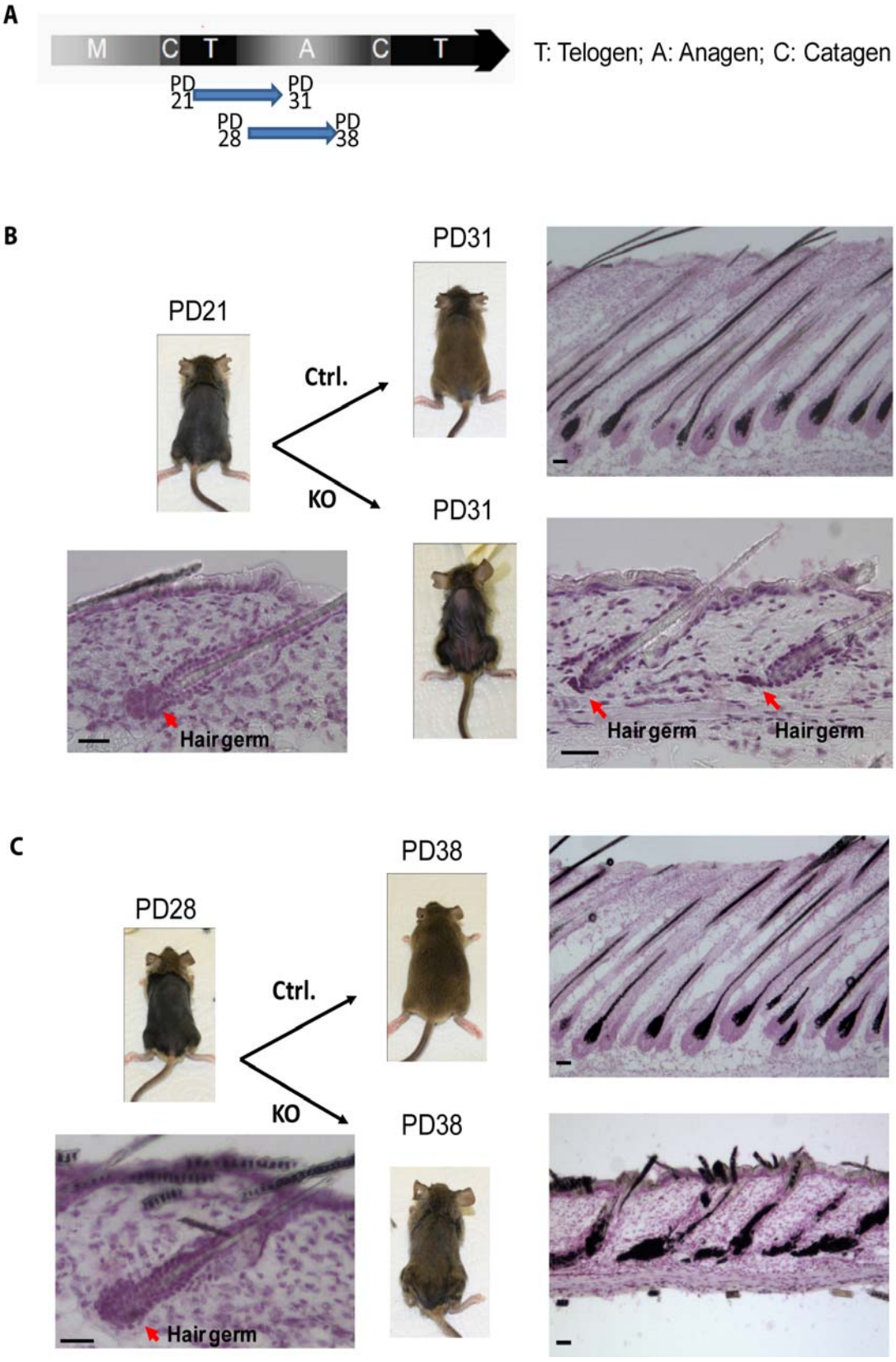
A
M
C
T
A
C
T
T: Telogen; A: Anagen; C: Catagen
PD 21
PD 31
PD 28
PD 38
B
PD21
Ctrl.
KO
PD31
PD31
Hair germ
Hair germ
Hair germ
C
PD28
Ctrl.
KO
PD38
PD38
Hair germ

revealed that the hair follicle from the control mice proceeded to full anagen after 10 days. The hair follicles on the *Gata6* knockout mice were blocked in the quiescent telogen stage. Moreover, the hair germ compartments were degenerated in most of the hair follicles after 10 days post tamoxifen injection (Fig. 4.2B). These data suggested that *Gata6* is required for the initiation of new hair growth and the maintenance of the progenitor zone during the quiescent stage of hair cycle.

In order to study if *Gata6* is necessary for the matrix progenitors after the hair growth initiation step, I shifted the knockout induction to a later stage at PD28 when the hair germs have already enlarged to become matrix (Fig. 4.2A,C). When I analyzed the skin at PD38, the control mice again had emerged new hair on the skin, whereas the *Gata6* knockout mice showed little new hair growth (Fig. 4.2C). In skin sections, the hair follicles from the knockout mice displayed disorganization of inner differentiated layers of the hair follicle which caused the malfunctioning cortex cells or unaffected melanocytes (K14 negative) to form aggregates throughout the hair shaft canal (Fig. 4.2C). This phenotype of the *Gata6* knockout mice in anagen suggested that *Gata6* not only maintains progenitors during quiescence but also regulates the proper function of progenitors during new hair growth.

Gata6 regulates progenitor cell differentiation, proliferation, and survival in the hair follicle and at the inter-follicular epidermis

I further characterized the *Gata6* knockout phenotype by examining the distribution of known differentiation markers in the skin epithelium. Studies have shown that integrins have important roles in regulating tissue homeostasis in the skin (Blanpain and Fuchs, 2006; Raghavan et al., 2000). The expression of α6 integrin at the epidermis basal layer and the out root sheath of the hair was lost in the knockout skin (Fig. 4.3). The supra-basal layer specific keratin 1 expression was also missing in

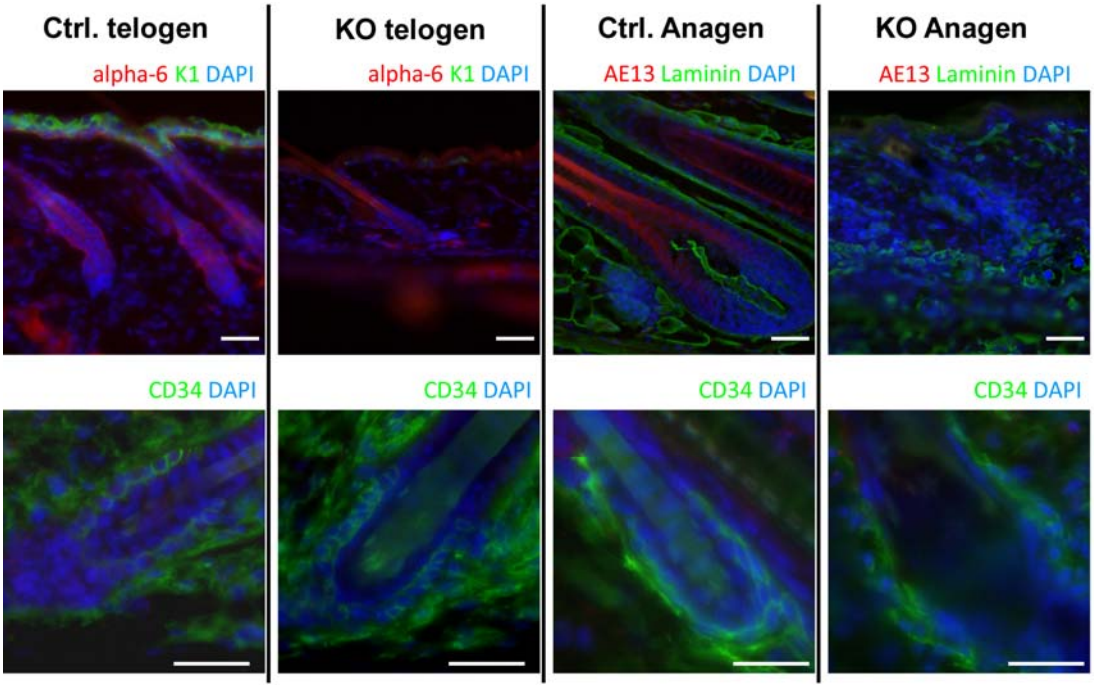

Figure 4.3. Differentiation defects in the *Gata6* knockout skin.

20 um skin sections were stained with various differentiation markers (upper panel) and bulge stem cell maker CD34 (lower panel). At telogen, epidermal differentiation marker Keratin 1 was lost in the knockout skin along with α6 integrin at the basal layer and outer root sheath. At anagen, hair follicle differentiation marker AE13 and Laminin expression were disturbed in the knockout skin. However, positive CD34 staining was detected in both control and knockout skin at both stage. N>=3 at each stage for control and knockout mice. Scale bars, 50 um.

the *Gata6* knockout mice suggesting the malfunction of epidermal progenitor differentiation (Fig. 4.3). AE13 is an inner root sheath marker for the hair, and Laminin is normally expressed in the out root sheath layers (Blanpain and Fuchs, 2006). In the anagen knockout mice, AE13 positive cells no longer existed, while the Laminin staining pattern was largely disturbed (Fig. 4.3). Although the production of differentiated lineages was severely affected by the loss of *Gata6*, the stem cells in the bulge were detectable for the longest period of time, with strong CD34 staining on the cell surface, until eventually the entire hair morphology becomes unrecognizable (Fig. 4.3).

To find out how the degeneration of hair follicle occurred in anagen *Gata6* knockout mice, I analyzed the *Gata6* knockout mouse skin at short time-points after tamoxifen induction (Fig. 4.4A). Skin sections revealed that the new hair growth was affected in the matrix 2 days after tamoxifen injection with dis-organized melanin. At 4 days, the regression of hair structure was already prominent (Fig. 4.4B). In addition, I analyzed the cell proliferation activity by 6 hour BrdU pulse before sacrificing the mice. The number of BrdU positive cells in the matrix was significantly reduced at 4 days after tamoxifen injection (Fig. 4.4C). I also detect ectopic apoptosis in the matrix by Caspase3 staining at the same stage in the knockout hair follicles, suggesting the matrix progenitors failed to survive even with reduced proliferation (Fig. 4.4D). Similar defects in proliferation and apoptosis were also found at the basal layer of inter-follicular epidermis (data not shown).

The above phenotype characterized in the conditional *Gata6* knockout suggested *Gata6* as a key regulator for skin homeostasis. To further investigate the long term effect of *Gata6* knockout, I grafted newborn mice skin to immune-deficient nude mice and induced *Gata6* knockout by tamoxifen injection to the recipient mice. I found that

Figure 4.4. *Gata6* is required for hair follicle matrix progenitor maintenance.

(A) Scheme of short-term knockout experiments at telogen PD28. Blue arrows indicate the wait time from the tamoxifen injection to sample collection. (B) Skin sections stained with hematoxylin showed that initial abnormality started in the matrix compartment of the hair follicle (red arrows). (C). Skin sections from control and knockout mice stained for BrdU revealed reduced proliferation in the matrix progenitors 4 days after tamoxifen injection. (D) Skin sections from wild-type catagen, control mice, and knockout mice stained for apoptotic marker Caspase3. *Gata6* knockout hair follicles displayed ectopic Caspase3 staining in the matrix (arrow) at PD32. Wild-type catagen tissue serves as a positive control for Caspase3 staining. Skin sections were 20um thick. N>=3 at each stage for control and knockout mice Scale bars, 50 um.

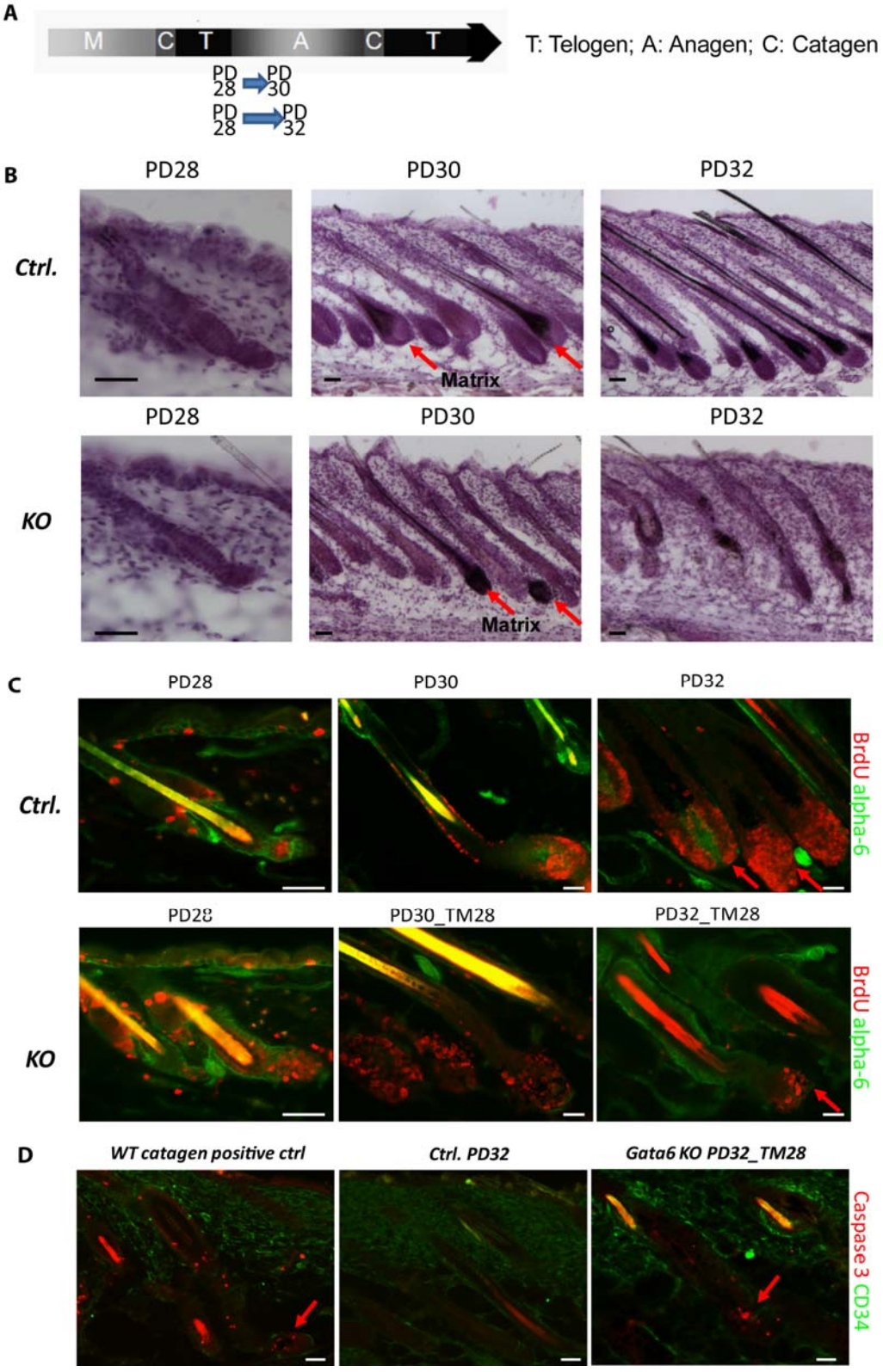
A
M
C
T
A
C
T
T: Telogen; A: Anagen; C: Catagen
PD 28
PD 30
PD 28
PD 32
B
PD28
PD30
PD32
Ctrl.
Matrix
PD28
PD30
PD32
KO
Matrix
C
PD28
PD30
PD32
Ctrl.
BrdU alpha-6
PD28
PD30_TM28
PD32_TM28
KO
BrdU alpha-6
D
WT catagen positive ctrl
Ctrl. PD32
Gata6 KO PD32_TM28
Caspase 3 CD34

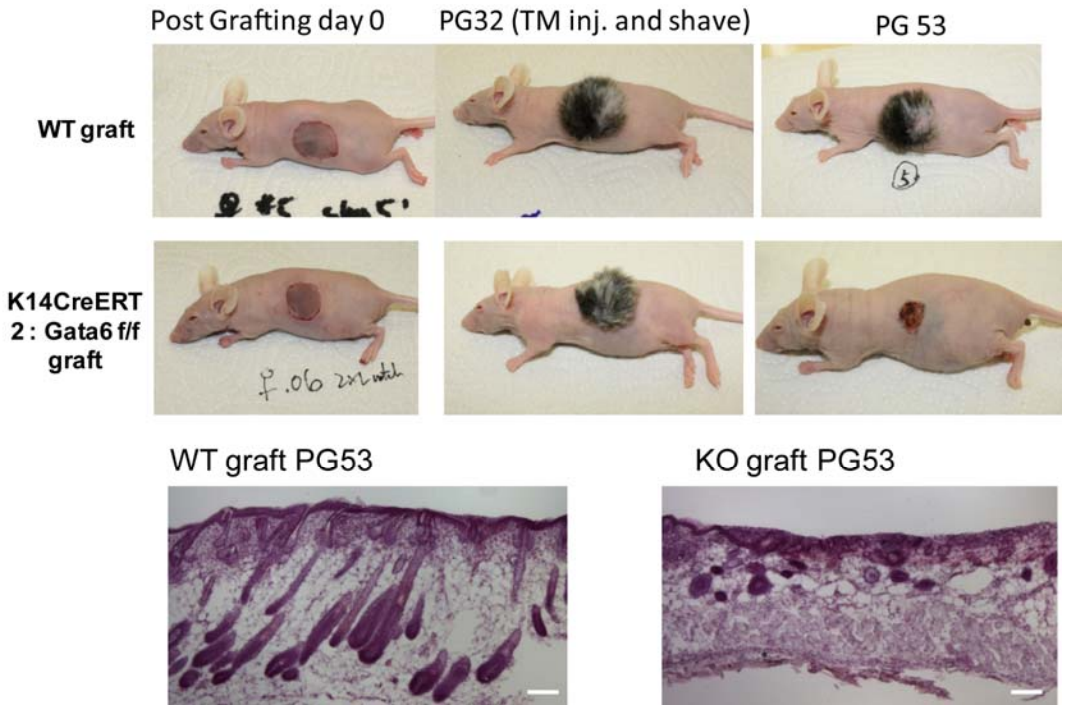

Figure 4.5. *Gata6* knockout skin phenotype in the graft.

Newborn skin from wild-type mice (upper panel) and *K14CreERT2 : Gata6 flox/flox* mice (middle panel) were grafted onto nude mice. On post grafting day (PG) 32, both grafts grew abundant hair on the recipient mice. The grafts were shaved and mice were injected with tamoxifen on PG32 after pictures were taken. On PG53, wild-type grafts showed additional hair growth. The knockout graft didn't grow more hair while the entire grafted area was shrinking. 20um Skin sections from PG53 grafts were stained with Hematoxylin (lower panel). N=2 for wild-type newborn skin; N=3 for knockout skin. Scale bars, 50 um.

both control and pre-induction knockout skin grafts grew hair after 32 days from the surgery. After shaving and waiting for another 20 days, the control skin grafts showed new hair growth again. In contrast, the *Gata6* knockout skin grafts failed to grow any hair shafts and the follicles started shrinking – a sign for total skin degeneration (Fig. 4.5). These results confirmed that the *Gata6* skin phenotype is a direct result from the loss of *Gata6* in the skin epithelium, and more importantly allowed us to asses the long term effect of *Gata6* loss.

Together, these results showed that *Gata6* orchestrates a wide range of activities in the progenitors in the skin epithelium. The loss of *Gata6* blocks the generation of differentiated cell lineages, limits the self-renewal of progenitor pool, and ultimately leads to cell death and tissue failure.

Gata6 is required for the maintenance of mouse keratinocytes in culture

The data so far have indicated the requirement of *Gata6* for progenitor cell functions in the native hair follicle and epidermis tissues. In an attempt to rescue the degeneration phenotype and uncover the molecular mechanisms, I explored in the keratinocyte cell culture system for the function of *Gata6*. First, I accessed the colony formation capability of primary keratinocytes from newborn skin. I injected new born mice with tamoxifen on PD1 and extracted keratinocytes on PD3. After 7 days of culture since plating on irradiated fibroblast feeders, control keratinocytes formed >100 colonies. In contrast, *Gata6* knockout keratinocytes only formed ~5 small colonies in the Petri-dish (Fig. 4.6A). After another week, the control dishes had almost grown to confluency, while only several big colonies were found in the knockout dish probably formed by cells that escaped the *Gata6* knockout (Fig. 4.6A). Thus, *Gata6* is essential for primary keratinocytes to self-renew and expand *in vitro*, which is consistent with our finding in the hair follicle matrix where progenitors

Figure 4.6. Gata6 is required for keratinocyte proliferation *in vitro*.

(A). Primary keratinocytes from control and knockout PD3 mice were plated on feeders. After 7 days, cells were stained with hematoxylin (upper left panel), and the number of colonies were quantified (upper right panel). Phase contrast images of cells were showed below. (B) After two passages of control and *K14CreERT2 : Gata6 flox/flox* keratinocytes, we added tamoxifen (500nmol) to the dish. In 3 days, cells in the knockout dish displayed significant detachment and abonomal cell shape compared to those in the control dishes. N=3. Scale bars, 10 um.

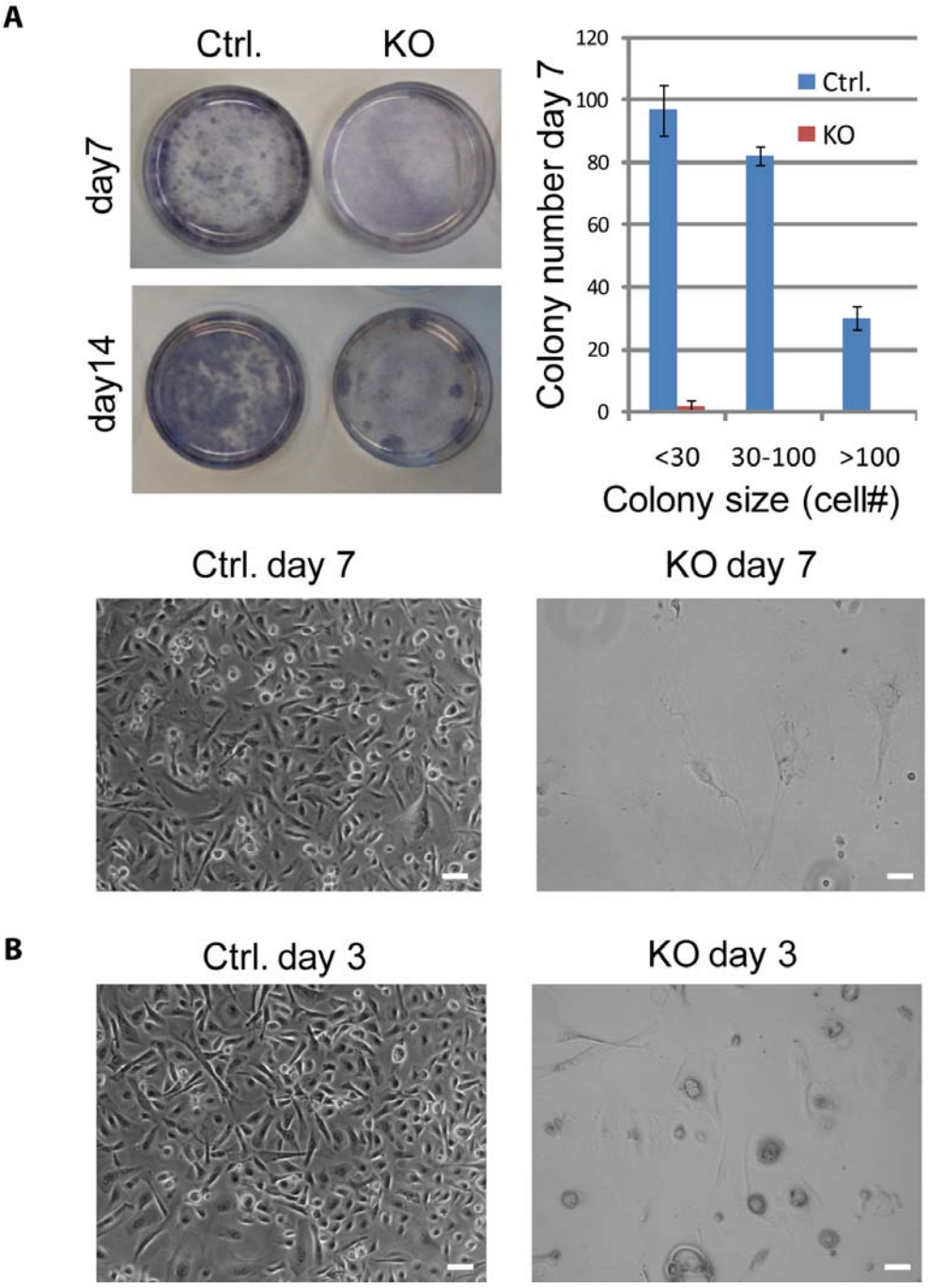
A
Ctrl.
KO
day7
day14
Colony number day 7
120
100
80
60
40
20
0
Ctrl.
KO
<30
30-100
>100
Colony size (cell#)
Ctrl. day 7
KO day 7
B
Ctrl. day 3
KO day 3

ceased to proliferate upon *Gata6* knockout. Next, I tested the function of *Gata6* in established keratinocytes cell lines. New born primary keratinocytes from control mice and pre-induction knockout mice showed comparable colonies formation ability (data not shown). After 2 passages, I added tamoxifen into the culture media to induce *Gata6* knockout. In 3 days, the knockout cells started detaching from the dish and began to die. The remaining cells also displayed abnormal morphology compared to the control cells (Fig. 4.6B). This result is in line with the telogen knockout phenotype in the hair follicle that hair germ progenitor cells fail to survive when *Gata6* is lost. In essence, knockout of *Gata6* recapitulates the phenotype in the skin epithelium. In the future, I will utilize this *in vitro* system to rescue the phenotype with exogenous *Gata6* construct via transfection, and to identify the downstream factors of *Gata6* using microarrays and biochemical assays.

The status of WNT signaling in the Gata6 knockout mice

It has been shown in the heart and lung tissue of mouse that *Gata6* forms a forward feedback loop in regulating WNT signaling in differentiated cell lineages (Alexandrovich et al., 2006; Tian et al., 2010; Weidenfeld et al., 2002; Zhang et al., 2008). WNT signaling has been implicated in hair follicle homeostasis such that the blocking of WNT signaling will lead to premature catagen (Blanpain and Fuchs, 2006; Millar, 2006). To examine the effect of *Gata6* knockout on WNT signaling in the hair follicle, I introduced the BAT-GAL transgene into the *Gata6* knockout background. When WNT signaling is active in a cell, the TCF/LEF binding sites in the BAT-GAL transgene will be activated leading to expression of LacZ reporter gene (Maretto et al., 2003). I repeated the PD28 anagen tamoxifen injections in these *K14CreERT2 het : BAT-GAL het : Gata6 flox/flox* mice. After 4 days, hair follicles in the control mice displayed strong X-Gal staining in the inner layers of the newly grown hair, indicating

active WNT signaling in those compartments as described before (Blanpain and Fuchs, 2006; Tumbar, 2006). In contrast, no significant X-Gal staining was detected in the regressing hair follicles from the *Gata6* knockout mice (Fig. 4.7). In order to conclude that WNT signaling was diminished in the inner layer of the hair follicle upon the loss of *Gata6*, I need to examine specific markers and the structure of the hair at this stage to see if the cells normally active for WNT signaling are still present in the hair follicles.

Preliminary Conclusions

We identified the preferential expression of the transcription factor *GATA6* in the differentiating progenitor zone of the hair follicles: the hair germ at telogen and the matrix at anagen. Conditional knockout of *Gata6* at telogen led to hair cycle arrest and degeneration of the hair germ compartment. In anagen, the loss of *Gata6* affected the proliferation, differentiation, and survival of progenitors in the matrix. These results were reiterated in both cell culture and skin grafting assays suggesting *Gata6* directly regulates the function of keratinocytes progenitors. In addition, I found *Gata6* knockout leads to the loss of super-basal layer differentiation at the inter-follicular epidermis, which implied that *Gata6* might be a universal progenitor regulator responsible for the maintenance of epidermis progenitors in the basal layer. Collectively, our findings provide an opportunity to study in detail the transcriptional mechanism governing the stem cell differentiation pathway in the skin. This, along with stem cell self-renewal studies, will unveil the complex genetic regulations for stem cell function in the mammalian tissue.

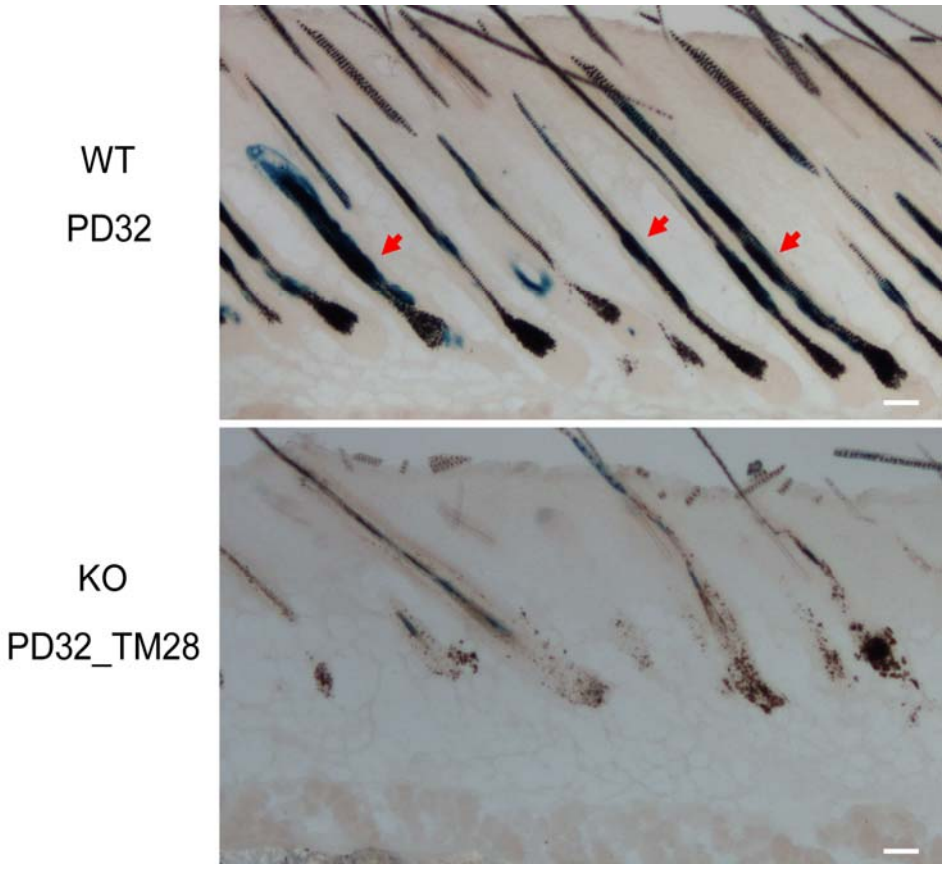

Figure 4.7. Reduced WNT signalling in Gata6 knockout hair follicles.

Skin sections stained with X-gal showed that WNT signaling in differentiated lineages from the wildtype mice at PD32 (arrows in the upper panel). In the regressing knockout hair follicles, only residue blue staining was found in the hair shaft. Skin sections were 20um. N=3. Scale bars, 50um.

CHAPTER 5

CONCLUSIONS AND FUTURE DIRECTIONS

Infrequently Dividing Hair Follicle Stem Cells in the Bulge

The three defining characteristics of stem cells are the self-renewal capability, differentiation potential, and long term contribution to tissue regeneration (Smith, 2001; Weissman et al., 2001). In the mouse hair follicle system, single stem cell culture assays have confirmed that some cells from the bulge can form self-renewing colonies *in vitro* (Blanpain et al., 2004; Claudinot et al., 2005). Upon transplantation, these cultured stem cells locate back to their native niche and generate differentiated lineages for the new hair growth (Claudinot et al., 2005). In addition, results from serial transplantations using descendents from the initial single bulge cell colonies suggest these cells have the long term proliferation and differentiation potential (Claudinot et al., 2005). Although these and other studies have provided abundant evidence supporting the bulge cells as the hair follicle stem cells, concerns remain that the disturbance or change of bulge cell property could occur during cell culture or transplantations. In addition, recently lineage tracing study using Lgr5 to mark cells in the hair germ proposed that the hair germ cells are the active stem cells for normal hair regeneration while the bulge are just the residence for quiescent inactive stem cells (Jaks et al., 2008). Thus, in order to investigate the true identity of hair follicle stem cells, it is essential to determine whether the bulge cells directly contribute to hair regeneration under normal physiological condition. Using two cell tracking systems in the intact mouse skin, we provide evidence supporting the bulge cells as the functional hair follicle stem cells.

First, we used a tet-off H2B-GFP expression to label the infrequently dividing bulge cells (Tumbar et al., 2004; Waghmare et al., 2008). We labeled bulge cells with high level of H2B-GFP retention after doxy chase in the first hair cycle (Fig. 2.1 and 2.5). As the hair follicles were approaching the beginning of the next quiescent stage of the hair cycle, we closely monitored the migration and proliferation activity in the bulge and hair germ. We found that before any cell division occurred, the number of hair germ cells increased during the quiescent stage. The number of the brightest H2B-GFP retaining cells, which had only divided 1-2 times in the previous hair cycle, almost doubled in the hair germ (Fig. 2.5). Later, proliferation started in the hair germ and was restricted to the hair germ while no significant apoptosis is detected (Fig. 2.5). These findings suggest that some bulge cells migrate into the hair germ at the beginning of the quiescent stage of the hair cycle and become transient amplifying progenitors upon the new hair growth.

Furthermore, we genetically labeled single bulge cells at the quiescent stage using the inducible K14CreER transgenic mice (Vasioukhin et al., 1999). We found that after one hair cycle, ~80% of the labeled single bulge cells stayed in the bulge and generated ~4 daughter cells (Fig. 2.8). ~17% of the labeled single bulge cells migrated out of the niche at the quiescent stage and produced differentiated cell lineages during new hair growth (Fig. 2.8, 2.10), which confirmed our observation in the H2B-GFP mice. Long-term lineage tracing results showed that the progeny from the labeled single bugle cells can self-renew in the bulge and contribute to all differentiated layers of the hair after even 1 year (Fig. 2.11). These results, along with the cell tracking data in the H2B-GFP mice, provide direct evidence for bulge cell's self-renewal, differentiation, and long-term potential in undisturbed mouse skin. Per the definition of stem cells, the bulge cells are the functional stem cells for hair follicle regenerations.

Another interesting feature of adult stem cells is that they divide infrequently. Studies in hematopoietic stem cells using the H2B-GFP system have suggested that the most infrequently dividing hematopoietic cells from a putatively heterogeneous stem cell pool and have higher proliferative potential and differentiation capability (Foudi et al., 2009; Wilson et al., 2008). However, recent evidence from unperturbed tissue, including epidermis, hair follicle, and intestine, seemed to challenge the "slow-cycling" stem cell model (Barker et al., 2007; Clayton et al., 2007; Jaks et al., 2008). Combining the H2B-GFP system with Fluorescence Activated Cell Sorting and confocal microscopy, we precisely measured the proliferation dynamics of bulge cells in one hair cycle under normal physiological conditions (Fig 2.1). Our data indicated that bulge cells began to divide at the quiescence-growth transition stage of the hair cycle, and continued on in the growth stage. The cells slowed-down divisions by the late growth stage and became dormant in the regression stage. Most bulge cells divided infrequently (0-5 times) during one hair cycle, confirming results from previous studies (Cotsarelis, 2006; Waghmare et al., 2008). Moreover, we analyzed the alleged Lgr5+ "actively dividing stem cell" in the hair germ for proliferation activity. Our finding suggests that at the quiescence stage, the hair germ is made of cells that have divided 2-4 times in the previous hair cycle (Fig. 2.5). Since these H2B-GFP cells were not detected in the differentiation zone of the hair follicle during the growth stage (data not shown), we conclude that the initial hair germ cells are also "slow-cycling" cells which probably originate from the region right below the bulge during the growth stage. We also characterized the proliferation dynamics of another Lrig1+ stem cell population at the junctional zone in the skin (Fig. 3.4). Compared to the bulge cells, the junctional zone cells divided more vigorously such that the H2B-GFP label was diluted to undetectable level (>5 divisions) within two weeks of doxy chase. Collectively, our data confirms the bulge cells divide infrequently in the intact

tissue. The proliferation activity of bulge cells fluctuates according to the hair regeneration stages. The hair germ cells are also infrequently dividing cells. It's possible that the hair germ cells also contribute to the hair regeneration, but further investigation is needed to elucidate the origin and function of this cell population. Yet we shouldn't be in haste to apply the "slow cycling" model to all types of adult stem cells. Whether or not a stem cell population would divide infrequently will largely depend on the homeostasis of specific tissues. In highly proliferative tissues, such as the intestine, stem cells may adopt different cell cycle mechanisms to achieve stable self-renewal and differentiation.

Alternating of Differentiation and Self-renewal in the Storage Stem Cell Niche of Hair Follicles

From the three types of stem cell niches, intensive studies have been done for the mechanism governing stem cell differentiation and self-renewal in simple niches and complex niches (Ohlstein et al., 2004). Stem cell – niche junction directed asymmetric cell division has been the dominant mechanism in those models: one daughter cell will stay attached to the niche becoming a renewed stem cell; the other daughter cell will depart the niche and start differentiating (Morrison and Kimble, 2006). For the storage niche model, however, little is known about how stem cells achieve differentiation and self-renewal. Here we describe a new temporal-spatial regulatory mechanism for stem cell function in a storage niche (Fig. 5.1).

At quiescence-growth transition stage of the hair cycle, cells in the hair germ and at the bulge/germ transition zone started proliferating first, followed by more extensive bulge cell proliferation in anagen (Cotsarelis, 2006; Greco et al., 2009; Tumbar et al., 2004). According to the asymmetric stem cell division model, the later

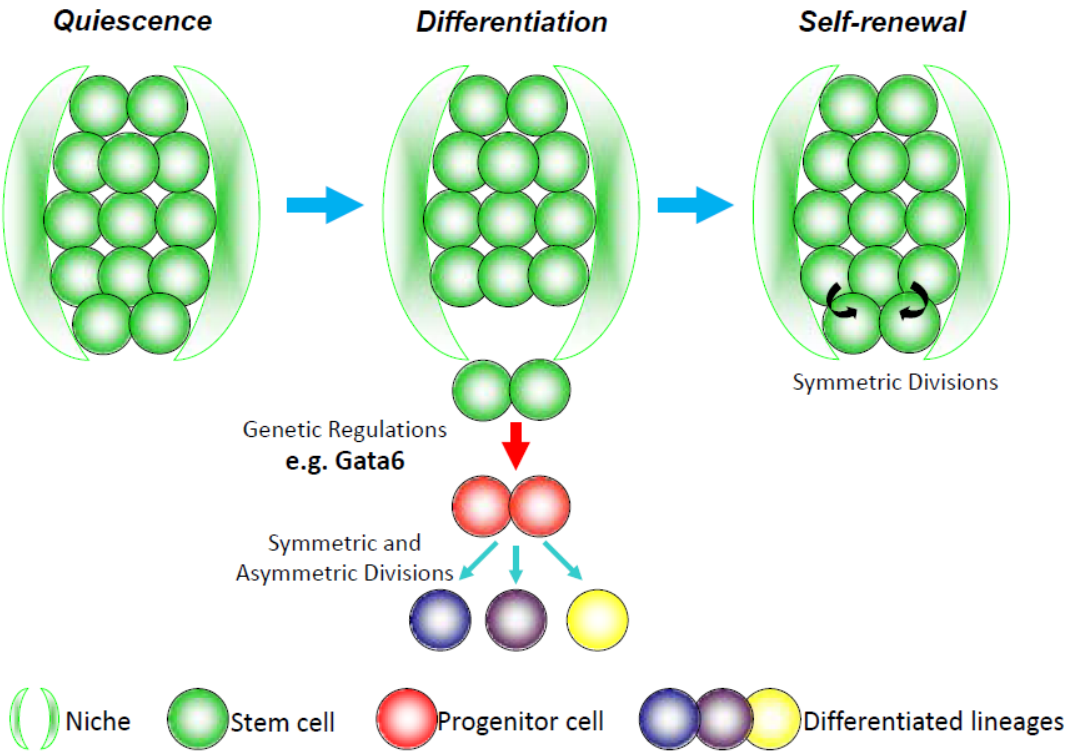

Figure 4.1. Stem cell maintenance in the storage niche.

Infrequently dividing stem cells reside in the storage niche at the quiescence stage of tissue regeneration. Upon activation signals for new tissue growth, the niche switches to differentiation state. Some stem cells migrate out of the niche without proliferation and become progenitors by genetic regulatory mechanisms (e.g., Gata6 up-regulation in the hair progenitors). The progenitors will further produce terminal differentiated lineages for the tissue growth by both symmetric and asymmetric divisions. In a later self-renewal stage of tissue regeneration, the remaining stem cells in the niche divide symmetrically to fill the gap left by the migrating stem cells.

bulge cell proliferation will produce new stem cell to replenish the stem cell pool and differentiating cells to contribute to the new hair growth. Our data, however, showed that a divergent fate of bulge cell progeny at two distinctive proliferation phases (Fig. 2.13A). First, bulge stem cells departed the storage niche in the absence of simultaneous self-renewing divisions during quiescence stage, and subsided to a fate of proliferation and differentiation, most likely upon encountering additional inductive signals outside the niche, and/or the removal of differentiation inhibitory signals supplied in the niche, as suggested in previous models of the field (Oshima et al., 2001; Plikus et al., 2008). On the contrary, the remaining bulge stem cells in the storage niche divide at the later growth stage to replenish the stem cell pool. In addition, the hair follicle labeling patterns from early to full growth stage maintained the same distribution, indicating that progeny made by the remaining bulge stem cells did not contribute to the new hair growth in the current hair cycle. Moreover, we detected more migration/differentiation of bulge cells when we shifted the labeling point to a later growth stage of the hair cycle. Furthermore, the gene expression studies of bulge progeny generated at quiescence stage and growth stage showed distinct profiles suggesting differentiation fate and self-renewal fate, respectively (Fig. 2.1; 2.3). Together, these data show that individual bulge stem cells either leave the storage niche to differentiate at the beginning of tissue regeneration, or stay in the niche and self-renew their pool at a different time point. The storage niche of the hair follicle stem cells oscillates between differentiation and self-renewal proliferation phases separated by quiescence stages. Self-renewal of stem cells occurs at distinct tissue location and time from the differentiation of progenitors. This population mechanism for stem cell differentiation and self-renewal is similar to that of *C. elegans* germ line stem cells where the original two stem cells divide symmetrically along larval development to produce a stem cell/progenitor pool of ~ 2000 cells in the

adult gonad (Kimble and White, 1981). In both systems, the loss of a fraction of the stem cell population does not affect the maintenance of the stem cell pool, and duplication of the niche results in the expansion of stem cell populations (data not shown and (Kipreos et al., 2000; Kostic et al., 2003; Lam et al., 2006)). Yet, the storage niche in the hair follicles still possess unique properties that every stem cell is positioned in a strict cellular environment with direct contact to other cells, whereas in the *C. elegans* germ line, putative stem cells can intermingle with only themselves. In essence, we propose a population mechanism for stem cell function in the storage niche at native mammalian tissue: stem cells as a population accomplish differentiation and self-renewal in which individual "citizen" have equal right and potential to adopt any of two possible fates to respond to the tissue's need for either more differentiated cells or more stem cells at distinct times and tissue locations. The decisions are likely influenced by the location relative to activating signals, underscoring again the essential role of the niche in stem cell fates.

Symmetric Fate Decisions and Divisions for Hair Follicle Stem Cells

The simple and efficient asymmetric stem cell division has been widely used by stem cells in invertebrate tissues, whereas mammalian stem cells show more flexibility and are able to switch between asymmetric and symmetric divisions upon tissue conditions (Clevers, 2005; Morrison and Kimble, 2006; Spradling et al., 2008). Our single-cell lineage tracing data within one hair cycle strongly suggest that the bulge stem cells might have adopted symmetric division/fate decision. However, it's still possible that the storage niche contains both stem cells and progenitors made from growth stage stem cell proliferation and stored until the next hair cycle for distinct fate

assignments. Our long-term lineage tracing data have provided further evidence for symmetric fate decision for hair follicle stem cells:

Bulge cell migration to the hair germ was again observed at the quiescence-growth transition stage of the second hair cycle (Fig. 2.11). At the full growth stage of the second hair cycle and after 1 year, the majority of labeled HFs showed complex patterns with single bulge cell descendants in both the niche and the differentiation zone, which was expected from random fate assignment of multiple labeled bulge cells at the start of second anagen. Importantly, we still detected significant fractions of HFs with niche-only or differentiation zone-only labeling patterns. These results rule out the possibility that bulge cell proliferation is strictly asymmetric producing stem cell daughters that remain confined to their niche, and progenitor daughters that might away simultaneously. In fact, the bulge cells can rely solely on symmetric fate determination and decision to fulfill their function during tissue homeostasis.

This conclusion is further supported by our analyses of the placement of two daughter cells from one stem cell division with respect to an important stem cell niche component – the basement membrane, which has been implicated in directing asymmetric cell division for stem cells in the inter-follicular epidermis (Lechler and Fuchs, 2005). Our findings suggest that when a stem cell leaves the storage niche and moves into the differentiating progenitor zone, it either divides symmetrically along the basement membrane likely to expand the progenitor pool, or asymmetrically perpendicular to the basement membrane producing a differentiating inner layer precursor and a renewed progenitor. When remaining stem cells divide in the later growth stage, the two daughter cells always align parallel to the basement membrane, indicating symmetric division. In order to ultimately determine the nature of cell divisions in the niche, we have analyzed the sub-cellular localization of the conserved asymmetric fate determinants from other stem cell systems including Par3 and Numb,

and the spindle orientation in dividing bulge cells (data not shown). But the ubiquitous expression of these markers and the scarcity of division in the bulge have prevented us from excluding the possibility that the bulge cells could divide asymmetrically. In fact, asymmetric division might be utilized for reasons other than stem cell daughter fate decisions, such as creating tissue polarity.

In short, we propose that hair follicle stem cells use symmetric fate divisions with temporal-spatial fate assignment of progeny to maintain tissue homeostasis. This provides an alternative mechanism for steady-state stem cells in mammalian tissues to achieve differentiation and self-renewal for extended periods of time.

Dynamic Cell Re-localization in the Hair Follicle Stem Cell Niche

Previous nucleotide label-retaining studies have implied only little cellular turnover in the hair follicle stem cell niche (Cotsarelis, 2006). This was supported by a genetic mosaic analysis during hair regeneration, which indicates that only 4 bulge cells are needed for new hair growth (Kopan et al., 2002). Our H2B-GFP cell division counting system, however, detected significant proliferation activity for most bulge cells during one hair cycle (>95%) with an anverage division time of 3 (Waghmare et al., 2008; Zhang et al., 2009). Such extent of bulge cell proliferation suggested the existence of compensating mechanisms for the equilibrium of the stem cell pool.

One aspect of stem cell dynamics is the export of stem cells to the differentiation zone upon new hair growth. Our lineage tracing data suggested that >10% of the bulge cells left the niche at the quiescence/growth transition stage (Fig. 2.8). Considering the entire bulge contains 100-150 cells, at least ~12 bulge cells migrated to the hair germ. These results, along with our ongoing mosaic analysis (data not shown), challenged the previous 4-cell contribution model. In addition, Drs. David

Shalloway and Brian White simulated bulge cell proliferation in mathematical models and calculated an upper bound on the expansion of bulge cell population fold changes (Fig. 3.5). Our data suggested that a minimum 42% cell loss occurred in the stem cell niche during one hair cycle, which was in part reflected by the impact of differentiation loss.

The second compensating mechanism takes place within the niche during tissue morphology changes. From the first to the second hair cycle, the area of CD34+ bulge compartment almost doubled due to the addition of the second club hair (Fig. 3.4). Over-crowding of bulge cells around the old club hair site might therefore force the newly generated cells to re-localize to the new bulge site surrounding the second club hair. This hypothesis was affirmed by our detection of the lateral movements in the H2B-GFP label-retaining bulge cells from the old club hair towards the newly generated club hair in catagen (Fig. 3.4). Together with the vertical migration discussed earlier, our finding suggested a 3-D inductive signaling network to direct the localization of bugle cells in the storage niche during tissue regenerations. The identification of these signaling molecules will contribute to the thorough understanding of stem cell – niche interactions in the future.

Future directions

The work presented in Chapter 2 and 3 proposed a temporal-spatial regulatory model for stem cell differentiation and self-renewal. Our gene expression profiling data have provided the foundation for future studies on how this symmetric stem cell fate/division mechanism is genetically regulated. As briefly described in Chapter 4, we started investigating the function of *Gata6* as one of the transcription factors upregulated during stem cell differentiation but not self-renewal. Our preliminary data

showed that the conditional knockout of *Gata6* led to hair cycle arrest and degeneration of the hair germ at telogen. In anagen, the loss of *Gata6* resulted in reduced proliferation, differentiation, and survival of progenitors in the matrix. *Gata6* also appeared to regulate epidermal progenitor function at the basal layer of inter-follicular epidermis. To elucidate the underlying mechanism for *Gata6* function in progenitor cell maintenance, I will perform the following experiments.

First, I'd like to know which gene expressions were affected in the *Gata6* knockout skin. In order to achieve this goal, the best approach would be sorting hair germ or matrix cells from the skin shortly after tamoxifen was injected to the mice. This method will reflect what happened in the native skin microenvironment avoiding the possible disturbance in cell culture condition. However, limitations also exist for such experiment: enrichment of our target cell populations could be hard due to their limited numbers in the tissue; specific cell surface marker for those two population might not work in the flow-cytometry to our satisfaction; as the progenitors are dying, it will be hard to distinguish them from dying cells by the experimental procedures. An alternative approach is to use the keratinocyte culture system where we have already used to show that the skin phenotype was recapitulated such that the proliferation and survival of progenitors are disrupted (Chapter 4). In that case, we can maintain the control and knockout (before induction) cell lines, and collect enough cells at various time points following the tamoxifen administration. As such, we would be able to track the gradual changes in *Gata6* knockout cells to reveal additional information for the molecular mechanism. After performing RT-PCR for interested genes and possibly microarray analyses, we will try to confirm the affected genes in the skin again to access the representativeness of cell culture phenotype for that in the native tissue.

Second, I will investigate the effect of *Gata6* over-expression in the cell culture system. We have obtained Flag tagged *Gata6* constructs from collaborators (Capo-Chichi et al., 2005). By transfecting the constructs into keratinocytes, we will yield cells transiently express *Gata6* at high levels. Similar RT-CPR and microarray assays can be utilized to provide how *Gata6* over-expression affects the global expression profile. By comparing this data set with that from the knockout, we will have a comprehensive understanding on how *Gata6* regulates its downstream factors. In addition, we plan to use biochemical approaches, such as chromatin IP, to investigate in depth several *Gata6* regulated downstream factors' expression levels.

Last but not least, I will pursue the *Gata6*-WNT regulatory pathway in the hair follicles. It has been shown that *Gata6* forms a forward feedback loop in regulating WNT signaling for stem cell differentiation in the lung and heart (Alexandrovich et al., 2006; Tian et al., 2010; Weidenfeld et al., 2002; Zhang et al., 2008). Our preliminary data also showed down-regulation of WNT signaling in differentiated layers of *Gata6* knockout hair follicles. To further examine the effect of *Gata6* knockout on WNT signaling in the hair follicle, I will first test the expression of important WNT signaling pathway factors in either sorted or culture *Gata6* knockout cells. Next, I will examine in cell culture how WNT signaling affects *Gata6* expression by transfecting WNT activators or WNT3a protein directly. Furthermore, I will search for *Gata6* binding sites in the promoter region of critical WNT signaling factors and test if *Gata6* directly regulates the expression of those factors. Understanding the molecular pathways that control hair follicle stem cell function will pave the road for elucidating in the future how perturbation of these pathways might lead to skin diseases including cancer.

APPENDIX 1

EXAMMING THE HETEROGENEITY IN THE NICHE OF HAIR FOLLICLE STEM CELLS IN MOUSE *MUS MUSCULUS*

This appendix describes the preliminary analyses of cellular heterogeneity in the niche of mouse hair follicle stem cells. As described in detail in Chapter 2, cells in the bulge stem cell niche divide infrequently through hair regenerations (Zhang et al., 2009). In one hair cycle, bulge residents display a division activity from 0 to more than 5 times with an average at 3 times. Our mathematical modeling of such proliferation dynamics captured by Fluorescence Activated Cell Sorting (FACS) (Fig. 2.1) implies the possible existence of more than one cell populations in the bulge compartment (data not shown). The simplest model consists of two cell populations: one divides rarely giving rise to the most quiescent bulge residents; the other population proliferates more actively contributing to the >5 division cell fraction after one hair cycle.

In order to examine the property of bulge cells with distinct proliferation history and test the possible heterogeneity implied by theoretical prediction, I sorted 4 bulge cell fractions based on their cell division numbers in one hair cycle and performed microarray (Fig. A1.1A; microarray procedures are described in Materials and Methods of Chapter 2). Among the genes that were differentially expressed between the most quiescent and proliferative bulge cell fractions, we first focused on cell surface markers which would facilitate the sorting of distinct bulge populations. The microarray signals of 5 cell surface markers preferentially expressed in most actively dividing cells are shown (Fig. A1.1A), among which ITM2A (integral membrane

Figure A1.1. ITM2A expression defines two cell populations in the bulge.

(A) Microarray analyses of bulge cell fraction by division number in one hair cycle. Bulge cells were isolated by different H2B-GFP intensity gatings from PD21-42 chased H2B-GFP mice (red double-head arrows). Microarray signal for 5 cell surfaces markers were plotted. N=2 mice. (See Fig. 2.1, 2.3 for detailed description of cell sorting and microarray). (B) QRT-PCR analyses for *Itm2a* and *CD53* expression level in different bulge cell fractions from PD21-42 chased H2B-GFP mice. N=2 mice. (C) FACS plots for skin cells from PD42 non-GFP mice. CD34+/α6+ bulge cells were further analyzed for ITM2A-FITC staining (lower panel). N=3 mice. (D) FACS plots for skin cells from PD21-PD42 chased H2B-GFP mice. CD34+/α6+/ITM2A+ or – bulge cells were analyzed for H2B-GFP intensity. N=3 mice.

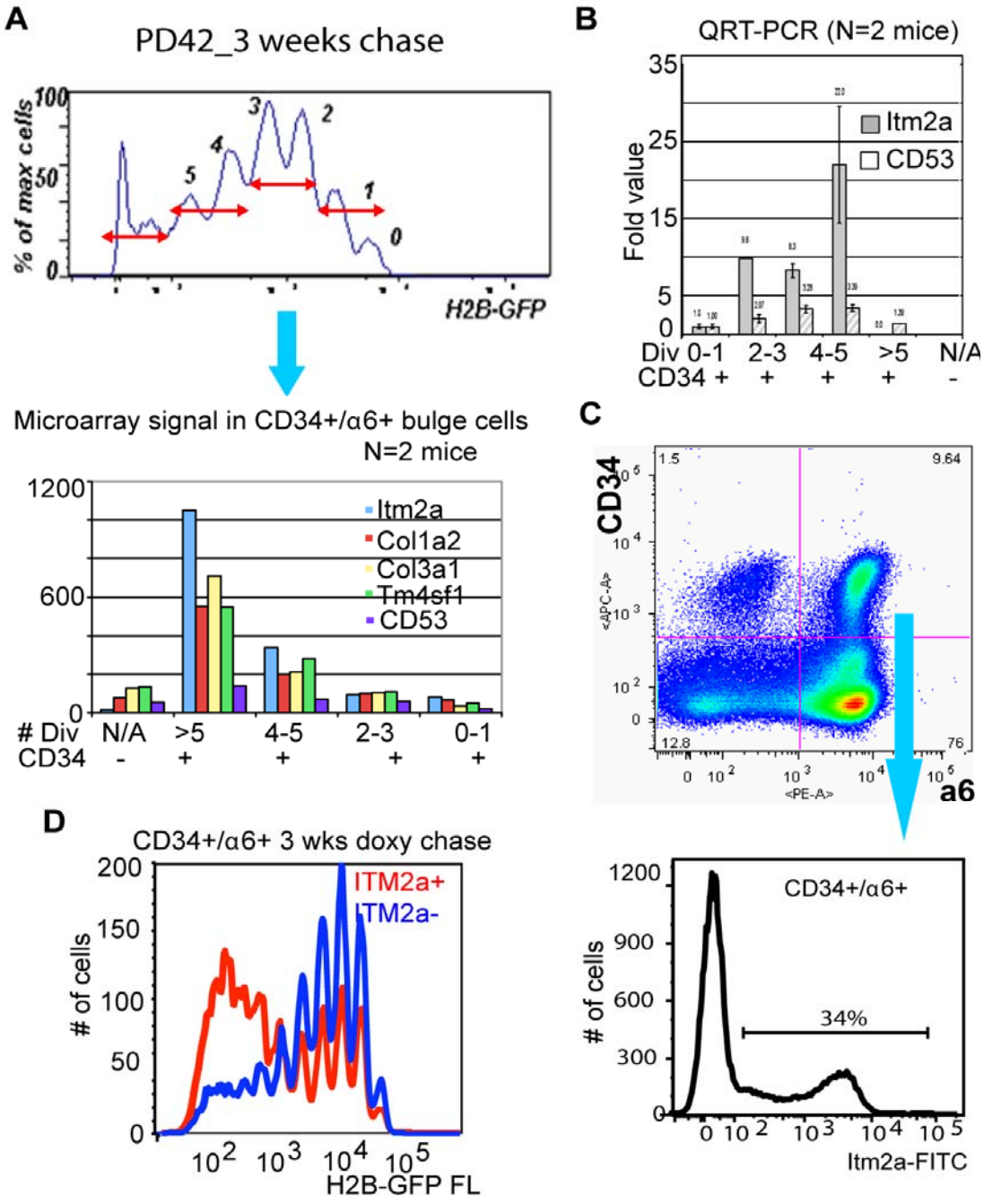
A
PD42_3 weeks chase
% of max cells
100
50
0
H2B-GFP
Microarray signal in CD34+/α6+ bulge cells
N=2 mice
1200
600
0
Itm2a
Col1a2
Col3a1
Tm4sf1
CD53
Div N/A >5 4-5 2-3 0-1
CD34 - + + + +
B
QRT-PCR (N=2 mice)
Fold value
35
25
15
5
0
Itm2a
CD53
Div 0-1 2-3 4-5 >5 N/A
CD34 + + + + -
C
CD34
a6
1.5
9.64
12.8
76
D
CD34+/α6+ 3 wks doxy chase
# of cells
200
150
100
50
0
ITM2a+
ITM2a-
H2B-GFP FL
CD34+/α6+
1200
900
600
300
0
34%
# of cells
Itm2a-FITC

protein 2A) and CD53are reconfirmed for their mRNA level by QRT-PCR experiments (Fig. A1.1B; QRT-PCR procedures are described in Materials and Methods of Chapter2. *Itm2a* forward primer: 5'-GCAAGTGGCAAGTATTTGCCT-3'; *Itm2a* reverse primer: 5'-GCATTTGTCAATGGCACGCTT-3'. *CD53* forward primer: 5'- GACCATAGCCATCCTGCTCTT -3'; *CD53* reverse primer: 5'-CTGAACATCTGCACCTGATGG -3').

To confirm and physically separate Itm2A + or – bulge cell populations for further analysis, I adopted two FACS experiment designs. First, I extracted skin cells from non-GFP littermates in the H2B-GFP mating (for details see Chapter 2), and stained with CD34-APC, α6-PE, and ITM2A-FITC antibodies. When analyzing the CD34+/ α6+ bulge populations for their ITM2A-FITC intensity, I found ~ 34% of bulge cells were ITM2A positive at post-natal day (PD) 42 (Fig. A1.1C). On the other hand, I stained H2B-GFP mice chased from PD21 to PD42 with CD34-APC, α6-PE, and ITM2A-PacificBlu antibodies. When I plotted ITM2A + or – bulge populations for their H2B-GFP intensity, the ITM2A+ bulge cells divide significantly more than the ITM2A- bulge residents (Fig. A1.1D).

Collectively, my data were indicative of the existence of two cellular populations in the bulge distinguished by the expression of *Itm2a*. ITM2A + bulge cells divided more frequently than the ITM2A- bulge cells in one hair cycle. Future studies are needed to determine the function and property of these two cellular populations in the stem cell niche of mouse hair follicles. Whether they have both similar potential and function with respect to hair follicle stem cells, or whether one is long-sought maintenance niche cells, or a temporary residing progenitor population remains to be established in the future by cell transplantation and lineage tracing assays.

REFERENCE

Alexandrovich, A., Arno, M., Patient, R.K., Shah, A.M., Pizzey, J.A., and Brewer, A.C. (2006). Wnt2 is a direct downstream target of GATA6 during early cardiogenesis. Mech Dev *123*, 297-311.

Alvarez-Buylla, A., and Lim, D.A. (2004). For the long run: maintaining germinal niches in the adult brain. Neuron *41*, 683-686.

Barker, N., van Es, J.H., Kuipers, J., Kujala, P., van den Born, M., Cozijnsen, M., Haegebarth, A., Korving, J., Begthel, H., Peters, P.J., *et al.* (2007). Identification of stem cells in small intestine and colon by marker gene Lgr5. Nature *449*, 1003-1007.

Betschinger, J., and Knoblich, J.A. (2004). Dare to be different: asymmetric cell division in Drosophila, C. elegans and vertebrates. Curr Biol *14*, R674-685.

Blanpain, C., and Fuchs, E. (2006). Epidermal stem cells of the skin. Annu Rev Cell Dev Biol *22*, 339-373.

Blanpain, C., Lowry, W.E., Geoghegan, A., Polak, L., and Fuchs, E. (2004). Self-renewal, multipotency, and the existence of two cell populations within an epithelial stem cell niche. Cell *118*, 635-648.

Bodine, D.M., Seidel, N.E., and Orlic, D. (1996). Bone marrow collected 14 days after in vivo administration of granulocyte colony-stimulating factor and stem cell factor to mice has 10-fold more repopulating ability than untreated bone marrow. Blood *88*, 89-97.

Braun, K.M., Niemann, C., Jensen, U.B., Sundberg, J.P., Silva-Vargas, V., and Watt, F.M. (2003). Manipulation of stem cell proliferation and lineage commitment: visualisation of label-retaining cells in wholemounts of mouse epidermis. Development *130*, 5241-5255.

Bresnick, E.H., Martowicz, M.L., Pal, S., and Johnson, K.D. (2005). Developmental control via GATA factor interplay at chromatin domains. J Cell Physiol *205*, 1-9.

Calvi, L.M., Adams, G.B., Weibrecht, K.W., Weber, J.M., Olson, D.P., Knight, M.C., Martin, R.P., Schipani, E., Divieti, P., Bringhurst, F.R., *et al.* (2003). Osteoblastic cells regulate the haematopoietic stem cell niche. Nature *425*, 841-846.

Capo-Chichi, C.D., Rula, M.E., Smedberg, J.L., Vanderveer, L., Parmacek, M.S., Morrisey, E.E., Godwin, A.K., and Xu, X.X. (2005). Perception of differentiation cues by GATA factors in primitive endoderm lineage determination of mouse embryonic stem cells. Dev Biol *286*, 574-586.

Cayouette, M., and Raff, M. (2002). Asymmetric segregation of Numb: a mechanism for neural specification from Drosophila to mammals. Nat Neurosci *5*, 1265-1269.

Chen, H.J., Lin, C.M., Lin, C.S., Perez-Olle, R., Leung, C.L., and Liem, R.K. (2006). The role of microtubule actin cross-linking factor 1 (MACF1) in the Wnt signaling pathway. Genes Dev *20*, 1933-1945.

Claudinot, S., Nicolas, M., Oshima, H., Rochat, A., and Barrandon, Y. (2005). Long-term renewal of hair follicles from clonogenic multipotent stem cells. Proc Natl Acad Sci U S A *102*, 14677-14682.

Clayton, E., Doupe, D.P., Klein, A.M., Winton, D.J., Simons, B.D., and Jones, P.H. (2007). A single type of progenitor cell maintains normal epidermis. Nature *446*, 185-189.

Clevers, H. (2005). Stem cells, asymmetric division and cancer. Nat Genet *37*, 1027-1028.

Conboy, I.M., and Rando, T.A. (2002). The regulation of Notch signaling controls satellite cell activation and cell fate determination in postnatal myogenesis. Dev Cell *3*, 397-409.

Cotsarelis, G. (2006). Epithelial stem cells: a folliculocentric view. J Invest Dermatol *126*, 1459-1468.

Cotsarelis, G., Sun, T.T., and Lavker, R.M. (1990). Label-retaining cells reside in the bulge area of pilosebaceous unit: implications for follicular stem cells, hair cycle, and skin carcinogenesis. Cell *61*, 1329-1337.

Decotto, E., and Spradling, A.C. (2005). The Drosophila ovarian and testis stem cell niches: similar somatic stem cells and signals. Dev Cell *9*, 501-510.

Diamond, I., Owolabi, T., Marco, M., Lam, C., and Glick, A. (2000). Conditional gene expression in the epidermis of transgenic mice using the tetracycline-regulated transactivators tTA and rTA linked to the keratin 5 promoter. J Invest Dermatol *115*, 788-794.

Doe, C.Q., and Bowerman, B. (2001). Asymmetric cell division: fly neuroblast meets worm zygote. Curr Opin Cell Biol *13*, 68-75.

Doetsch, F., Petreanu, L., Caille, I., Garcia-Verdugo, J.M., and Alvarez-Buylla, A. (2002). EGF converts transit-amplifying neurogenic precursors in the adult brain into multipotent stem cells. Neuron *36*, 1021-1034.

Dor, Y., and Melton, D.A. (2004). How important are adult stem cells for tissue maintenance? Cell Cycle *3*, 1104-1106.

Foudi, A., Hochedlinger, K., Van Buren, D., Schindler, J.W., Jaenisch, R., Carey, V., and Hock, H. (2009). Analysis of histone 2B-GFP retention reveals slowly cycling hematopoietic stem cells. Nat Biotechnol *27*, 84-90.

Frye, M., Gardner, C., Li, E.R., Arnold, I., and Watt, F.M. (2003). Evidence that Myc activation depletes the epidermal stem cell compartment by modulating adhesive interactions with the local microenvironment. Development *130*, 2793-2808.

Fuchs, E. (2009). The tortoise and the hair: slow-cycling cells in the stem cell race. Cell *137*, 811-819.

Fuchs, E., and Raghavan, S. (2002). Getting under the skin of epidermal morphogenesis. Nat Rev Genet *3*, 199-209.

Ghazizadeh, S., and Taichman, L.B. (2001). Multiple classes of stem cells in cutaneous epithelium: a lineage analysis of adult mouse skin. Embo J *20*, 1215-1222.

Greco, V., Chen, T., Rendl, M., Schober, M., Pasolli, H.A., Stokes, N., Dela Cruz-Racelis, J., and Fuchs, E. (2009). A two-step mechanism for stem cell activation during hair regeneration. Cell Stem Cell *4*, 155-169.

Guo, S., and Kemphues, K.J. (1996). Molecular genetics of asymmetric cleavage in the early Caenorhabditis elegans embryo. Curr Opin Genet Dev *6*, 408-415.

Hoffman, R.M. (2006). The pluripotency of hair follicle stem cells. Cell Cycle *5*, 232-233.

Holtzinger, A., and Evans, T. (2007). Gata5 and Gata6 are functionally redundant in zebrafish for specification of cardiomyocytes. Dev Biol *312*, 613-622.

Horsley, V., O'Carroll, D., Tooze, R., Ohinata, Y., Saitou, M., Obukhanych, T., Nussenzweig, M., Tarakhovsky, A., and Fuchs, E. (2006). Blimp1 defines a progenitor population that governs cellular input to the sebaceous gland. Cell *126*, 597-609.

Huttner, W.B., and Kosodo, Y. (2005). Symmetric versus asymmetric cell division during neurogenesis in the developing vertebrate central nervous system. Curr Opin Cell Biol *17*, 648-657.

Hynes, R.O. (2009). The extracellular matrix: not just pretty fibrils. Science *326*, 1216-1219.

Il-Hoan, O., and Kyung-Rim, K. (2010). Multiple Niches for Hematopoietic Stem Cell Regulations. Stem Cells.

Iscove, N.N., and Nawa, K. (1997). Hematopoietic stem cells expand during serial transplantation in vivo without apparent exhaustion. Curr Biol *7*, 805-808.

Ito, M., Kizawa, K., Hamada, K., and Cotsarelis, G. (2004). Hair follicle stem cells in the lower bulge form the secondary germ, a biochemically distinct but functionally equivalent progenitor cell population, at the termination of catagen. Differentiation *72*, 548-557.

Ito, M., Liu, Y., Yang, Z., Nguyen, J., Liang, F., Morris, R.J., and Cotsarelis, G. (2005). Stem cells in the hair follicle bulge contribute to wound repair but not to homeostasis of the epidermis. Nat Med *11*, 1351-1354.

Jaks, V., Barker, N., Kasper, M., van Es, J.H., Snippert, H.J., Clevers, H., and Toftgard, R. (2008). Lgr5 marks cycling, yet long-lived, hair follicle stem cells. Nat Genet.

Jensen, K.B., Collins, C.A., Nascimento, E., Tan, D.W., Frye, M., Itami, S., and Watt, F.M. (2009). Lrig1 expression defines a distinct multipotent stem cell population in mammalian epidermis. Cell Stem Cell *4*, 427-439.

Jones, C.L., and Reiners, J.J., Jr. (1997). Differentiation status of cultured murine keratinocytes modulates induction of genes responsive to 2,3,7,8-tetrachlorodibenzo-p-dioxin. Arch Biochem Biophys *347*, 163-173.

Kaufman, C.K., Zhou, P., Pasolli, H.A., Rendl, M., Bolotin, D., Lim, K.C., Dai, X., Alegre, M.L., and Fuchs, E. (2003). GATA-3: an unexpected regulator of cell lineage determination in skin. Genes Dev *17*, 2108-2122.

Kimble, J., and Crittenden, S.L. (2007). Controls of germline stem cells, entry into meiosis, and the sperm/oocyte decision in Caenorhabditis elegans. Annu Rev Cell Dev Biol *23*, 405-433.

Kimble, J.E., and White, J.G. (1981). On the control of germ cell development in Caenorhabditis elegans. Dev Biol *81*, 208-219.

Kipreos, E.T., Gohel, S.P., and Hedgecock, E.M. (2000). The C. elegans F-box/WD-repeat protein LIN-23 functions to limit cell division during development. Development *127*, 5071-5082.

Kobayashi, K., Rochat, A., and Barrandon, Y. (1993). Segregation of keratinocyte colony-forming cells in the bulge of the rat vibrissa. Proc Natl Acad Sci U S A *90*, 7391-7395.

Kopan, R., Lee, J., Lin, M.H., Syder, A.J., Kesterson, J., Crutchfield, N., Li, C.R., Wu, W., Books, J., and Gordon, J.I. (2002). Genetic mosaic analysis indicates that the bulb region of coat hair follicles contains a resident population of several active multipotent epithelial lineage progenitors. Dev Biol *242*, 44-57.

Kostic, I., Li, S., and Roy, R. (2003). cki-1 links cell division and cell fate acquisition in the C. elegans somatic gonad. Dev Biol *263*, 242-252.

Lam, N., Chesney, M.A., and Kimble, J. (2006). Wnt signaling and CEH-22/tinman/Nkx2.5 specify a stem cell niche in C. elegans. Curr Biol *16*, 287-295.

Lansdorp, P.M. (2007). Immortal strands? Give me a break. Cell *129*, 1244-1247.

Lechler, T., and Fuchs, E. (2005). Asymmetric cell divisions promote stratification and differentiation of mammalian skin. Nature *437*, 275-280.

Legue, E., and Nicolas, J.F. (2005). Hair follicle renewal: organization of stem cells in the matrix and the role of stereotyped lineages and behaviors. Development *132*, 4143-4154.

Li, L., and Clevers, H. (2010). Coexistence of quiescent and active adult stem cells in mammals. Science *327*, 542-545.

Li, M., Indra, A.K., Warot, X., Brocard, J., Messaddeq, N., Kato, S., Metzger, D., and Chambon, P. (2000). Skin abnormalities generated by temporally controlled RXRalpha mutations in mouse epidermis. Nature *407*, 633-636.

Lien, W.H., Klezovitch, O., and Vasioukhin, V. (2006). Cadherin-catenin proteins in vertebrate development. Curr Opin Cell Biol *18*, 499-506.

Lin, H. (2002). The stem-cell niche theory: lessons from flies. Nat Rev Genet *3*, 931-940.

Luong, M.X., van der Meijden, C.M., Xing, D., Hesselton, R., Monuki, E.S., Jones, S.N., Lian, J.B., Stein, J.L., Stein, G.S., Neufeld, E.J., *et al.* (2002). Genetic ablation of the CDP/Cux protein C terminus results in hair cycle defects and reduced male fertility. Mol Cell Biol *22*, 1424-1437.

Maretto, S., Cordenonsi, M., Dupont, S., Braghetta, P., Broccoli, V., Hassan, A.B., Volpin, D., Bressan, G.M., and Piccolo, S. (2003). Mapping Wnt/beta-catenin signaling during mouse development and in colorectal tumors. Proc Natl Acad Sci U S A *100*, 3299-3304.

Millar, S.E. (2006). Smad7: licensed to kill beta-catenin. Dev Cell *11*, 274-276.

Morris, R.J., Liu, Y., Marles, L., Yang, Z., Trempus, C., Li, S., Lin, J.S., Sawicki, J.A., and Cotsarelis, G. (2004). Capturing and profiling adult hair follicle stem cells. Nat Biotechnol *22*, 411-417.

Morris, R.J., and Potten, C.S. (1999). Highly persistent label-retaining cells in the hair follicles of mice and their fate following induction of anagen. J Invest Dermatol *112*, 470-475.

Morrisey, E.E., Tang, Z., Sigrist, K., Lu, M.M., Jiang, F., Ip, H.S., and Parmacek, M.S. (1998). GATA6 regulates HNF4 and is required for differentiation of visceral endoderm in the mouse embryo. Genes Dev *12*, 3579-3590.

Morrison, S.J., Hemmati, H.D., Wandycz, A.M., and Weissman, I.L. (1995). The purification and characterization of fetal liver hematopoietic stem cells. Proc Natl Acad Sci U S A *92*, 10302-10306.

Morrison, S.J., and Kimble, J. (2006). Asymmetric and symmetric stem-cell divisions in development and cancer. Nature *441*, 1068-1074.

Morrison, S.J., Shah, N.M., and Anderson, D.J. (1997a). Regulatory mechanisms in stem cell biology. Cell *88*, 287-298.

Morrison, S.J., and Spradling, A.C. (2008). Stem cells and niches: mechanisms that promote stem cell maintenance throughout life. Cell *132*, 598-611.

Morrison, S.J., Wright, D.E., and Weissman, I.L. (1997b). Cyclophosphamide/granulocyte colony-stimulating factor induces hematopoietic stem cells to proliferate prior to mobilization. Proc Natl Acad Sci U S A *94*, 1908-1913.

Morshead, C.M., Craig, C.G., and van der Kooy, D. (1998). In vivo clonal analyses reveal the properties of endogenous neural stem cell proliferation in the adult mammalian forebrain. Development *125*, 2251-2261.

Muller-Rover, S., Handjiski, B., van der Veen, C., Eichmuller, S., Foitzik, K., McKay, I.A., Stenn, K.S., and Paus, R. (2001). A comprehensive guide for the accurate classification of murine hair follicles in distinct hair cycle stages. J Invest Dermatol *117*, 3-15.

Noctor, S.C., Martinez-Cerdeno, V., Ivic, L., and Kriegstein, A.R. (2004). Cortical neurons arise in symmetric and asymmetric division zones and migrate through specific phases. Nat Neurosci *7*, 136-144.

Ohlstein, B., Kai, T., Decotto, E., and Spradling, A. (2004). The stem cell niche: theme and variations. Curr Opin Cell Biol *16*, 693-699.

Orkin, S.H. (1992). GATA-binding transcription factors in hematopoietic cells. Blood *80*, 575-581.

Oshima, H., Rochat, A., Kedzia, C., Kobayashi, K., and Barrandon, Y. (2001). Morphogenesis and renewal of hair follicles from adult multipotent stem cells. Cell *104*, 233-245.

Osorio, K.M., Lee, S.E., McDermitt, D.J., Waghmare, S.K., Zhang, Y.V., Woo, H.N., and Tumbar, T. (2008). Runx1 modulates developmental, but not injury-driven, hair follicle stem cell activation. Development *135*, 1059-1068.

Papaioannou, V. (2001). Stem cells and Differentiation. Differentiation *68*, 153-154.

Plikus, M.V., Mayer, J.A., de la Cruz, D., Baker, R.E., Maini, P.K., Maxson, R., and Chuong, C.M. (2008). Cyclic dermal BMP signalling regulates stem cell activation during hair regeneration. Nature *451*, 340-344.

Purton, L.E., and Scadden, D.T. (2007). Limiting factors in murine hematopoietic stem cell assays. Cell Stem Cell *1*, 263-270.

Raghavan, S., Bauer, C., Mundschau, G., Li, Q., and Fuchs, E. (2000). Conditional ablation of beta1 integrin in skin. Severe defects in epidermal proliferation, basement membrane formation, and hair follicle invagination. J Cell Biol *150*, 1149-1160.

Reid, C.B., Tavazoie, S.F., and Walsh, C.A. (1997). Clonal dispersion and evidence for asymmetric cell division in ferret cortex. Development *124*, 2441-2450.

Rendl, M., Lewis, L., and Fuchs, E. (2005). Molecular dissection of mesenchymal-epithelial interactions in the hair follicle. PLoS Biol *3*, e331.

Rieger, E., Bijl, J.J., van Oostveen, J.W., Soyer, H.P., Oudejans, C.B., Jiwa, N.M., Walboomers, J.M., and Meijer, C.J. (1994). Expression of the homeobox gene HOXC4 in keratinocytes of normal skin and epithelial skin tumors is correlated with differentiation. J Invest Dermatol *103*, 341-346.

Ryu, B.Y., Orwig, K.E., Avarbock, M.R., and Brinster, R.L. (2003). Stem cell and niche development in the postnatal rat testis. Dev Biol *263*, 253-263.

Schmidt-Ullrich, R., and Paus, R. (2005). Molecular principles of hair follicle induction and morphogenesis. Bioessays *27*, 247-261.

Seery, J.P., and Watt, F.M. (2000). Asymmetric stem-cell divisions define the architecture of human oesophageal epithelium. Curr Biol *10*, 1447-1450.

Segre, J.A., Nemhauser, J.L., Taylor, B.A., Nadeau, J.H., and Lander, E.S. (1995). Positional cloning of the nude locus: genetic, physical, and transcription maps of the region and mutations in the mouse and rat. Genomics *28*, 549-559.

Shay, J.W., and Wright, W.E. (2000). Hayflick, his limit, and cellular ageing. Nat Rev Mol Cell Biol *1*, 72-76.

Shen, Q., Zhong, W., Jan, Y.N., and Temple, S. (2002). Asymmetric Numb distribution is critical for asymmetric cell division of mouse cerebral cortical stem cells and neuroblasts. Development *129*, 4843-4853.

Sherr, C.J., and DePinho, R.A. (2000). Cellular senescence: mitotic clock or culture shock? Cell *102*, 407-410.

Smith, A.G. (2001). Embryo-derived stem cells: of mice and men. Annu Rev Cell Dev Biol *17*, 435-462.

Sodhi, C.P., Li, J., and Duncan, S.A. (2006). Generation of mice harbouring a conditional loss-of-function allele of Gata6. BMC Dev Biol *6*, 19.

Song, X., Zhu, C.H., Doan, C., and Xie, T. (2002). Germline stem cells anchored by adherens junctions in the Drosophila ovary niches. Science *296*, 1855-1857.

Soriano, P. (1999). Generalized lacZ expression with the ROSA26 Cre reporter strain. Nat Genet *21*, 70-71.

Spradling, A., Drummond-Barbosa, D., and Kai, T. (2001). Stem cells find their niche. Nature *414*, 98-104.

Spradling, A.C., Nystul, T., Lighthouse, D., Morris, L., Fox, D., Cox, R., Tootle, T., Frederick, R., and Skora, A. (2008). Stem cells and their niches: integrated units that maintain Drosophila tissues. Cold Spring Harb Symp Quant Biol *73*, 49-57.

Sun, T.T., and Lavker, R.M. (2004). Corneal epithelial stem cells: past, present, and future. J Investig Dermatol Symp Proc *9*, 202-207.

Sur, I., Rozell, B., Jaks, V., Bergstrom, A., and Toftgard, R. (2006). Epidermal and craniofacial defects in mice overexpressing Klf5 in the basal layer of the epidermis. J Cell Sci *119*, 3593-3601.

Tanahashi, H., and Tabira, T. (2000). Alkaline treatment after X-Gal staining reaction for Escherichia coli beta-galactosidase enhances sensitivity. Anal Biochem *279*, 122-123.

Taylor, G., Lehrer, M.S., Jensen, P.J., Sun, T.T., and Lavker, R.M. (2000). Involvement of follicular stem cells in forming not only the follicle but also the epidermis. Cell *102*, 451-461.

Tian, Y., Yuan, L., Goss, A.M., Wang, T., Yang, J., Lepore, J.J., Zhou, D., Schwartz, R.J., Patel, V., Cohen, E.D., *et al.* (2010). Characterization and in vivo pharmacological rescue of a Wnt2-Gata6 pathway required for cardiac inflow tract development. Dev Cell *18*, 275-287.

Trempus, C.S., Morris, R.J., Bortner, C.D., Cotsarelis, G., Faircloth, R.S., Reece, J.M., and Tennant, R.W. (2003). Enrichment for living murine keratinocytes from the hair follicle bulge with the cell surface marker CD34. J Invest Dermatol *120*, 501-511.

Tudorita Tumbar, and Fuchs, E. (2006). Epithelial Skin Stem Cells. In Essentials of Stem Cell Biology, R. Lanza, ed. (Elsevier Academic Press), pp. 169-177.

Tumbar, T. (2006). Epithelial skin stem cells. Methods Enzymol *419*, 73-99.

Tumbar, T., Guasch, G., Greco, V., Blanpain, C., Lowry, W.E., Rendl, M., and Fuchs, E. (2004). Defining the epithelial stem cell niche in skin. Science *303*, 359-363.

van der Kooy, D., and Weiss, S. (2000). Why stem cells? Science *287*, 1439-1441.

Vasioukhin, V., Degenstein, L., Wise, B., and Fuchs, E. (1999). The magical touch: genome targeting in epidermal stem cells induced by tamoxifen application to mouse skin. Proc Natl Acad Sci U S A *96*, 8551-8556.

Viger, R.S., Guittot, S.M., Anttonen, M., Wilson, D.B., and Heikinheimo, M. (2008). Role of the GATA family of transcription factors in endocrine development, function, and disease. Mol Endocrinol *22*, 781-798.

Waghmare, S.K., Bansal, R., Lee, J., Zhang, Y.V., McDermitt, D.J., and Tumbar, T. (2008). Quantitative proliferation dynamics and random chromosome segregation of hair follicle stem cells. Embo J *27*, 1309-1320.

Wakamatsu, Y., Maynard, T.M., Jones, S.U., and Weston, J.A. (1999). NUMB localizes in the basal cortex of mitotic avian neuroepithelial cells and modulates neuronal differentiation by binding to NOTCH-1. Neuron *23*, 71-81.

Weidenfeld, J., Shu, W., Zhang, L., Millar, S.E., and Morrisey, E.E. (2002). The WNT7b promoter is regulated by TTF-1, GATA6, and Foxa2 in lung epithelium. J Biol Chem *277*, 21061-21070.

Weissman, I.L., Anderson, D.J., and Gage, F. (2001). Stem and progenitor cells: origins, phenotypes, lineage commitments, and transdifferentiations. Annu Rev Cell Dev Biol *17*, 387-403.

Wilson, A., Laurenti, E., Oser, G., van der Wath, R.C., Blanco-Bose, W., Jaworski, M., Offner, S., Dunant, C.F., Eshkind, L., Bockamp, E.*, et al.* (2008). Hematopoietic stem cells reversibly switch from dormancy to self-renewal during homeostasis and repair. Cell *135*, 1118-1129.

Wodarz, A. (2005). Molecular control of cell polarity and asymmetric cell division in Drosophila neuroblasts. Curr Opin Cell Biol *17*, 475-481.

Wright, D.E., Cheshier, S.H., Wagers, A.J., Randall, T.D., Christensen, J.L., and Weissman, I.L. (2001). Cyclophosphamide/granulocyte colony-stimulating factor causes selective mobilization of bone marrow hematopoietic stem cells into the blood after M phase of the cell cycle. Blood *97*, 2278-2285.

Xie, T., and Spradling, A.C. (2000). A niche maintaining germ line stem cells in the Drosophila ovary. Science *290*, 328-330.

Yamashita, Y.M., Fuller, M.T., and Jones, D.L. (2005). Signaling in stem cell niches: lessons from the Drosophila germline. J Cell Sci *118*, 665-672.

Yamashita, Y.M., Jones, D.L., and Fuller, M.T. (2003). Orientation of asymmetric stem cell division by the APC tumor suppressor and centrosome. Science *301*, 1547-1550.

Zhang, R., Zhang, Z., Zhang, C., Zhang, L., Robin, A., Wang, Y., Lu, M., and Chopp, M. (2004). Stroke transiently increases subventricular zone cell division from asymmetric to symmetric and increases neuronal differentiation in the adult rat. J Neurosci *24*, 5810-5815.

Zhang, Y., Goss, A.M., Cohen, E.D., Kadzik, R., Lepore, J.J., Muthukumaraswamy, K., Yang, J., DeMayo, F.J., Whitsett, J.A., Parmacek, M.S., *et al.* (2008). A Gata6-Wnt pathway required for epithelial stem cell development and airway regeneration. Nat Genet *40*, 862-870.

Zhang, Y., Rath, N., Hannenhalli, S., Wang, Z., Cappola, T., Kimura, S., Atochina-Vasserman, E., Lu, M.M., Beers, M.F., and Morrisey, E.E. (2007). GATA and Nkx factors synergistically regulate tissue-specific gene expression and development in vivo. Development *134*, 189-198.

Zhang, Y.V., Cheong, J., Ciapurin, N., McDermitt, D.J., and Tumbar, T. (2009). Distinct self-renewal and differentiation phases in the niche of infrequently dividing hair follicle stem cells. Cell Stem Cell *5*, 267-278.

Zhang, Y.V., White, B.S., Shalloway, D.I., and Tumbar, T. (2010). Stem cell dynamics in mouse hair follicles: A story from cell division counting and single cell lineage tracing. Cell Cycle *9*.

Zhao, R., Watt, A.J., Li, J., Luebke-Wheeler, J., Morrisey, E.E., and Duncan, S.A. (2005). GATA6 is essential for embryonic development of the liver but dispensable for early heart formation. Mol Cell Biol *25*, 2622-2631.

Zhong, W., Feder, J.N., Jiang, M.M., Jan, L.Y., and Jan, Y.N. (1996). Asymmetric localization of a mammalian numb homolog during mouse cortical neurogenesis. Neuron *17*, 43-53.